# Soliton-Like Waves Of Nuclear Burning In The Neutron Multiplicating Media (Theory And Computational Approach)

Dissertation zur Erlangung des Doktorgrades
der Fakultät für Physic
der Universität Bielefeld

vorgelegt von
Olga Byegunova

Januar 2009

Gedruckt auf alterungsbeständigem Papier nach DIN-ISO 9706

# Contents

# List of Figures

# List of Tables

# Acknowledgements

This thesis would have not been ready without the support of many people who have helped me directly as well as indirectly. I would like to convey my gratitude to some of them for their efforts and best wishes.

First of all, I would like to express my gratitude to Professors Yuri Kondratiev, Philippe Blanchard and Michael Röckner for giving me the possibility to perform the PhD research at International Graduate College "Stochastics and Real World Models". It has been an interesting three years. Next, I would like to thank Prof. Yuri Kondratiev, my daily supervisor, for his valuable support, advice, encouragement and help about the project until the last period of writing this thesis.

Thanks are also due to people at the Department of Theoretical and Experimental Nuclear Physic of the National Politechnic University of Odessa, Ukraine. Especially I am indebted to Prof. Vitaly Rusov for his continuous assistance, constructive critics, valuable discussions and more important for patience and encouragement, although officially he had nothing to do with my thesis research. Furthermore I would like to thank Dr. V. A. Tarasov and Dr. S. I. Kosenko for teaching me the basic principles of reactor physics. Without them I will not be able to finish Chapter 4. A special appreciation goes to Prof. Tatjana Zelentsova for her collaboration and theoretical guidance.

I wish to express my thanks to Hannelore Litschewsky for her attention and caring when I arrived to Bielefeld; Nikole Zimmermann for her help and support; Gaby Windhorst for her caring especially during the last period of writing this thesis.

I would like also to thank all people in the IGC for the support, aid and fruitful environment. Thanks for everything: laughs, good conversation during coffee breaks and lunches, and so much more.

One person deserves a special mention, and that is Felipe Torres, who gradually evolved from my colleague to a good friend. I would like to thank him for his invaluable support in almost anything and assistance developing the simulation code, and for being my office mate during the last two years.

I also take this opportunity to thank Natalia Ohlerich for always encouraging me and giving moral support to finish this thesis and Sven Wiesinger for his help and making huge amount of organization work for us.

In this occasion I would like to express my gratitude to my parents, to whom this thesis is dedicated, for the support and for the love. Thanks for always encouraging and supporting me even when we are miles apart.

Finally, a very special appreciation is due to my beloved husband, Konstantin Zverev. Thanks for your constant encouragement and support, for always helping me when I was in a bad mood, and also for your love.

I also want to thank the Chinese part of IGC, who hosted me during the joint workshop in Beijing, March 19–23, 2007 at the Academy of Mathematics and Systems Science, Chinese Academy of Sciences. I had a very good time in China, and I learnt a lot.

Financial support by the International Graduate College "Stochastics and Real World Models"via a scholarship is gratefully acknowledged.

# Introduction

## Background

It is well-known that usable nuclear energy can be extracted from atomic nuclei via two types of physical processes - nuclear fission (breeding) and nuclear fusion (thermonuclear) reactions. However, from a variety of light nuclei fusion reactions only fusion reactions of hydrogen isotopes are actually suitable for nuclear power engineering. This is conditioned by the fact that Coulomb repulsion for nuclei with a big atomic number (charge) and appropriate radiation loss make fusion reaction on heavy nuclei unfeasible.

Meanwhile, well-known reaction between the nuclei of the two heavy forms (isotopes) of hydrogen - deuterium (D) and tritium (T) $D+T \rightarrow \alpha+n$, characterized by $He^5$ compound nucleus resonance in the nuclear projectile energy range 100 KeV, has an approximately 100 times higher reaction rate (after Maxwell averaging of hydrogen plasma in operating temperature range $5 \div 20\, KeV$) than seemingly similar $D + D$ reaction. This advantage of DT-reaction over other thermonuclear reactions is so definitive that with current technology the DT-reaction is most readily feasible. But even for Deuterium-Tritium fuel nowadays it remains unclear that an economically viable fusion plant is possible at all. The technically full-featured and functional prototype that considers the Lawson criterion does not exist as of yet. Several fusion reactors have been built, but none have produced more thermal energy than electrical energy consumed. Aforementioned concerns both Tokamak-type reactors, which confine a deuterium-tritium plasma magnetically, and impulse reactors, which accumulate energy either from laser beams or from heavy-ion accelerators.

Usual nuclear plants evolved for many decades with vigorous government support of the most developed countries. The ˝usual˝nuclear reactors deeply influenced electrical power engineering and power industry, entered the ice-breaker and submarine transportation systems, made their way into space industry, not mentioning the military uses. With the course of time it becomes clear that traditional nuclear power engineering has a lot of stimuli

and possibilities for future improvement. The implementation of fast neutron reactors, or simply fast reactors, is of great importance because they offer the prospect of vastly more efficient use of fuel. The hesitation to deploy these reactors is caused by the fact that the most common coolant - water - has to be replaced by liquid metal coolant (molten sodium, bismuth, or lead), which leads to price increase. On the other hand, the fast neutron reactors have a lot of advantages, including operational benefits (safety).

During last decades of reactor development, a lot of attention has been paid to reactor safety enhancements. The term ˝inherent safety˝or so-called ˝passive safety˝was invented. A reactor is called safe when under any circumstances, even uncontrolled and unpredicted, there is no radioactive pollution created outside of the reactor hall. Reactor with inherent safety is such a kind of safe reactor that prevents failure and appearance of reactivity-initiated accidents not by operator intervention, but automatically, by virtue of the physical principles that underlie its design [1]. In other words, the reactors with inherent safety are, by exact expression of famous Russian nuclear physicist L. Feoktistov, ˝The nuclear plants, which never explode˝[2, 3].

It is appropriate to mention here his book ˝A Weapon that Outlived itself ˝, where he wrote: ˝If the rods, as the result of act of terrorism or any other accident, fly out of an active zone... in this case none of currently existing protection systems can prevent a nuclear explosion. The pressure inside the reactor is 150 atmospheres. The rods fly out with the velocity of up to 200-300 meter per second. In the scale of those first microseconds and milliseconds none of the currently existing mechanisms works, if the rods are ejected with such a velocity˝[2].

Unfortunately this prediction almost came true. This hypothetical accident almost happened at Davis-Besse Nuclear Power Station located on the southwest shore of Lake Erie near Oak Harbor, Ohio, USA. In February 2002, the workers repairing a cracked control rod drive mechanism nozzle at the Davis-Besse Nuclear Power Station discovered a football-sized cavity in the reactor vessel head, the Unit 1 was immediately shutdown [4]. This cavity was 12.7 cm long, 15.2 cm deep and 10.2 cm wide. As it was discovered later, a small amount of boric acid leaking out of the emergency cooling system of the active zone onto the reactor vessel head corrodes carbon steel at a high rate.

The Nuclear Regulatory Commission noticed in the report of this event that: ˝a cavity had formed around that nozzle in the low-alloy steel portion of the reactor pressure vessel head, leaving only the stainless steel-clad (9 mm thick) material as the reactor coolant pressure boundary over an area of approximately 16.5 square-inches˝[4]. One can add that as the result of the potential failure of high pressure injection pumps the water jet could spurt

out with the pressure of 150 atmospheres. It is not out of place to mention here that so-called E scheme; the 2000-tonne top of 4-th unit of Chernobyl nuclear power plant, also known as ″cover Elena″, was torn and thrown up by the stream explosion of much lower pressure.

This real-life example illustrates the colossal importance of Feoktistov concept, which is that the main constraint and perfect protection system against the explosion in such type of nuclear constructions has to be a physical law, which means a Law of Nature, but can neither be an automatic system, even the perfect one, nor the multistage safety barrier, nor the human being, which is the weakest and the most dangerous part of the nuclear object control system.

On the other hand, it is obvious that just stating an idea is not enough. It is necessary to find the new pragmatic ways of the realization of inherent safety concept at the level of fundamental physical laws. The solutions of this problem were proposed independently by russian physicist Lev Feoktistov and american physicist Edward Teller. It's only fair that the solutions were first obtained by same scientists, who worked on the nuclear weapon development and hydrogen bomb design.

## Objectives of the research

The first objective of this research is to obtain a preliminary model of nuclear fast reactor of Feoktistov type. The model in question should satisfy the following requirements:

- Inherent safety. The model reactor should possess a property of inherent safety. In other words, model of such a safe reactor that prevents failure and appearance of reactivity-initiated accidents not by operator intervention, but automatically, by virtue of the physical principles that underlie its design should be obtained.

- Self-regulation. The model reactor should be completely automatic, with no powered mechanisms, no operator controls and no provision for human access during their operational lifetime, in order to avoid both error and misuse. This implies the soliton-like nuclear burning wave as a working principle of the reactor model.

The second objective of these work is to obtain the physical conditions of nuclear burning wave origin and propagation.

The third objective is to offer the mathematical solution for the provided physical model of the reactor. In oder to verify theoretical model the computational experiment has to be performed.

The research project consist of three parts. The first part is concerned with the concept of inherent safety deals with the soliton-like fast reactors. This includes an overview of existing reactor models, w.r.t. property of inherent safety and the analysis of Feoktistov concept of the soliton-like propagation of neutron-fission nuclear burning wave in the neutron multiplicating media. The aim of this investigation is to satisfy the first objective.

The second part deals with physical condition of nuclear burning wave origin and propagation. The aim of this part is to fulfill the second objective.

The third part of this project is related to the mathematical solution for the suggested physical model. Numerical models of neutrons and nuclei dynamics are developed. The aim of this part is to satisfy the third objective.

## Outline of this thesis

In chapter 1 the concept of the inherent safety is considered. A concise description of the related reactor types is presented along with the advantages and the drawbacks. In the same chapter the kinetics of self-stabilising fast uranium-plutonium reactor, which generates Feoktistov self-propagating nuclear burning wave and satisfies all conditions of inherent safety is considering. Furthermore, an overview of the modern models of soliton-like fast reactors available at the time of starting this PhD project is presented.

In chapter 2 some relevant for this thesis elements of fundamental analysis of self-stabilizing criticality burning waves in the neutron multiplicating medium will be considered. In this chapter the existing fundamental models and their analytical solutions are studied. Using the pattern of transition from quantum mechanics framework to the classical mechanics the necessary and sufficient conditions of nuclear burning wave origin and propagation in the neutron multiplicating medium are obtained.

In chapter 3 the simplified one-dimentional model of plutonium accumulation and uranium burnup kinetics is proposed. Taking into account delayed neutrons three-dimentional model for one-group diffusion approximation is offered. The numerical solution using the method of mesh points in the implicit form is obtained. Finally, the simulation results and its verification w.r.t. obtained in the chapter 2 necessary and suffycient conditions of nuclear burning wave origin are given in this chapter.

Chapter 4 consists of an alternative view on the hypothesis of existence of a natural nuclear reactor within the Earth's core. Assuming the existence of soliton-like reactor on the boundary of the solid and liquid phases of the Earth's core the $^3He/^4He$ distribution in the Earth's interior is calculated. An alternative description of the data produced in the KamLAND exper-

iment is proposed. Finally, a tentative estimation of the geoantineutrino intensity and spectrum on the Earths surface is given.

In chapter 5 the final conclusions are drawn.

# Chapter 1

# Feoktistov neutron-fission burning wave. Research problem statement.

In this chapter the concept of the inherently safe nuclear reactor is considered. The description of related reactor types is presented in section 1.1. In the section 1.2 the kinetics of self-stabilising fast uranium-plutonium reactor, which generates Feoktistov self-propagating nuclear burning wave and satises all conditions of inherent safety is considering. And finally, in section 1.3 the overview of the modern models of soliton-like fast reactors available at the time of starting this PhD project is presented.

## 1.1 Concept of reactor with inherent safety.

According to Feoktistov, the pragmatic development of new generation of nuclear power plants can be illustrated with table 1.1 [1] The first row of this table lists the types of nuclear fission reactors with inherent safety, the second row contains the first generation of fusion reactors, the third row shows the ultimate thermonuclear power systems. Although having the different level of technical development, all of them are inherently safe.

The reactor types shown in table 1.1 should be considered as an example of pragmatic way of thinking necessary for development of new generation reactors. In his book "From past to the future: from hopes about bomb to safe reactor"[3], Feoktistov described in detail the operating principles of these reactors. The characteristic feature of all the reactors types is that each of them uses some physical law, a constraint, which prevents an explosive development of energy release. The table 1.2 shows a corresponding law for

Table 1.1: The reactors with inherent safety. Adapted from [9]

| **"All these will never explode"L.P. Feoktistov** | | |
|---|---|---|
| Nuclear reactions | | |
| Neutron-fission wave reactor (NFWR) | Boiling water reactor (BWR) | Ideal reactor (IR)<br><br>fast neutron reactor with substitution of core and blanket |
| Thermonuclear reactions | | |
| Hybrid reactor (HR) | Laser nuclear fusion - Laser inertial devices | Thermo-nuclear space engine (TNSE) |
| Fusion detonation | | |
| DT - cord | DD - cord | Aneutronic fusion reactions |

each reactor type.

For example, the boiling water thermal neutron reactor (BWR) is shown in figure 1.1. The table 1.3 lists the bowling water type thermal neutron reactor characteristics obtained in [1].

In this reactor natural unenriched uranium is used as a fuel and heavy water as a neutron moderator. The figure 1.2 shows the dependence of neutron multiplication factor $K_\infty$ in an infinite medium on uranium dilution rate $\chi = N_{D_2O} \backslash N_U^{238}$. As follows from the figure 1.2, for such a mixture of $D_2O + U_{238}$ a multiplication factor is bigger than one $K_\infty > 1$ at the region where the stationary reactor can exist, i.e. at the region with the dilution coefficient $10 < \chi < 1000$. The dip in the curve at the right-hand side of the diagram is explained by a neutron absorption in heavy water. The dip at the left-hand side is caused by neutron spectrum changes. The neutron spectrum becomes harder and enters the resonance absorption region of $U_{238}$. It is precisely this left-hand side dip which is interesting for us because it illustrates Feoktistov idea of reactor controlled by physical law [1, 3]. This is a considerable difference of Feoktistov boiling water reactor in comparison with usual BWR, such as CANDU reactor which uses natural unenriched uranium as a fuel as well.

The physics of Feoktistov heavy water reactor is pretty simple. At the

Table 1.2: The physical law - a constraint, which prevents an explosive development of chain reaction. From [9]

| | | |
|---|---|---|
| **1.** | The double $\beta$ -decay with a longn life time $$U_{238} + n \rightarrow U_{239} \rightarrow Np_{239} \rightarrow Pu_{239}$$ | NFWR, IR |
| **2.** | The considerable change of moderator density in boiling process (going away from the supercriticality) | BWR |
| **3.** | The fissile material tends to an equilibrium isotopic composition | IR |
| **4.** | The neutrons lack in blanket without thermonuclear burst | HR TNSE |

initial stage the concentration of active atoms increases, as a result of an activity intensification and intensive water vaporization, this causes the change of neutron energy spectrum. The concentration of natural uranium increases and dilution rate $\chi = N_{D_2O} \backslash N_U^{238}$ decreases. This, and resonance inclusion (neutrons absorption region of $U_{238}$, causes the shift of plutonium equilibrium concentration to the left, see figure 1.2, and the process of plutonium accumulation continues. After a while, only plutonium burns, and, as a result, the fuel burn-up strongly increases. The velocity of heat generation reduces, as the core overheats, via reduction of moderator density. Therefore in a case of emergency temperature increase the moderator evaporates intensively and $D_2O$ steam flows from the core through the inverted valve. This auto-regulating model of core operation is a good demonstration of a concept of inherent safety based on a physical law. In other words, the emergency increase of heat generation velocity causes an additional moderator evaporation and immediate reaction shut-down, resulted from the neutron spectrum hardening and the neutron leakage.

This concerns serious accidents, such as loss-of-coolant accidents or loss-of-decay-heat-removal-function accidents, as well. To remove a generated heat from reactor and convert it into useful electrical power, a coolant system is used. If the coolant flow is reduced, or lost altogether, the heat can increase

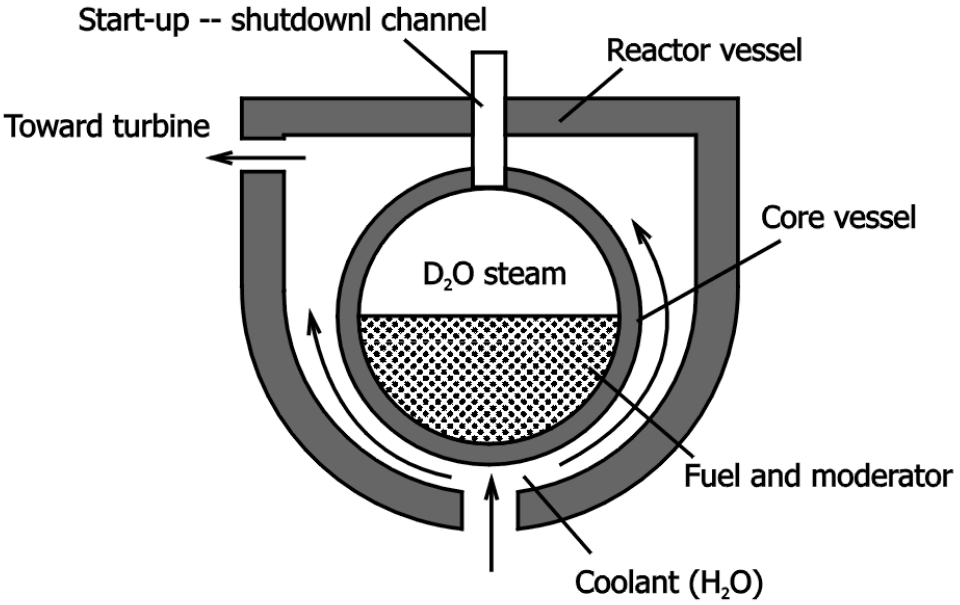


Figure 1.1: Boiling water type thermal neutron reactor. From [1].

Table 1.3: Boiling water type thermal neutron reactor. From [1].

| | |
|---|---|
| The reactor power | 30 MW |
| The core radius | 3 m |
| The reactor fueling - the initial core load | Natural Uranium 20000kg |
| | heavy water 50000 kg |
| The steam pressure in the chamber | $\backsim$100 atmosphere |
| Uranium burnup | $\approx$ 2% |

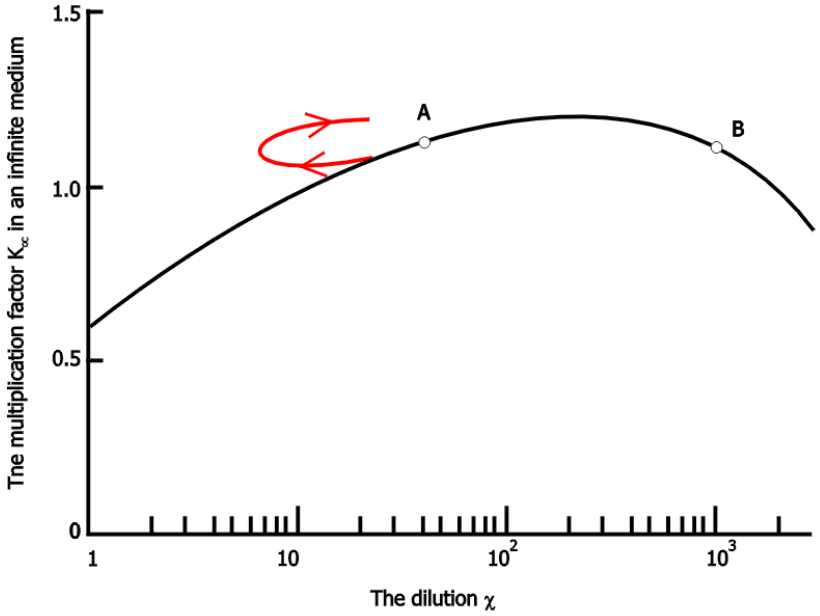


Figure 1.2: The dependence of neutron multiplication factor on uranium dilution rate.The point A is stable, in opposite to point B [1]: a small increase of power (steam) moves the operating point to the left and makes the system subcritical. The arrow shows the dilution rate variation during long burning process (years). Adopted from [1].

the fuel temperature to the point of damaging the reactor. This type of accident develops very slowly. Tens of minutes are required for the water in reactor to boil away. In fact it takes even more time. The chain reaction stops automatically because of increase of uranium concentration in heavy water, i.e. because of sharp decrease of the dilution rate $\chi < 10$ with corresponding neutron multiplication factor smaller than one $K_\infty < 1$, see figure 1.2. That means complete shutdown of neutron multiplication chain reaction. Here it's important to note, that specific afterheat, which is proportional to reactor specific power, decreases so strongly that fuel doesn't melt even without water.

As we can see, Feoktistov boiling water reactor (BWR) is designed in such a way, that the physical principle that underlies its design prevents reactor's failure. This is a significant advantage of Feoktistov BWR in comparison with usual BWR, such as CANDU reactor in which reactivity control were

designed to be achieved by control rods.

According to the information from New Scientist magazine [12], the reactor, known as the Rapid-L, was conceived of as a power source for colonies on the Moon. The new operator-free fast reactor is characterized by RAPID (Refueling by All Pins Integrated Design) refueling concept, which enable quick and simplified refueling 2 months after reactor shutdown [10, 11, 12]. The reactor called Rapid is designed for a terrestrial power system, which enables quick and simplified refueling. The Rapid-L is designed for lunar base power system. The conceptual design of RAPID consists of a $10MW$ (thermal)-$1MW$ (electric) $U - Pu - Zr$ metal fueled, sodium cooled, fast spectrum reactor with lithium ($Li$) inlet and outlet temperatures of 380℃, and 530℃, respectively. This power level is sufficient for 500 private residences. The reactor is basically a loop type configuration and a reactor vessel of $3.0m$ in diameter and $6.8m$ depth.

"Unlike traditional nuclear reactors the Rapid has no control rods to initiate the reaction. The new revolutionary technology uses reservoirs of liquid lithium-6, an isotope that is effective at absorbing neutrons $^6Li$. The $^6Li$ reservoirs are connected to a vertical tube that fits into the reactor core. During normal operation the tube contains an inert gas, see figure 1.3. But as the temperature of the reactor rises, the liquid lithium expands, compressing the inert gas and entering the core to absorb neutrons and slow down the reaction. The lithium acts as a liquid control rod. And unlike solid control rods, which have to be inserted mechanically, the liquid expands naturally when the core gets warm.The Rapid uses the same principle to start up and close down the reaction. The reactor would be cooled by molten sodium and run at about 530℃. Kambe's main concern now is to test the fail-safe system's long-term durability"[12].

A significant advantage of Rapid-L and Rapid is the introduction of the innovative reactivity control systems: Lithium Expansion Modules (LEM) for inherent reactivity feedback, Lithium Injection Modules (LIM) for inherent ultimate shutdown, and Lithium Release Modules (LRM) for automated reactor startup. All these systems adopt $^6Li$ as a liquid poison instead of conventional $B_4C$ rods or $Be$ reflectors. These systems are effective independent of the magnitude and direction of the gravity force. "This concept enables operator-free reactor and excludes human error and terrorists' intervention", says Mitsuru Kambe, head of the research team at Japan's Central Research Institute of Electrical Power Industry (CRIEPI) in his article "RAPID Operator-Free Fast Reactor Concept without Any Control Rods"[10]. Let us concider this systems in more details.

The LEM is actuated by the volume expansion of $^6Li$ itself, see figure 1.3. It is composed of an envelope of refractory metal in which liquid poison

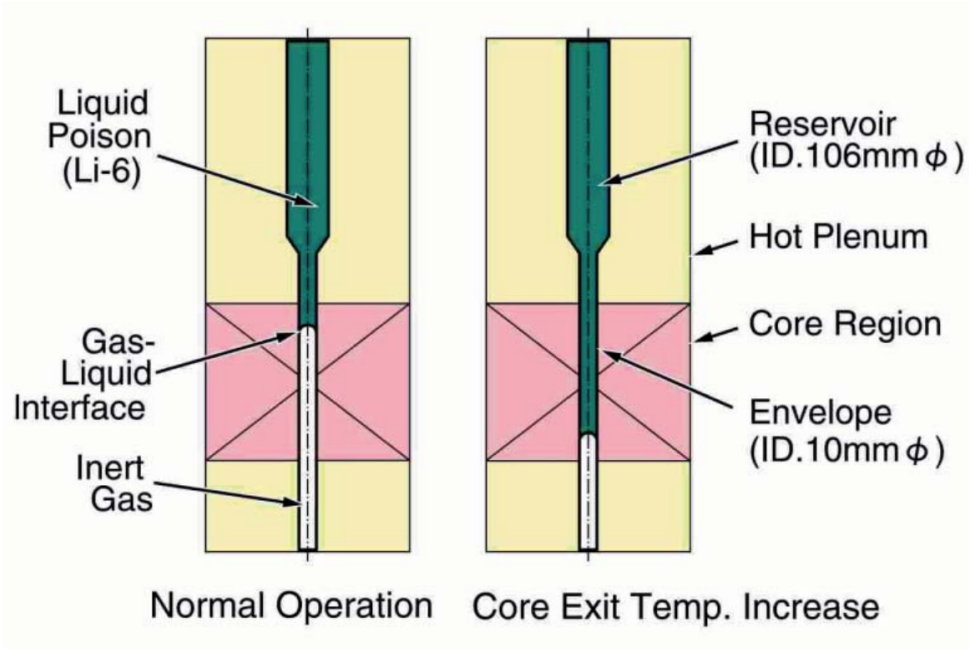


Figure 1.3: LEM concept. From [10].

of 95% enriched $^6Li$ is enclosed. $^6Li$ is suspended in the upper part of the envelope by surface tension exerted on the gas-liquid interface. The gas-liquid interface goes up and down in accordance with temperature. If the core exit temperature increases, the gas-liquid interface goes down and negative reactivity insertion can be achieved. In case the core outlet temperature decreases, the gas-liquid interface goes up and no positive reactivity insertion is expected.

LIM, figure 1.4 is also composed of an envelope in which 95% enriched $^6Li$ is enclosed. In case that the core outlet temperature exceeds the melting point of the freeze seal, $^6Li$ is injected by a pneumatic mechanism from upper to lower region to achieve negative reactivity insertion. In this way the reactor is automatically brought into a permanently subcritical state and temperatures are kept well below the boiling point of sodium (960℃).

LRM concept is shown in figure 1.5. An automated startup can be achieved by gradually increasing the primary coolant temperature by the primary pump circulation. The freeze seal of LRMs melts at the hot standby temperature (380 ℃), and $^6Li$ is released from lower level (active core level) to upper level to achieve positive reactivity addition. An almost constant reactivity insertion rate is ensured by the LRM because the liquid poison flows through a very small orifice due to the gas pressure in the bottom

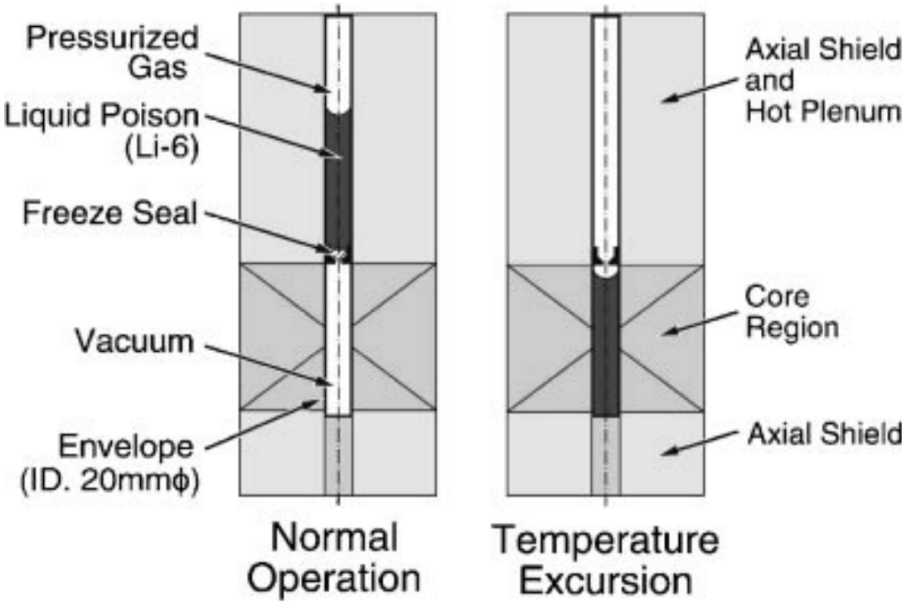


Figure 1.4: LIM concept. From [10].

chamber. It would take almost 14 hour for the liquid poison to move into the top chamber. Prior to refueling, the LRM bundle should be released in lower part of the core so that liquid poison can be located in the active core region again. In this case, the LRM bundle acts as a poison rod. Once released, it is clumped at the bottom and is impossible to pull out again.

From the reactor design description it became clear that the lithium acts as a liquid control rod. In the Rapid reactor the mechanical movement of solid control rods replaced with the liquid expansion, which occurs, when the core gets warm.

"The reactor is controlled by LEM, LIM, and LRM instead of the conventional control rods. The LEM is a thermometer-like device actuated by the volume expansion of $^6Li$ itself. This "liquid control rod"can keep the reactor power almost constant throughout the design life", is written in JAERI Annual Research Report 2002 [49].

If the Rapid reactor has just "liquid lithium control rods"instead of solid ones, that means that any mechanical damage or failure of an envelope with enriched $^6Li$ can cause an explosive development of energy release and reactivity accident. So it's early to say that Rapid reactor concept "exclude human error and terrorists' intervention"[10]. Thus we can conclude that the Rapid reactor design doesn't match the Feoktistov definition of inher-

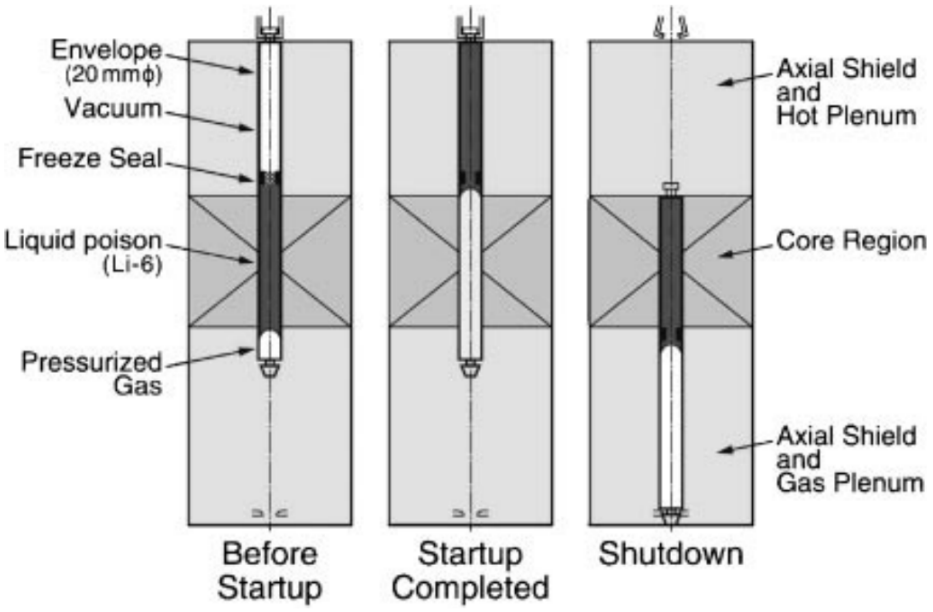


Figure 1.5: LRM concept. From [10].

ent safety, because its design is not based on any physical law, which would prevent the accident.

Therefore it's very important to consider here the concept of inherently safe reactor concerning fast reactor, to show that not only thermal reactors, but also fast neutron reactors could be safe by virtue of the physical principles that underlie their design.

The modern fast reactor (FR) consists of two regions: core and blanket. The energy releases in the core fuelled with plutonium-uranium mixture with an enrichment of plutonium $75\%U_{238} + 25\%Pu_{239}$. The core is surrounded by a zone of fertile material constituting a blanket, where plutonium is accumulated via absorption of neutrons emitted from core. This scheme is optimized for cumulative breeding ratio (BR) but presupposes the permanent removal of plutonium from blanket region, and the closed fuel cycle with reuse of self produced plutonium. Besides a lot of chemical operations necessary for this fuel cycle, it causes creation of big amount of pure plutonium, which does for not only peaceful, but also military use. This fact forms a negative opinion about fast reactors as means of nuclear weapon proliferation.

Feoktistov offers a possibility [1] to avoid the risk of nuclear weapon proliferation by substitution of two regions of usual fast reactor (core and blanket) by one region in which plutonium will both accumulate and burn. For this

purpose these regions has to be combined in such a way, that it allows both criticality and breeding.

It doesn't take a lot of effort to prove this. It's proven experimentally that fast reactor can have $BR > 1$. Let us write BR in the following form:

$$BR = \frac{\tilde{n}_{Pu}}{n_{crit}} U_8 > 1 \tag{1.1}$$

where $U_8 \approx 1 - n_{crit}$ is the concentration of $U_{238}$ in a mixture with plutonium critical concentration $n_{crit}$, $\tilde{n}_{Pu}$ is so-called plutonium equilibrium concentration, to which plutonium concentration tends during burning, regardless of its initial value. If plutonium initial concentration is bigger than equilibrium $n_0 > \tilde{n}_{Pu}$ (fast reactor core) plutonium burns (tends to $\tilde{n}_{Pu}$ from above), and if $n_0 < \tilde{n}_{Pu}$ plutonium accumulates (tends to $\tilde{n}_{Pu}$ from below, like in blanket region), see figure 1.6.

Now, what happens if we create one-region reactor with $n_{crit} < \tilde{n}_{Pu}$ ($BR > 1$)? Feoktistov asserts that such system, left to its own devices can not go supercritical (above its thermodynamic critical point), despite it tends to plutonium equilibrium concentration $\tilde{n}_{Pu} > n_{crit}$. How to explaine this seemingly paradoxical situation?

Two time parameters are used for the description of nuclear chain reaction and transmutation of chemical elements:

- The average time between the emission of neutrons and either their absorption in the system or their escape from the system $t_{neutron} \backsim 10^{-6} - 10^{-7}$ is called neutron lifetime.

- Instead of fissioned atom of plutonium the new atom of $Pu_{239}$ is created by neutron capture in $U_{238}$ through two beta-decays with a half-life time $t_{1/2} = 2,3 days$.

These two time parameters greatly differ in scale and course of further development always defines by bigger time scale. If reactor works for years, then a few days delay in plutonium production is irrelevant. That's quite another story if the system is brought to a supercriticality. Excess plutonium, which causes supercriticality, capture neutrons and fission in a time $t_{neutron}$, and system is brought back to a subcritical state. Emitted neutrons cause production of an additional plutonium in a time $t_{1/2}$, what meant in two and half days and drugged out in time.

The new time parameter, halflife $t_{1/2}$ appeared in the system. Since plutonium accumulates "from below"characteristic time necessary for power increasing has an order of days that adds an important safety feature to the system.

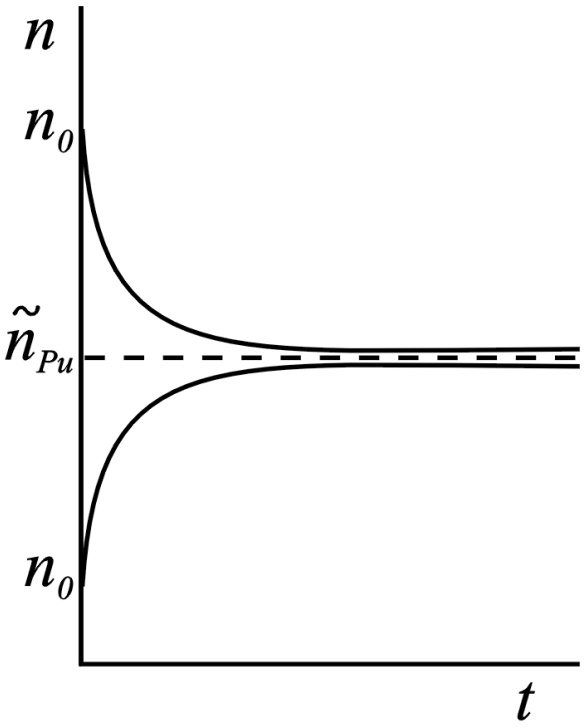


Figure 1.6: Dependence of neutron concentration on time. The upper curve shows plutonium burnup, the lower shows plutonium accumulation. Plutonium equilibrium concentration for FR and BWR equals 10 and 0.25 respectively. From [1].

The critical state of a system maintains automatically because $n \to \tilde{n}_{Pu}$ but can not become bigger than $n_{crit}$. In other words the control through control rods and operator manual intervention is not anymore necessary. If this reactor is left to its own devices, at first its power (neutron flux) will increase, and then, together with burnup of $U_{238}$ power will decrease. One can say, that in such ˝self-contained˝reactor several days duration ˝explosion˝develops (for BR 1.5 burnup time is about $10 * t_{1/2} = 1month$). The reaction stops because $\tilde{n}_{Pu}$ is proportional to $U_{238}$ concentration and sooner or later $BR$ becomes smaller than 1 $n_{crit} < \tilde{n}_{Pu}$. It happens if the fuel burnup is about 50%. High burnup is an additional advantage of this reactor [1]. Table 1.4 shows the parameters of such self-development system.

Table 1.4: The burning of reactor left to its own devices.

| Breeding ratio (BR) | Burning time (days) | $U_{238}$ burnup (%) |
|---|---|---|
| 1 | 970 | 20 |
| 1.3 | 250 | 40 |
| 1.5 | 50 | 60 |
| 1.7 | 30 | 70 |
| 1.9 | 20 | 77 |

If neutron lifetime $t_n \approx 10^{-6} sek$ and $\beta$ -decay half-life $\tilde{n}_{1/2} \approx 2.5\, days$

$$neutron + {}^{238}_{92}U(n,\gamma) \rightarrow {}^{239}_{92}U \xrightarrow{\beta^-} {}^{239}_{92}Np \xrightarrow{\beta^-} {}^{239}_{92}Pu$$

burning time defines by bigger time scale

Thus, the main concept of inherently safe reactor is that the fuel components have to be composed in such a way that characteristic time $t1/2$ is considerably greater than one minute and its functioning includes elements of self-regulation. As Feoktistov showed in [5, 6, 7, 8] this can be achieved if among other reactions in the reactor core the following chain reaction occurs

$$ {}^{238}_{92}U(n,\gamma) \rightarrow {}^{239}_{92}U \xrightarrow{\beta^-} {}^{239}_{93}Np \xrightarrow{\beta^-} {}^{239}_{94}Pu(n, fission) \tag{1.2}$$

where ${}^{238}_{92}U$, ${}^{239}_{92}U$, ${}^{239}_{93}Np$, and ${}^{239}_{94}Pu$ are isotopes of uranium, neptunium, and plutonium respectively, $n$ is a neutron, $\beta^-$ denotes $\beta$-decay. In this case appeared plutonium is used immediately like a fuel. Characteristic time of such reaction is a time of two $\beta$-decays and is approximately equal $\tau = 2.3/\ln 2 = 3.3 days$, that is nearly four order more than for delayed neutron.

The self-regulation effect is caused by the fact that the increase of neutron flux lead to faster burnup of plutonium, decrease the plutonium concentrations, and, consequently, the neutron flux (new nuclei of ${}^{239}Pu$ will be generated in about 3.3 days). If, however, the netron flux drop (due to, for example, an external intervention), then the burnup slows down, and the plutonium generation rate increases, which will then lead to the increase of neutron generation after an approximately same time (several days). The aforementioned transmutations take place also in traditional thermal reactors, for example, [13] describes one-group approximation, and another two-group approximation solution was achieved in [14], which in some cases could be interpreted as a slow nuclear burning wave. However, in traditional re-

actors they are considered secondary for an energy release, since they are mostly used for plutonium generation purposes.

$$\frac{dN_{Pu}}{dt} = \upsilon n \left[ {}^{8}\sigma_a N_8 - \left( {}^{Pu}\sigma_a + {}^{Pu}\,\sigma_f \right) N_{Pu} \right] \tag{1.3}$$

Sufficiently complete mathematical model of a reactor core should include models of non-stationary 3D processes of neutron transfer in heavily heterogeneous medium, models of fuel burn-up and reactor kinetics, and a model of heat removal.

## 1.2 Self-stabilizing criticality burning waves

It is well-known, that in order to test the physical hypothesis it is sufficient to use quite simple models. First simplification we can make is a separate analysis of neutronic-nuclear processes and heat removal process (which is justified for long regulation times). The neutronic processes themselves can be studied in single-dimension geometry, considering also the diffusinal and one-energy-group approximation. Latter means that the neutron spectral charasteristics are averaged out on fixed neutron energy interval, and the problem is solved using fixed neutron energy value.

Let us consider, according to [5], [8], kinetics of self-stabilising fast uranium-plutonium reactor, which generates self-propagating neutron-fission nuclear burning wave (Feoktistov wave), which satisfies all conditions of inherent safety.

Main transmutations chain reflects the uranium-plutonium fuel cycle (1.2). Let us consider a semi-space filled with $U^{238}$, which is bombarded with neutrons from the external surface. Let us also assume for simplicity that the neutron spectrum is the fission spectrum. The characteristic neutron energy in the medium depends mostly on the moderating properties of the medium. Following Feoktistov [8], let us consider a case with little or no moderator and the neutron spectrum being the same as the initial neutron spectrum.

The main goal of this simplified model is to obtain the auto-wave solution for the transmutation chain with necessary condition $n_{crit} < \tilde{n}_{Pu}$.

Let us write the plutonium concentration balance equation

$$\frac{dn}{dt} = n\upsilon N_8 \left[ (\nu - 1)\, {}^{Pu}\sigma_f n_{Pu} - \sum_i {}^{i}\sigma_a n_i \right] \tag{1.4}$$

where $N_{Pu}$ is the $^{239}Pu$ concentration, $N_8$ is the concentration of $^{238}U$, $n$ is the concentration of neutrons, $\upsilon$ is the neutron velocity for one-group

approximation, $\sigma_a$ and $\sigma_f$ are the absorption cross-section and fission cross-section, respectively.

For this, let us define an equilibrium plutonium concentration, where the derivative turns to zero

$$\tilde{n}_{Pu} = \frac{\tilde{N}_P u}{N_8} = \frac{{}^{8}\sigma_a}{{}^{Pu}\sigma_a + {}^{Pu}\sigma_f} \tag{1.5}$$

Here $N_{Pu}|_{t=0} = 0$ and current concentration $N_{Pu}(t)$ cannot exceed $\tilde{N}_{Pu}$ (see figure 1.6). Let us remind that the value of constant $\tilde{n}_{Pu}$ varies greatly depending on the neutron energy: for thermal reactor $\tilde{n}_{Pu} = 0.25\%$, for fast reactor $\tilde{n}_{Pu} = 10\%$.

The other property of of the uranium-plutonium medium is a critical plutonium concentration $n_{crit}$. When $n_{Pu} > n_{crit}$ the system becomes supercritical and capable of self-propagation, and, conversly, when $n_{Pu} < n_{crit}$ the system is subcritical and the neutron density decays with time.

The value $n_{crit}$ is derived from the neutron balance equation

$$\frac{dn}{dt} = n\upsilon N_8 \left[ (\nu - 1)^{Pu}\sigma_f n_{Pu} - \sum_i {}^{i}\sigma_a N_i \right], \tag{1.6}$$

where $n_i$ are the concentrations of the elements taking part in reaction, $\nu$ is an average number of prompt neutrons per ssion for $^{239}Pu$, ${}^{i}\sigma_a$ is the absorption micro cross-section of $i$-th element including $u$ and $Pu$ (neutron leakage can be also included).

The value

$$n_{Pu} = n_{crit}^{Pu} = \frac{\sum_i {}^{i}\sigma_a n_i}{(\nu - 1)^{Pu}\sigma_f} \tag{1.7}$$

defines the plutonium concentration when the medium is critical (stationary). Value $n_{crit}$ is also a function of neutron energy. Since two dimensionless numbers $\tilde{n}_P u$ and $n_{crit}$ are derived from two different combination of constants, all variants are posible: $\tilde{n}_{Pu} > n_{crit}$, $\tilde{n}_{Pu} < n_{crit}$ $\tilde{n}_{Pu} = n_{crit}$.

As it gets, for thermal neutrons $n_{Pu} < n_{crit}$ for fast neutrons $\tilde{n}_{Pu} > n_{crit}$ . In the first case the system is only viable if the neutron source is present. If there is no external source, or if it is turned off, the reaction immediately stops. In the other case, which is the one we will be considering from now on, there exists one solution in the form of stationary running wave, and this solution is asymptotical and does not depend on initial conditions. There is nothing paradoxical about it if the aforementioned explanations of physical meaning of expression (1.1) are considered.

Thus, it is getting clear that it is impossible to cross the criticality threshold in the case of slow burning of $^{238}U$ caused by fast neutrons. This leads

to the possibility of neglecting the partial derivative in time in the neutron transmission equation. This can be imagined as follows: neutrons emitted from the neutron source are absorbed at the depth equal to the neutron free path, and they turn uranium into plutonium. As the plutonium accumulates, the fission process intensifies, and there are enough neutrons released in order to "process"the next, more distant, area of the core. At last, the energy release area shifts along the core axis away from the neutron sourse, whose influence decreases, and the system enters the stationary running state. In other words, all functions now depend on the argument $z = x+ut$, which is a wave going from left to right with the velocity $u$, and its order is proportional to $u \sim L/\tau$, where $L = 5cm$ is a diffusional absorption length of a neutron, and $\tau = 3.3\ days$ is a time needed for transmutation of $^{238}U$ into $^{239}Pu$.

Now, in order to obtain a system of kinetic equations for neutrons and nuclei which take part in the transmutation chain (1.2) , let us rewrite this systems using "traditional"Cartesian coordinates $\{x, t\}$ as follows

$$\frac{d\tilde{n}\,(x,t)}{dt} = D\Delta\tilde{n}\,(x.t) + q\,(x,t) \tag{1.8}$$

where $\tilde{n}\,(x,t)$ is a neutron density, $D = \upsilon/3\Sigma_s$ is a neutron diffusion coefficient, $\upsilon$ is a neutron velocity in one-group approximation, $\Sigma_s$ denotes a macroscopic scattering cross-section, $q$ is an intensity of a neutron flux coming from external neutron source.

Obviously, the expression for density of neutron source can be written is as follows

$$q\,(x,t) = \tilde{n}\,(x,t)\,\upsilon\left[(\nu-1)\,{}^{Pu}\sigma_f N_{Pu} + \sum_i {}^{i}\sigma_a N_i\right] \tag{1.9}$$

where $N_i$ is the concentration of $i$-th isotope in the chain (1.2), ${}^{Pu}\sigma_f$ is the $^{239}_{94}Pu$ microscopic fission cross-section, ${}^{i}\sigma_a$ is the microscopic absorption cross-section of $i$-th isotope, and $\nu$ is an average number of prompt neutrons per ssion for $^{239}_{94}Pu$.

Further, using the expression (1.7) for relative critical concentration of plutonium, and simultaneously introducing the normalization of neutrons concentration and isotopes w.r.t. to $^{238}U$ concentration, we obtain diffusion equation (1.8) as follows

$$\frac{1}{D}\frac{dn(x,t)}{dt} = \Delta n(x,t) - \frac{N_8}{D}\upsilon\sum_i {}^{i}\sigma_a n_i(x,t)\left[1 - \frac{n_{Pu}(x,t)}{n_k^{Pu}(x,t)}\right]n(x,t) \tag{1.10}$$

where

$$n(x,t) = \frac{\tilde{n}(x,t)}{N_8(x,t)},\ n_i(x,t) = \frac{N_i(x,t)}{N_8(x,t)},$$
$$n_{Pu}(x,t) = \frac{N_{Pu}(x,t)}{N_8(x,t)},\ n_{crit}^{Pu}(x,t) = \frac{N_{crit}^{Pu}}{N_8(x,t)} \tag{1.11}$$

or, in other words, $n(x,t)$ and $n_i(x,t)$ are the relative concentration of neutrons and isotopes, respectively, $n_{Pu}$ and $n_{crit}^{Pu}$ are the relative equilibrium concentration and relative critical concentration of plutonium, respectively.

As it was noted earlier, the inequation $\tilde{n}_{Pu} > n_{crit}$ predetermines the stationary form of the kinetic equation. Since it turns out in [7] that for qualitative analysis of (1.8) it is sufficient to find an approximate solution for the stationary equation for the region ahead of the wave front, i.e. in the asymptotycal region $x \to -\infty$, then we can neglect the summands $n_9$ and $n_{Pu}$, which can be found together with $n_8 \cong 1$. The latter means that the stationary form of the kinetic equation (1.10) will have simplified form as follows

$$\frac{d^2 n(x,t)}{dx^2} = C_\infty \left[1 - \frac{n_{Pu}(x,t)}{n_{crit}^{Pu}(x,t)}\right] n(x,t), \tag{1.12}$$

where $C_\infty$ is equal

$$C_\infty = \frac{\upsilon}{D}\left({}^8\sigma_a\right) N_8(x,0) = \frac{1}{D\tau} = \frac{1}{L^2}, \tag{1.13}$$

and concentration $N_8(x,t)$ is equal to the initial concentration $N_8(x,0)$, since, following [7], we shall from now on look for an approximate solution of the stationary equation (1.12) in the region ahead of the wave front $x \to -\infty$.

Now let us express the kinetic equations for each of the isotopes taking part in chain reaction (1.2). First we write the equation for isotope $^{238}_{92}U$ as follows

$$\begin{aligned}\frac{dn_8(x,t)}{dt} = \ & -\upsilon n(x,t) N_8(x,0)\left({}^8\sigma_a + {}^8\sigma_f\right) N_8(x,t) \\ & + \upsilon n(x,t) N_8(x,0) \textstyle\sum_{9,Pu} {}^i\sigma_a n_i(x,t)\end{aligned} \tag{1.14}$$

The second summand in the right part of (1.14) is introduced in [7] according to the assumptions that the absorption of neutron for nuclei $^{239}_{92}U$ and $^{239}_{94}Pu$ leads to formation of $^{240}_{94}Pu$, whose properties are assumed to be

equivalent to those of the $^{239}_{92}U$. Obviously, this is done in order to simplify the problem or, in other words, for the satisfactory closure, without loss of generality, of the kinetic equation system for neutrons and nuclei taking part in the transmutation chain (1.2).

Assuming that $^{8}\sigma_f \ll^{8} \sigma_a$ [7] the kinetic equations for $^{238}_{92}U$ takes the following form

$$\frac{dn_8(x,t)}{dt} = -\left[c_8 n_8(x,t) - c_9 n_9(x,t) - c_{Pu} n_{Pu}(x,t)\right] n(x,t) \tag{1.15}$$

where

$$C_i = \upsilon N_8(x,0)^i \sigma_a, i = 8, 9, Pu \tag{1.16}$$

The kinetic equations for isotope $^{239}_{92}U$ takes the following form

$$\begin{aligned} \frac{dN_9(x,t)}{dt} &= \upsilon n(x,t) N_8(x,t) \\ &- \upsilon n(x,t) N_8(x,0) \left(^{9}\sigma_a +^{9} \sigma_f\right) N_9(x,t) - \frac{N_9(x,t)}{\tau_\beta} \end{aligned} \tag{1.17}$$

where $\tau_\beta = \tau_\beta^9 + \tau_\beta^{Np}$ is effective nucleus life-time for $^{239}_{92}U$ w.r.t. two $\beta$-decay of $^{239}_{92}$ and $^{239}_{93}Np$.

Taking into account that $^{9}\sigma_f \ll^{9} \sigma_a$ and normalizing w.r.t. $N_8(x,0)$ will get (1.17) in the following form

$$\frac{dn_9(x,t)}{dt} = c_9 n(x,t) n_8(x,t) - c_9 n(x,t) n_9(x,t) - \frac{n_9(x,t)}{\tau_\beta} \tag{1.18}$$

And finally we will write the kinetic equation for $^{239}_{94}Pu$ as

$$\frac{dN_{Pu}(x,t)}{dt} = \frac{N_9(x,t)}{\tau_\beta} - \upsilon n(x,t) N_8(x,0) \left(^{Pu}\sigma_a +^{Pu} \sigma_f\right) N_{Pu}(x,t). \tag{1.19}$$

Taking into account the expression for the equilibrium plutonium concentration (1.5) and normalizing w.r.t. initial $^{238}U$ concentration $N_8(x,0)$ will get the expression (1.19) in the following form

$$\frac{dn_{Pu}(x,t)}{dt} = \frac{n_9(x,t)}{\tau_\beta} - c_8 n(x,t) \frac{n_{Pu}(x,t)}{\tilde{n}_{Pu}} \tag{1.20}$$

Now we can rewrite the system of kinetic equations for the neutrons and nuclei that take part in the transmutations chain (1.2) w.r.t. to the dimensionless autowave variable $z = \xi/L = (x + ut)/L$, where $u$ is a velocity of stationary wave going from left to right [7], and $L$ is an average diffusional neutron free path.

For this purpose from now on we shell use the following operators

$$\frac{\partial}{\partial x} = \frac{d}{d\xi}, \ \frac{\partial}{\partial t} = \upsilon \frac{d}{d\xi}. \tag{1.21}$$

Following [7], let us assume, without loss of generality, that ${}^8\sigma_a \cong^9 \sigma_a \cong^{Pu} \sigma_a$. From this it follows that $c_8 = c_9 = c_{Pu}$. Then, introducing the dimensionless constant $\Lambda = u\tau_\beta/L$ and a variable $n_*(z) = c_1\tau_\beta n(z)$, and simultaneously performing in equations (1.12), (1.15), (1.18) and (1.20) the following coordinate transform

$$z = \frac{\xi}{L} = \frac{x + ut}{L} \tag{1.22}$$

we obtain the kinetic equations system relative to the dimensionless autowave variable $z$ in the following form

$$\frac{d^2 n_*}{dz^2} = \left[1 - \frac{n_{Pu}}{n_{crit}^{Pu}}\right] n_*, \tag{1.23}$$

$$\Lambda \frac{dn_8}{dt} = -\left[n_8 - n_9 - n_{Pu}\right] n_*, \tag{1.24}$$

$$\Lambda \frac{dn_9}{dz} = \left(n_8 - n_9\right) n_* - n_9, \tag{1.25}$$

$$\Lambda \frac{dn_{Pu}}{dz} = n_9 - \frac{n_{Pu}}{\tilde{n}_{Pu}} n_*. \tag{1.26}$$

The solution of the equations is based on the analogy[1] of the diffusion equation to the stationary Schrödinger equation in its quasiclassical approximation. Naturally, in this case the stationarity condition is satifsied integrally, because there are points where $n_{Pu} > n_{crit}$, and there are points where $n_{Pu} < n_{crit}$ . In this sense, the region with $n_{Pu} > n_{crit}$ corresponds to the

[1]It is necessary to note that nowadays we may speak not about the analogy, but about the direct link between some equation of Lagrange type (such as the diffusion equation), and the Schrödinger equation. This conclusion lies in the base of Bohm quantum mechanics [15], [16], augmented by Chetaev theorem [17], [18]. Moreover, this theorem was used in order to prove that Bohm mechanics in essense does not have any hidden parameters [18].

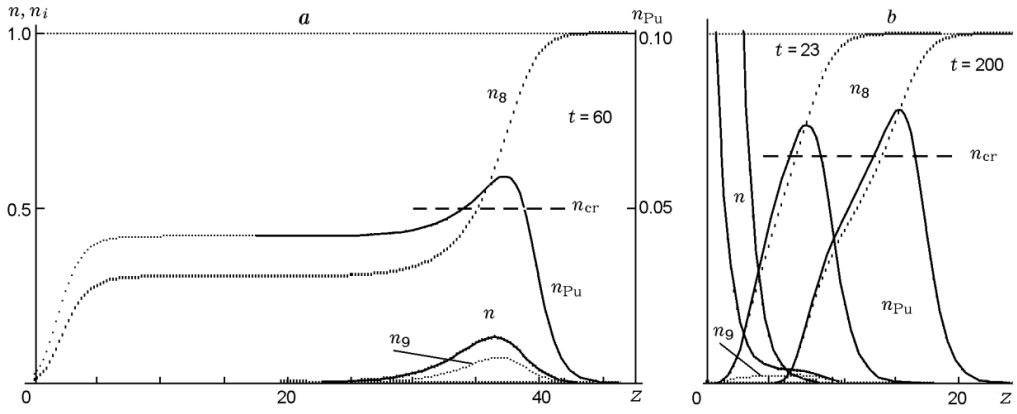


Figure 1.7: Dependence of neutron concentration on time. Propagating wave (a) and "locked"wave (b): a segment of the curve of $n_{Pu(z)}$ above the $n_{cr}$ line is the reactor core active zone; the scales of $n_{cr}$ and $n_{Pu}$ are given with $a \times 10$ magnification. From [19]

allowed region, while the regions with $n_{Pu} < n_{crit}$ corresponds to the subbarrier region. In other words, the role of potential well is played by (inverted) profile of the plutonium concentration in the $^{238}U$ medium (see figure 1.7).

In the region ahead of the wave front $z = -\infty$ the solution looks like follows

$$n = C \exp z, \tag{1.27}$$

$$n_8 = \exp\left(-\frac{C}{\Lambda} \exp z\right), \tag{1.28}$$

$$n_9 = \frac{C}{1+\Lambda} \exp z, \tag{1.29}$$

$$n_{Pu} = \frac{\tilde{n}_{Pu}}{1+\Lambda}\left[1 - \exp\left(-\frac{C}{\Lambda \tilde{n}_{Pu}} \exp z\right)\right]. \tag{1.30}$$

Let us remind that obtaining this solution we have neglected the summands $n_9$ and $n_{Pu}$ which can be obtained w.r.t. boundary condition $n_8 \cong 1$. Now let us assume that subbarrier region ends at $z = 0$, which automatically means $n_{Pu} = n_{crit}$ at this point, which allows us to find the value of constant C.

At the point $z = a$ according to Bohr-Sommerfeld quantization condition we obtain the following equation

$$\int_0^a \sqrt{\frac{n_{Pu}}{n_{crit}} - 1} dz = \frac{\pi}{2} \tag{1.31}$$

where the integral is taken over the supercritical region $n_{Pu} > n_{crit}$. While condition (1.31) simultaneously plays the role of the condition for finding of point $a$ with $n_{Pu} = n_{crit}$, i.e. when the transition into subbarrier region happens (see figure 1.7(a) and 1.8) due to burn-up.

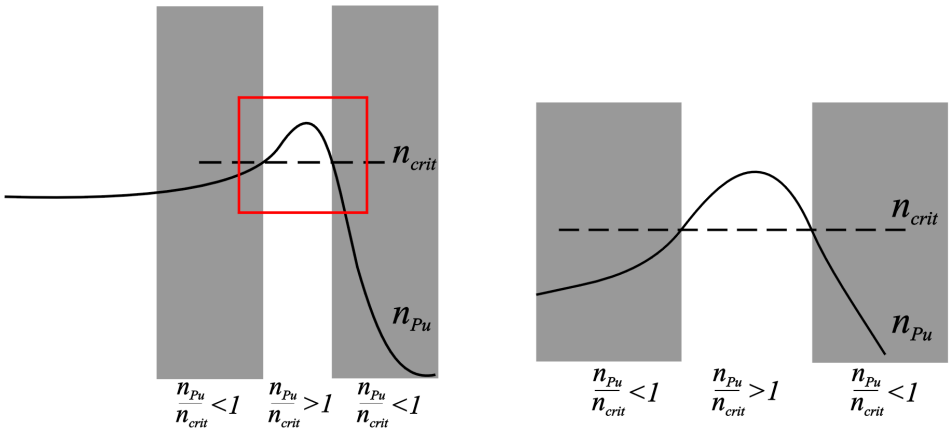


Figure 1.8: The schematic view of allowed and subbarier (gray colored) regions, corresponds the conditions $n_{Pu} > n_{crit}$ and $n_{Pu} < n_{crit}$ respectively.

Table 1.5: Feoktisov analytical estimations of parameter $\Lambda(a)$.

| $\eta = \frac{\tilde{n}_{Pu}=0.1}{ncrit}$ | 1.55 | 1.67 | 1.75 | 2.0 | 2.38 | 2.50 |
|---|---|---|---|---|---|---|
| $\Lambda(a)$ | 0 | 0.16 | 0.28 | 0.63 | 1.08 | 1.53 |

Here Feoktistov makes an important observation that the solution exists not for all possible values of $\eta$ (not for all possible values of $n_{crit}$). For example, for $n_{Pu} = 0.1$ the propagation of the nuclear burning wave in the neutron-multiplicating medium, such as $^{238}U$, takes place only when $n_{crit} < 0.0064$.

It is quite interesting in this regard to examine the physical processes in situation where $n_{Pu} > n_{crit}$, but the nuclear burning wave, contrary to our expectations, does not propagates. Following the numerical solutions of Feoktistov problem (1.24)-(1.26) done in [19], let us consider this process in

detail. Figure 1.7(a) shows the distribution of the main nuclei concentrations, which are determined in (1.24)-(1.26) with $n_{crit} = 0.05$ at the moment $t = 60$ (dimension of $\tau_\beta$). Autowave coordinate is in dimension of $L$. Normalized wave velocity $u = 0.625$. It is noted in [19] that in this mode about 70% of $^{238}U$ is burned up.

Now let us consider a case when, for $n_{crit} > 0.064$ ($\tilde{n}_{Pu} = 0.1$), the plutonium concentration can exceed the critical one, but the stationary wave does not develop. Figure 1.7(b) shows the calculation results for $n_{crit} > 0.065$ at the moments of time $t = 23$ and $t = 200$. Moreover, at $t = 200$ plutonium concentration $n_{Pu}$ is even bigger than in the previous case, but the diameter of possible burning zone is small, since the front of the wave moved very slowly. With time, the concentration of $^{239}U$ $n_9$ drops to levels unnoticeable at this scale.

Qualitatively, stopping or lock-out of the wave could be explained as follows. The plutonium accumulation speed drops approaching the limit, which is plutonium equilibrium concentration $\tilde{n}_{Pu}$, therefore the concentration itselfs grows slowly. The Bohr-Sommerfeld quantization condition (1.31) at small values of difference $n_{Pu} - n_{crit}$ requires the expansion of supercritical region (see (1.31)).

$$a \backsim \sqrt{\frac{n_{crit}}{n_{Pu} - n_{crit}}} \tag{1.32}$$

In fact, however, the characteristical wave width, defined by diffusion length $L$, does not increase with the increase of $n_{crit}$, but decreases instead. The situation is aggravated by the fact that the plutonium equilibtium concentration drops as the $^{238}U$ burns up, since $\tilde{N}_{Pu} = \tilde{n}_{Pu} N_8$ (see (1.5)).

The scales of figure 1.7 is such that for $\tilde{n}_{Pu} = 0.1$ the equality $\tilde{N}_{Pu} = n_{Pu}$ can only be satisfied at the point where the curves $n_8$ and $n_{Pu}$ intersect. As it's seen from the figure 1.7(b), from this moment on the concentration $n_{Pu}$ starts to decrease (on the figure it does indeed drop even earlier due to noticable concentration of intermediate product $n_9$), As a result, the criticality conditions are not satisfied in this barely moving reactor, and the neutron wave moves only because of the neutron flux from the external source on the boundary. As the wave moves away from the external neutron source, it is more and more difficult to propagate the wave, and distributions ˝freezes˝. Thus, when $n_{crit} > 0.064$ ($\tilde{n}_{Pu} = 0.1$), it is impossible to form self-sustaining critical region.

The described course of events can be compared with ˝immovable˝traditional reactor in working mode, when at the peripherial zone one control rod is in-

serted while the other (burned up) rod is being removed from the central region. The more rods one has, and the more movements they do while approaching the center, the more realistic this picture becomes. Ideally, each rod should have the same "lifetime". But since this is impossible to achieve in reality, and because the replacement of rods is accompanied by disturbance of the neutron field, the complex system of control rods have to be employed. In the autowave mode this happens automatically.

The fact that the critical state is maintained automatically when $\tilde{n}_{Pu} > n_{crit}$, as follows from [7], can be used not only for the propagating wave mode, but also in the stationary geometry of tradiotional reactor. In this reactor, once brought to the critical state and being left to its own devices, the reaction will develop automatically.

Thus Feoktistov **was first to show** [7] that the **soliton-like propagation of neutron-fission nuclear burning wave** is possible in $U_{238}$ *medium, but only under the condition of a certain ratio between equilibrium and critical plutonium concentration* ($\tilde{n}_{Pu} > n_{crit}$), which is characterized by **Bohr-Sommerfeld quantization condition**. In other words, only in this case the critical system state is maintained automaticaly without any external intervention. Consequently, only in this case the critical state of the system is fully characterized by inherent safety properties.

## 1.3 Modern innovation projects of soliton-like fast reactors

In 1996 Edward Teller et al [21] offered a concept of slow nuclear burning independently of Feoktistov. The burning wave propagates in thorium(Th)-uranium(U) neutron multiplication medium, but not uranium-plutonium as in Feoktistov model

$$^{232}_{x}Th(n,\gamma) \rightarrow ^{233}_{x}Pa \xrightarrow{\beta^-} ^{233}_{92}U(n, fission) \tag{1.33}$$

Based on this Th-U cycle they developed an inherently safe automatic reactor for long-term energy production (30 years) [21]. Bypassing the details of description of slow burning propagation in thorium-uranium core of this reactor (we shall discuss them later in 2), let us consider here some points of fundamental analysis of self-stabilizing properties of nuclear burning waves in neutron-multiplicating medium. Let us do it based on analysis of known base models and their possible theoretical solutions, which in their turn can be considered a test for corresponding computational experiments.

First, let us consider mentioned above Teller model of completely automated nuclear reactor for long-term operation.

In 1995Teller at all. develop their first model of completely automated nuclear reactor for long-term operation.

In this model a low-average-enrichment initial fuel loading which lasts the entire 30-year, full-power design life of the power-plant, and which is intended never to be removed from the reactor is featured [21].

The reactor core, comprised of a thorium cylindrical fuel stick with an enriched ignitor section on its left end, surrounded by a graphite reflector. The cylindrical core of the stick is hollowed out, with the radius of 10 cm, and filled with low-density material, in order to enhance to an optimal extent the near-axial transport of excess neutrons from the region of maximum neutron production. The outer radius of the stick is 25 cm, and the outer radius of the reflector is 40 cm, The axial length of the ignitor section is 0 cm, or one fuel stick diameter. The compositions and densities of the reactor core components are indicated in figure 1.9. A wave of nuclear breeding+deflagration is launched by the ignitors toward the right of the stick. This wave then propagates at a mean speed of $\sim 0.5\ meter/year$, releasing $\sim 1.5\ GW$ of steady-state thermal power as it advances.

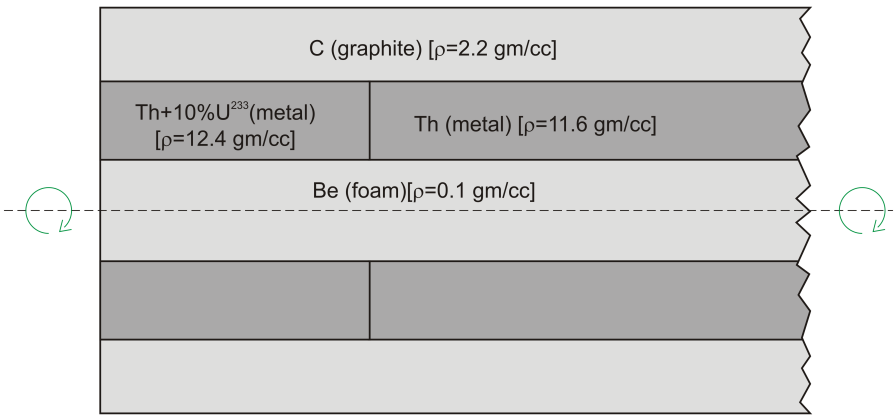


Figure 1.9: A diametral plane section of the reactor core. Adopted from [21]

The modeling results indicate that it is feasible to propagate in steady-state a nuclear burning wave down length of a stick of pure $^{232}Th$. apparently for an essentially arbitrary distance, from a small ignitor region at the stick's end. The figure 1.10 shows the masses of each of the 20 zones (each 10 cm

axial thickness) of the thorium-uranium section of the simulated reactor configuration of figure 1.9, at 2.0 years of simulation time, plotted as function of axial distance from the left side of the ignitor section. The ignitor section, initially enriched to 10% $^{233}U$ (i.e. zonal mass of 21.9 kg of $^{233}U$), extends from 0 to 50 cm, as is indicated by the persistent discontinuity in the slope of fission products vs. axial coordinate. The high burn-up of the thorium fuel is particularly notable $\sim$ 60% in the ignitor section, but is also quite high $\geq$ 50% in initially pure thorium which has passed through its epoch of peak burning, e.g. between 50 and 90 cm. The leading-edge of the nuclear [breeding+deflagration] front, defined as the location where the $^{233}U$ concentration has risen to the initial $^{233}U$ concentration in the ignitor section, has advanced to $\sim$ 155 $cm$, and the coordinate of the peak specific nuclear fission point has advanced from 0 $cm$ at $time = 0$ to $\sim$ 120 $cm$. The more than three-fold variation in specific nuclear fission rate from $z = 0$ to $z = 120$ $cm$ (specific nuclear power is given in relative units) is in marked contrast to the less that two difference in $^{233}U$ concentration between these two points. This is explained by the $\sim$ 5 times higher fission product concentration in the ignitor section, which competes effectively with the $^{233}U$ for neutrons at the smaller $z$ coordinates [21].

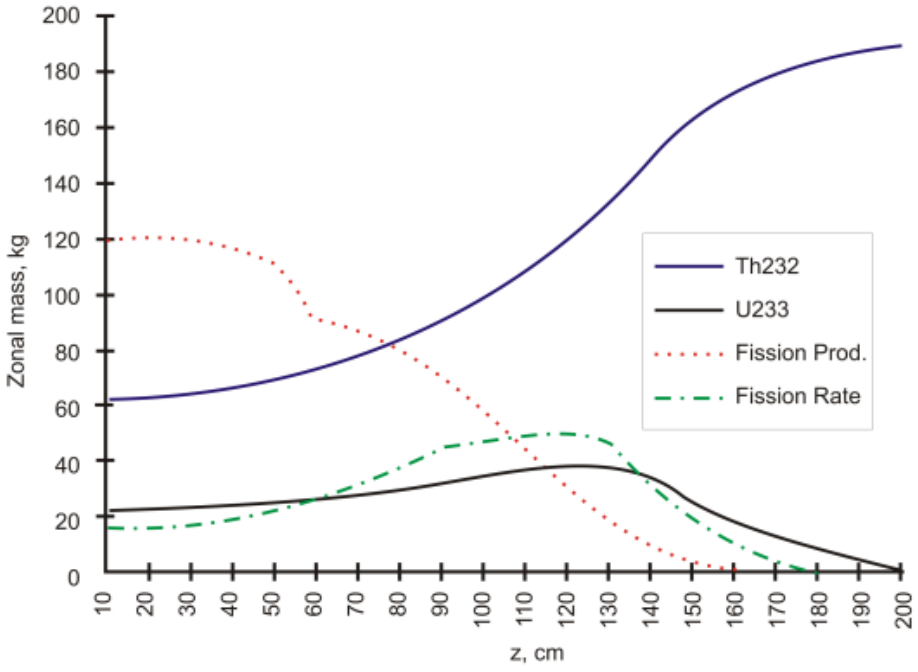


Figure 1.10: The modeling results. From [21]

Thus, this models demonstrates that a graphite reflector-clad thorium-cylinder of $< 1$ meter total diameter is seen to generate $> 1\,GW$ continuous power levels, at nuclear breeding/burn-front propagation speeds of $< 1\,meter\,year^{-1}$.

In 1996, the second model of reactor, the completely automated nuclear reactor for long-term operation II were presented by Teller group [22].

In this model, a neutron source – only necessary at the start of the operation – is located at the center of the core, surrounded by thorium on both sides. The thorium is thus converted into the fissile material $^{233}U$ and the burning region spontaneously moves from the center to both sides.

The reactor core is a right circular cylinder of approximately 3 meters diameter and 10 meters length. This core basically consists of a small nuclear ignition region containing fuel enriched in $^{235}U$ (albeit not to an extent supportive of diversion to assembly of a nuclear weapon), embedded in a much larger breeding+burning section containing $^{232}Th$. Core-averaged fissile isotopic content is $\sim 1\%$ by mass). This, together with the feasibility of very high average fuel burn-up in the considered design (e.g., 50%), indicates a total requirement for perhaps 100 tonnes (rather than 3000-4500 tonnes) of as-mined fuel for a 1 $GWe$ reactor's entire three-decade full-power operational life.

Management of nuclear power production in the reactor's core is fully automatic in all respects, over the entire three-decade interval between nuclear ignition and final core shutdown at the power plant's end-of-operational-life. Participation of human operators is needed only at the commencement of the core's ignition and at the final, irreversible negation of its reactivity.

Fully automatic regulation of nuclear power production is performed by uniformly distributed, functionally redundant thermostating modules. Each of these acts to absorb strongly the local neutron flux when the local material temperature exceeds the design-value, thereby quenching local nuclear power production and assuring thermal homeostasis of every portion of the core, over wide ranges of coolant flow and temperature, fuel composition, neutron spectrum and neutron flux. Each thermostating module acts by reversibly inserting neutron-avid liquid $^{6}Li$ into a small ($< 100\ cm^3$) compartment located in the coolant-flow from a source outside the neutron reflector, under the drive action of a thermostating bulb filled with neutron-indifferent liquid $^{7}Li$ which is emplaced in adjacent, substantially hotter nuclear fuel. A 3-D lattice of such thermostating modules, each functionally-independent from all of its fellows and emplaced during manufacture throughout the core, serves to regulate the matter temperatures everywhere, at all times.

A surrounding neutron reflector and radiation shield, distributed means for implementing a thermostating function on the reactivity and local power

density.

A redundant pressurized-gas coolant transport system, and automatic-and-redundant heat-dumping means to obviate concerns regarding all classes of loss-of-coolant accidents during the plant's operational and post-operational life. As core coolant, is planed to employ pressurized helium, rather than water. This permits the utilization of thermal energy at substantially higher temperature, avoids all hazards arising from water reactions with high temperature materials, and provides favorable independence of the core's neutronic reactivity on coolant-voiding. This reactor is proposed to be situated in suitable environments at $\sim 100\ meter$ depths underground.

At the commencement of the reactor's operational life, the centrally-positioned nuclear ignitor module is driven critical by one-time removal of neutronic poison and, through concurrent nuclear fission and high-gain breeding actions, commences to launch a nuclear deflagration wave into the adjacent unenriched fuel. This wave first diverges radially from the centrally positioned, on-axis nuclear ignitor until portions of it reach the outer edge of the cylindrical fuel mass, where it is resolved into two oppositely-directed, axially-propagating waves. One such wave moves toward each of the two ends of the cylindrical core at a (exceedingly low peak) speed determined at all times by the instantaneous thermal power demand on the reactor (and upper-bounded by the leisurely $\beta$-decay of $^{233}Pa$, the rate-limiting step in $^{232}Th$-$^{233}U$ breeding). When only very low power is demanded, the neutronic reactivity is driven to zero by action of the thermostatic controls, and the deflagration-wave stalls; when heat is removed from the core at a greater rate, the thermostating controls cool and thus raise the neutronic reactivity to slightly positive levels, and the [burning+breeding] wave re-commences its advance.

Fuel moderately enriched in fissile material is generated behind each of the two wave-fronts. These two increasing masses of enriched fuel then continue to burn, until fission product accumulation and fertile isotopic depletion (at a 50% core-averaged fuel burn-up) finally drives the core's neutronic reactivity negative. Figure 1.11 llustrates typical conditions ahead of, within, and behind this pair of nuclear deflagration waves.

As we can see, in this case the two burn-fronts propagate toward the two ends of the fuel-charge from a centrally-positioned nuclear ignitor.

Some of the salient features of the fuel-charge of the core of the reference reactor are depicted in figure 1.11, at four equi-spaced times during the operational life of the reactor after nuclear ignition is commanded and in a scenario in which the full $\sim 2\,GW$ of rated power is continuously demanded. The corresponding positions of the leading edge of the nuclear deflagration wave are indicated in the insert. Masses (in $gm$) of various isotopic compo-

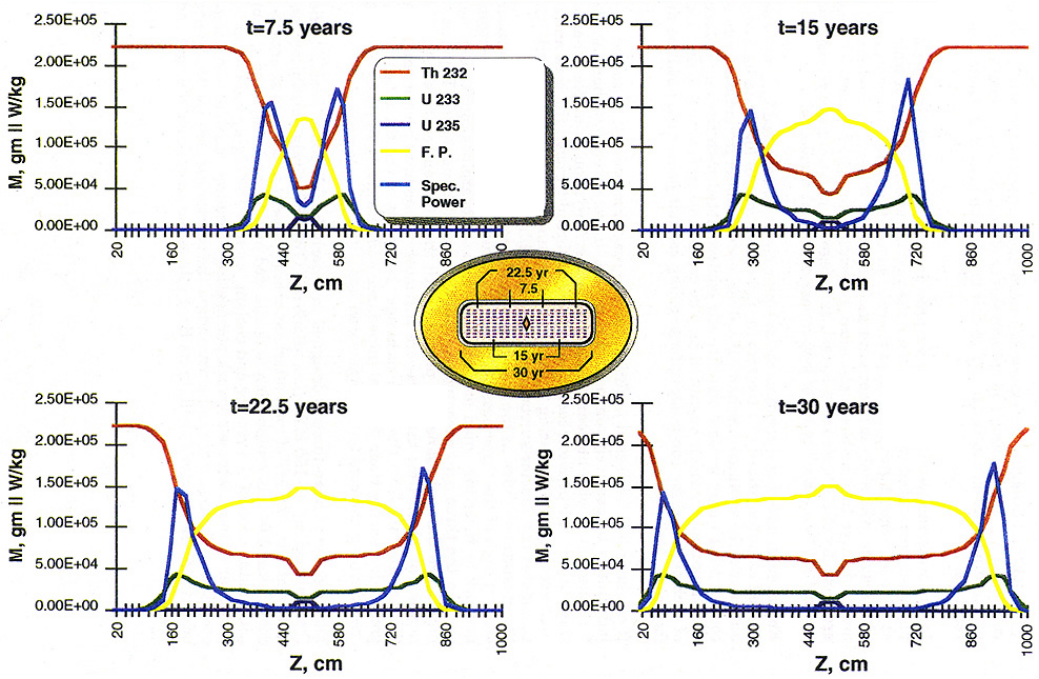


Figure 1.11: Salient features of nuclear deflagration wave propagation. From [22]

nents in a set of representative near-axial zones and fuel specific power (in $W/kg$) are the ordinate-values, while the axial position along the 10-meter-length of the fuel-charge is the abscissal value.

Note that the neutron flux from the most intensely burning region behind the wave-front necessarily breeds a fissile-rich region at the front's leading-edge, thereby serving to advance the wave. After the wave's front has swept over a given mass of fuel, the fissile atom concentration continues to rise for as long as radiative capture of neutrons on available fertile nuclei is considerably more likely than on fission product nuclei, while ongoing fission generates an ever-greater mass of fission products. Nuclear power-production density necessarily peaks in this region of the fuel-charge, at any given moment.

Finally, well behind the wave's advancing front, the concentration ratio of fission product nuclei (whose mass averages half that of a fissile nucleus) to fissile ones climbs to a value comparable to the ratio of the fissile fission to the fission product radiative capture cross-sections, the "local neutronic reactivity" goes negative, and both burning and breeding effectively cease - as is clear from comparing the various snapshots with each other, far behind the wave-front.

Thus, Teller group presented two models of soliton-like fast reactor. In

the first model, one nuclear burning wave moves from the ignitor section on the left end of the reactor core, to the right along the cylinder axis. In the second model, two nuclear burning waves move towards the tho ends of the cylinder from the centrally-positioned ignitor region.

The simulation results shows, that in both cases the nuclear burning wave (or two waves in opposite directions) appears and propagates along the reactor core.

In 2005 Hiroshi Sekimoto and Yutaka Udagava suggested a model of a fast reactor with natural uranium as a fresh fuel, i.e. $U - Pu$ fuel cycle (1.2) [23].

CANDLE is a new burnup strategy for nuclear reactors. The acronym stands for Constant Axial Shape of Neutron Flux, Nuclide Densities and Power Shape During Life of Energy Production, but also represents the candle-like burnup. As it shown in figure 1.12 this burn up strategy is adopted, although the fuel is fixed in a reactor core, the burning region moves, at a speed proportionate to the power output, along the direction of the core axis without changing the spatial distribution of the number density of the nuclides, neutron flux, and power density.

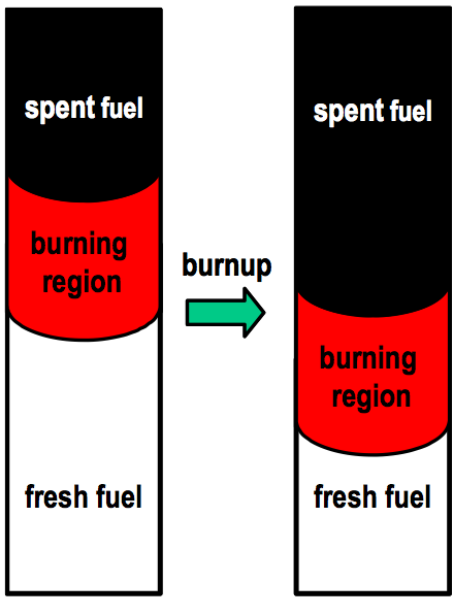


Figure 1.12: CANDLE burnup strategy. From [23]

The neutron transport equation is written as follows

$$\frac{1}{r}\frac{\partial}{\partial r}rD_g\frac{\partial}{\partial r}\phi_g + \frac{\partial}{\partial z}D_g\frac{\partial}{\partial z}\phi_g - \sum_n N_n\sigma_{R,n,g}\phi_g + \sum_n N_n\sigma_{n,g-1\to g}\phi_{g-1} + \frac{\chi_g}{k_{eff}}\sum_{g'}\sum_n N_n\nu\sigma_{F,n,g'}\phi_{g'} = 0 \quad (1.34)$$

The nuclide transformation equation is expressed in the next equation

$$\frac{\partial N_n}{\partial t} = -N_n\left(\lambda_n + \sum_g \sigma_{A,n,g}\phi_g\right) + \sum_{n'} N_{n'}\lambda_{n'\to n} + \sum_{n'} N_{n'}\sum_g \sigma_{n'\to n,g}\phi_g \quad (1.35)$$

A coordinate system that moves along with the burning region was considered. In this case, even as burnup progresses, the burning region does not move. The transformation to this type of coordinate system is the Galilean transformation. Under this transformation, the neutron diffusion equation and nuclide transformation equation become as follows

$$\frac{1}{r}\frac{\partial}{\partial r}rD_g\frac{\partial}{\partial r}\phi_g + \frac{\partial}{\partial z}D_g\frac{\partial}{\partial z}\phi_g - \sum_n N_n\sigma_{R,n,g}\phi_g + \sum_n N_n\sigma_{n,g-1\to g}\phi_{g-1} + \frac{\chi_g}{k_{eff}}\sum_{g'}\sum_n N_n\nu\sigma_{F,n,g'}\phi_{g'} = 0 \quad (1.36)$$

$$-V\frac{\partial N_n}{\partial z'} - N_n\left(\lambda_n + \sum_g \sigma_{A,n,g}\phi_g\right) + \sum_{n'} N_{n'}\lambda_{n'\to n} + \sum_{n'} N_{n'}\sum_g \sigma_{n'\to n,g}\phi_g = 0 \quad (1.37)$$

Here $V$ stands for the moving speed of the burning region. $V$ is determined below. These equations are solved by iteration. Equation (1.36) does not change under the Galilean transformation, and is the same as equation (1.34). The important fact is that the time variable has disappeared in equations (1.36) and (1.37). The neutron transport equation corresponding to equation (1.36) would also not change under the Galilean transformation even if the strict transport equation was considered instead of the diffusion equation. Several characteristics can be derived from the obtained equations and here a few of the most important aspects are described. In equation (1.37), there are two kinds of nuclear transformation, neutron induced reaction and radioactive decay; however, radioactive decay can be generally ignored. If $\Phi_g = \phi_g/V$ is used instead of $\phi_g$, $V$ is removed from equations (1.36) and (1.37)

$$\frac{1}{r}\frac{\partial}{\partial r}rD_g\frac{\partial}{\partial r}\Phi_g+\frac{\partial}{\partial z}D_g\frac{\partial}{\partial z}\Phi_g-\sum_n N_n\sigma_{R,n,g}\Phi_g+\sum_n N_n\sigma_{n,g-1\to g}\Phi_{g-1}$$
$$+\frac{\chi_g}{k_{eff}}\sum_{g'}\sum_n N_n\nu\sigma_{F,n,g'}\Phi_{g'}=0$$

$$-\frac{\partial N_n}{\partial z'}-N_n\left(\sum_g\sigma_{A,n,g}\Phi_g\right)+\sum_{n'}N_{n'}\sum_g\sigma_{n'\to n,g}\Phi_g=0$$

This indicates the following. If the neutron flux, namely the power, is increased by a factor of $m$, the moving speed of the burning region also increases by $m$. Even the absolute value of the power becomes $m$ times greater, though the relative shape does not change. That is, when the power is changed, the moving speed of the burning region and the absolute value of the power density change, however, the power density distribution does not change. These results, however, do not hold when radioactive decay cannot be ignored. In this case, a change in the neutron multiplication factor poses a bigger problem than a change in the power distribution. The relationship between the moving speed of the burning region, burnup of spent fuel, and total power is expressed by the following equation, which has no approximation

$$\int_{-\infty}^{\infty}\sum_{g'}\sum_n N_n\sigma_{F,n,g'}\phi_{g'}dz=V\int_{-\infty}^{\infty}\sum_{g'}\sum_n N_n\sigma_{F,n,g'}\phi_{g'}dt \tag{1.38}$$

Here the left side is the total number of nuclear fissions integrated along the axis at a certain radial position. The integral on the right side is proportional to the burnup of the spent fuel at the same radial position.

CANDLE burnup is possible in a core designed so that the infinite medium neutron multiplication factor $k_{infty}$ (the neutron multiplication factor considering the reactor to be of infinite size) of the fuel changes with burnup specifically as shown in figure 1.13.

On the left is the fresh fuel side and on the right is the spent fuel side. On the left side of the peak, $k_{infty}$ increases with burnup, and on the right side it decreases. Accordingly, the peak shifts to the left side, namely, to the fresh fuel side.

Since a fast reactor has excellent neutron economy, CANDLE burnup in this model was tried with natural uranium or depleted uranium used as fresh fuel. The principle behind this is that the $^{238}U$ in the fresh fuel region

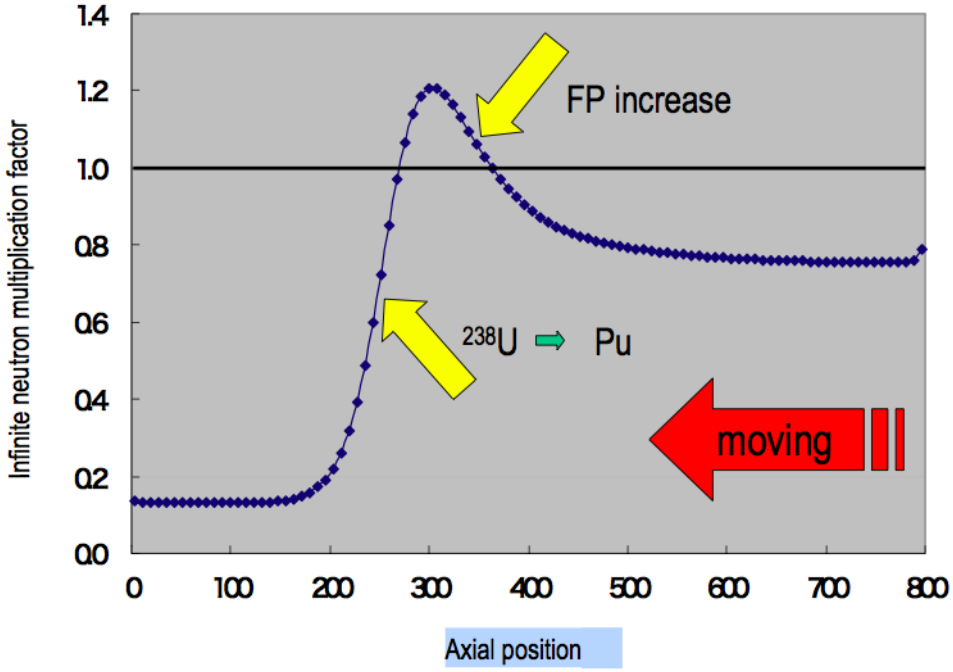


Figure 1.13: Principle of CANDLE Burnup. From [25]

absorbs neutrons leaking from the burning region and changes into $^{239}Pu$. Burnup and fuel change in this reactor are shown in figure 1.14. In this figure, changes in nuclide densities of important nuclides and neutron flux (speed weighted average number density of neutrons) along the core axis are shown.

Since natural uranium is highly sub-critical, many neutrons must be absorbed by $^{238}U$ to bring the system to a critical state. Thus, it is important to have a nuclear reactor with excellent neutron economy. For this purpose, the neutron spectrum should be extremely hard (i.e., the effective neutron energy should be extremely high.). The burnup of fuel is increased by supplying many neutrons to the fresh fuel region. This also results in a reduction in the moving speed of the burning region.

Natural uranium was used as fresh fuel for this investigation, however the same design is possible for depleted uranium. To increase the neutron economy with a hard neutron spectrum, the percentage of fuel volume was set to 50%, which is larger than used in current reactors. In this case, the cooling capability of the coolant decreases. In this design, the fuel has a similar structure to the fuel block employed in the high-temperature gas-cooled reactor and the coolant flows through holes in the block. In this way,

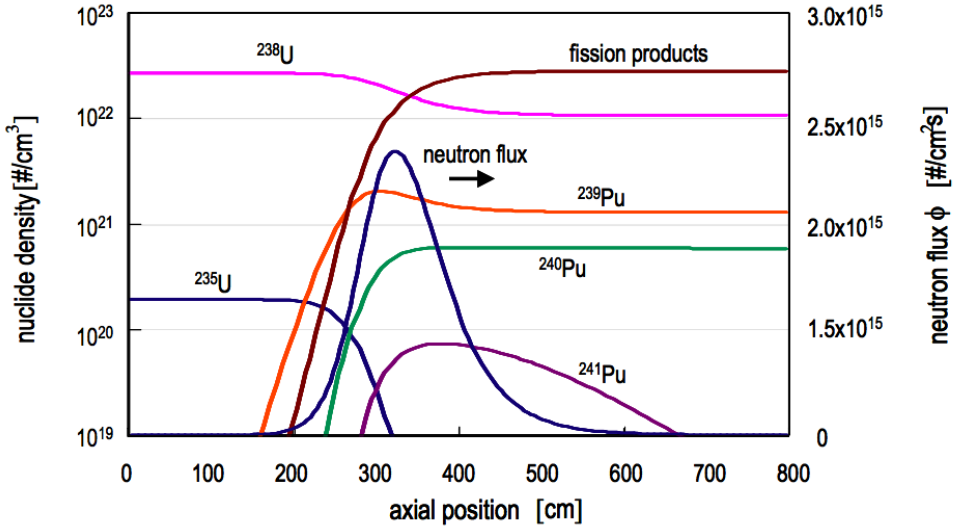


Figure 1.14: CANDLE burnup in a fast reactor. From [25]

a high cooling capability can be obtained with a small amount of coolant. This structure is also suitable for CANDLE burnup from a viewpoint of refueling. For the calculation, 21-group diffusion equations were used. It was confirmed that CANDLE burnup can be established for this design. The results are shown in table 1.6.

Table 1.6: Calculation results for a fast reactor loaded with natural uranium.

| fuel | oxide | nitride | metal |
|---|---|---|---|
| effective neutron multiplication factor | 0.926 | 0.990 | 1.015 |
| moving speed of burning region | 4.7cm/year | 3.5cm/year | 3.8cm/year |
| average burnup of spent fuel | 452GWd/t | 445GWd/t | 426GWd/t |

As we can see now, both Teller and Sekimoto groups, made numerical experiments of nuclear reactor with thorium-uranium and uranium-plutonium fuel cycle, respectively, and obtained, under different initial and boundary condition, the solution in the form of progressive burning wave.

The open question now is: ″what is the necessary and sufficient conditions of nuclear burning wave origin and propagation in the neutron multiplicating medium?″In the chapter 2 we will look for answer to this question.

# Chapter 2

# Physical conditions of nuclear burning (NB) wave origin

In this chapter some relevant for this thesis elements of fundamental analysis of self-stabilizing criticality burning waves in the neutron multiplicating medium will be considered. In this chapter we will first analyze the existing fundamental models and their analytical solutions, which can be used for verification of computing experiments results. And then, in the section 2.2 and 2.3 using the pattern of transition from quantum mechanics framework to the classical mechanics we will obtain the necessary and sufficient conditions of nuclear burning wave origin and propagation in the neutron multiplicating medium. This will be done here without going into details of heuristic description of the slow burning process propagation in the reactor core. The heuristic description will be given in chapter 3.

## 2.1 Negative feedback and Van Damm neutronic model

Now, let us consider the physical reasons, which predetermine soliton-like propagation of criticality wave in initially subcritical infinite-length medium with multiplication rate $k_\infty < 1$. It is obvious that subcritical region with $k_\infty > 1$ has to be created by some external neutron source, such as accelerator or another sabcritical region. Generally speaking, subcritical region is a product of either neutron multiplication effects in fast nuclear systems, or burning of flammable absorber (a fuel component) in thermonuclear systems. Due to gradual burn-up of neutron-multiplicating medium in the subcritical region, the region itself stops being subcritical, as $k_\infty$ decreases below 1. In the usual case the subcriticality wave would have stopped and extinguished,

but since neutrons that were produced in this region during the multiplication stage have ″infected″neighboring regions via diffusion mechanism, the ″virgin″region ahead of the wave front becomes subcritical, and the wave propagates in this direction. It is obvious that for stable movement of this soliton-like wave there has to exist some stabilizing mechanism, such as negative autocatalysis, or, speaking more broadly, any other negative feedback mechanism. In traditional nuclear reactors it is called ″negative reactivity feedback″. Then, let us consider the following example.

Let us write non-stationary one-dimensional equation for a reactor in one-group approximation and with negative reactivity feedback:

$$D\frac{\partial^2\phi}{\partial x^2} + (k_\infty - 1 + \gamma\phi)\,\Sigma_a\phi = \frac{1}{\upsilon}\frac{\partial\phi}{\partial t} \tag{2.1}$$

where $\phi$ is a neutron flux $[cm\cdot sec^{-1}]$, $D$ is a diffusion coefficient $[cm]$,$\gamma\phi$ is a reactivity (dimensionless quantity), $\Sigma_a$ is a macroscopic absorbtion cross-section; $\upsilon$ is a neutron speed. In our case a negative feedback coefficient $\gamma$ is mostly defined by the fact that expression (2.1) uses neutron multiplication rate in infinite medium, and therefore the flux density has to be corrected.

We will search for a solution in form of autowave

$$\phi(x,t) = \phi(x - ut) \equiv \phi(\xi) \tag{2.2}$$

where $u$ is a phase velocity of the wave, $\xi$ coordinate in the system of axes, which moves with phase velocity $u$. Then

$$\frac{1}{\upsilon}\frac{\partial\phi}{\partial t} = -\frac{u}{\upsilon}\frac{\partial\phi}{\partial t} \tag{2.3}$$

Since we know [42] that ratio $u/\upsilon$ in (2.2) is a number of order of magnitude $10^{-13}$ for fast neutron systems and $10^{-11}$ for thermonuclear systems, respectively, it is obvious that we can neglect the partial derivative in (2.1) without loss of generality.

Taking into consideration (2.2), we rewrite (2.1) in the following way

$$L^2\frac{\partial^2\phi}{\partial\xi^2} + [k_\infty(\psi) - 1 + \gamma\phi]\,\phi = 0 \tag{2.4}$$

where $L = D/\Sigma_a$ is a $1/2$ of neutron diffusion length and $\phi$ is co-called neutron fluence function

$$\psi(x,t) = \int_0^t \phi(x,t')dt' \tag{2.5}$$

If we use an expansion of $\phi(\xi)$ in order to a small parameter $\varepsilon = k_\infty - 1$ in (2.4), then, taking into account $\mid \gamma\phi \mid \ll O(1)$, we obtain a very well known Korteweg-de Vries (KdV) equation

$$\varepsilon L^2 \phi_{\xi\xi\xi} + \varepsilon\phi_\xi + \gamma\phi\phi_\xi = 0 \tag{2.6}$$

which has a stable solution of soliton-type wave only when $\gamma < 0$.

$$\phi = \phi_m \sec h^2(\alpha\xi) = \phi_m \sec h^2[\alpha(x - ut)] \tag{2.7}$$

where $\phi_m$ is a neutron flux amplitude, $1/\alpha$ is a characteristic length, which is proportional to the soliton wave breadth, which by definition is full with at half maximum (FWHM) and equals

$$\Delta_{1/2} = FWHM = 2\ln\left(1 + \sqrt{2}\right)\alpha^{-1}, [cm] \tag{2.8}$$

Obviously that through integration of equation (2.7) one can calculate the soliton area

$$S_{area} = 2\phi_m/\alpha \tag{2.9}$$

We have to note here that even a superficial analysis allows us to make one very important conclusion: stable soliton-like wave of nuclear burning (subcritical wave) is only possible when there is a negative feedback, such as a negative reactivity feedback.

In order to find physically meaningful analytical solution of (2.4) by expanding it with (2.6), it is necessary to define function $k_\infty(\psi)$, which is called a burn-up function in literature, in a realistic way. Since we know that burn-up function has a bell-shaped dependency on fluence normalized by its maximum value $\psi_{max}$ (see figure 2.1), then, according to [42], we can without a loss of generality define it as

$$k_\infty = k_{max} + (k_0 - k_{max})\left(\frac{\psi}{\psi_{max}} - 1\right)^2 \tag{2.10}$$

where $k_0$ and $k_\infty$ are initial and maximal neutron multiplication factor, respectively. Using (2.10) we can rewrite (2.4)

$$L^2\phi_{\xi\xi} + \rho_{max}\phi + \gamma\phi^2 - \delta\left[\frac{\int_\xi^\infty \phi d\xi}{u\psi_m} - 1\right]^2 \phi = 0 \tag{2.11}$$

where $\rho_{max} = k_{max} - 1$, $\delta = k_{max} - k_0$.

Now it is not difficult to find the parameters of soliton-like solution by direct substitution of (2.7) into equation (2.11). This procedure, which was

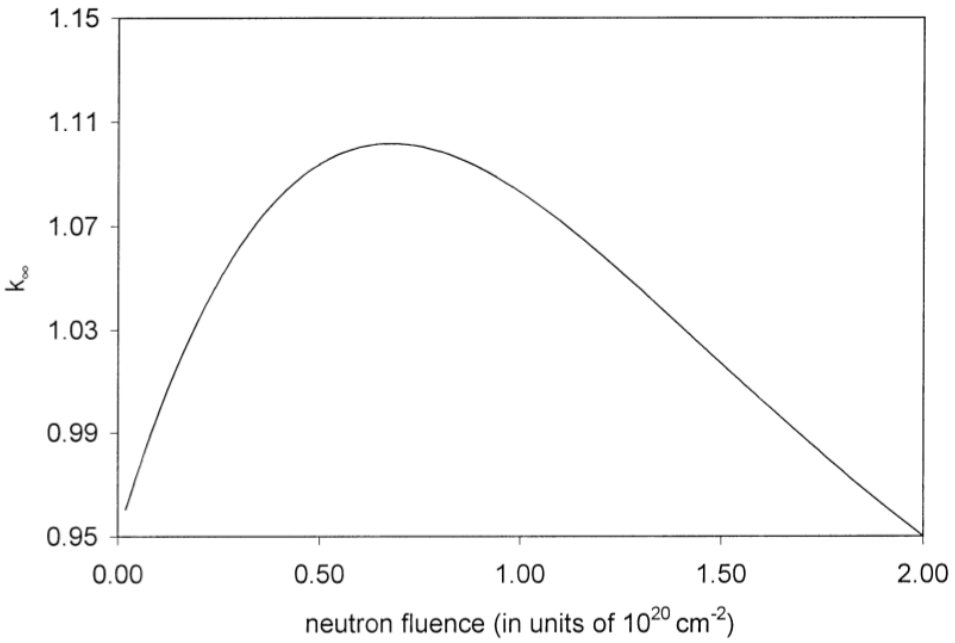


Figure 2.1: Asymmetric burn-up function as characteristic for realistic burn-up function.

first suggested and discussed in [42], lets us find values of the amplitude, phase and phase velocity of soliton-like wave.

$$\phi_m = \frac{\delta - 3\rho_{max}}{2\gamma}, \alpha = \frac{\sqrt{\delta - \rho_{max}}}{2L}, u = \frac{1}{\alpha}\frac{\phi_m}{\psi_{max}} \tag{2.12}$$

But most important we can conclude from it (based on negativity of $\gamma$) the existence (fire-up) requirement of autowave for one-dimensional ($1D$) case [42]

$$\rho_{max} - 2\alpha^2 L^2 - 2k_{max} + k_0 - 3 > 0 \tag{2.13}$$

Let us demonstrate it by emulating the disturbance of soliton solution in the framework of $3D$ model of Van Dam reactor [44], and by analyzing of this solution's stability in case of expanded model (2.1). For simplicity let us consider cylindrical reactor. In this case we can consider neutron leakage by using so-called transverse geometric buckling [39, 40, 41], or, in other words, transverse geometrical parameter of neutron-multiplicating medium, which, as opposed to material buckling, characterizes exclusively the specifics of reactor's active zone geometry and the boundary conditions for neutron

flux density (e.g., $\phi = 0$ at the external extrapolated boundary of the reactor core).

First and foremost, it is connected with the fact that in many neutronic computational systems functions exist permitting the conversion of core models from $3D$ to $2D$ or $1D$. Usually, as in collapsing the core model one or two dimensions are lost, the equivalence process to pass from the $3D$ model to the reduced one, evaluates a transverse buckling distribution that takes into account for the neutron leakage in the lost direction. The most used method to compute this distribution is based on the $3D$ leakage conservation [1].

This formulation is also stipulated by the fact that, according to linear diffusion theory for reactors with homogenous reactor core, transverse geometrical buckling is much higher than longitudinal geometric buckling. Therefore, following [44], we will take the value of transverse geometrical buckling as a basis for perturbance of soliton solution for $3D$ reactor model (2.1). Introducing the geometrical multiplier factor $k_{\mathcal{B}}$, we can rewrite (2.1) as follows

$$L^2(\phi_{xx} + \phi_{yy}) + (k_{\mathcal{B}} - 1)\phi + L^2\phi_{zz} + (k_\infty - k_{\mathcal{B}} + \gamma\phi)\phi = 0 \tag{2.14}$$

For the perturbation formalism we assume further that $k$ is quite close to $k_{\mathcal{B}}$ and $\gamma\phi$ much smaller than unity. Thus, we have

$$\phi_{zz} \ll \phi_{xx}, \phi_{zz} \ll \phi_{yy} \tag{2.15}$$

$$\mid k_\infty - k_{\mathcal{B}} \mid \ll \mid k_{\mathcal{B}} - 1 \mid, \mid \gamma\phi \mid \ll O(1) \tag{2.16}$$

According to a usual perturbation scheme, $\phi$ is expanded in the form

$$\phi = \phi_0 + \phi_1 + \dots \tag{2.17}$$

where $\phi_0$ is the leading-order solution and $\phi_1$ is the first higher-order one.

Substituting (2.17) into (2.14) and collecting equal order terms, we obtain the leading order equation

$$L^2\left(\frac{\partial^2\phi_0}{\partial x^2} + \frac{\partial^2\phi_0}{\partial y}\right) + (k_{\mathcal{B}} - 1)\,\phi_0 = 0 \tag{2.18}$$

[1] In multigroup nucleonic models this method could give poor results in trying to match $2D$ models with a strongly non-uniform composition distribution. The method presented in [45] permits the computation of a transverse buckling distribution that gives a good equivalence in these difficult configurations. This method can be used to make an equivalence between two $3D$ models. This capability is useful in resetting computer models on measurements.

and the first higher order equation

$$L^2\left(\frac{\partial^2\phi_1}{\partial x^2}+\frac{\partial^2\phi_1}{\partial y}\right)+\left(k_{\mathcal{B}}-1\right)\phi_1=L^2\frac{\partial^2\phi_0}{\partial z^2}-\left(k_\infty-k_{\mathcal{B}}+\gamma\phi_0\right)\phi_0\equiv f(\phi_0) \tag{2.19}$$

From (2.18) and (2.19) we obtain respectively

$$\Delta_{xy}^2\phi_0=-\frac{k_{\mathcal{B}}-1}{L^2}\phi_0 \tag{2.20}$$

$$\Delta_{xy}^2\phi_1=\frac{f(\phi_0)-\left(k_{\mathcal{B}}-1\right)\phi_1}{L^2} \tag{2.21}$$

Substituting (2.21) and (2.21) into second Green [32] formula we obtain, we obtain the solvability condition for Van Dam equation

$$\int_S\left(\phi_0\Delta_{xy}^2\phi_1-\phi_1\Delta_{xy}^2\phi_0\right)dS=\frac{1}{L^2}\int_S\phi_0 f(\phi_0)dS=0 \tag{2.22}$$

Thus, by using parabolic burn-up function for $k_\infty$ (2.10) and assuming that

$$\phi_0=\Phi(\xi)\phi_0(r),\xi=z-ut,\psi_m(r)=\Psi_m\psi_0(r)$$

the right-hand side of (2.19) leads to

$$\begin{aligned}-f(\phi_0)&=L^2\frac{\partial^2\phi}{\partial z^2}+(k_{max}-k_{\mathcal{B}})\phi_0\\&-(k_{max}-k_0)\left[\frac{\int_\xi^\infty\phi_0 d\xi}{u\psi_m}-1\right]^2\phi_0+\gamma\phi_0^2\end{aligned} \tag{2.23}$$

Furthermore, the integration of $\phi_0 f(\phi_0)$ in solvability condition (2.22) gives

$$\begin{aligned}-\int_S\phi_0 f(\phi_0)dS&=\left[L^2\Delta_{\xi\xi}^2\Phi+(k_\infty-k_{\mathcal{B}})\Phi\right]dS\\&-(k_\infty-k_{\mathcal{B}})\Phi\left[\frac{\int_\xi^\infty\Phi d\xi}{u\Psi_m}-1\right]^2\int\phi_0^2dS+\gamma\Phi^2\int_S\phi_0^3dS\end{aligned} \tag{2.24}$$

The solvability condition (2.22) leads to an amplitude equation of $\Phi$, which has an identical form to the $1D$ model by Van Dam (2.11)

$$L^2\frac{\partial^2\Phi}{\partial\xi^2}+(k_{max}-k\mathcal{B})\Phi-(k_{max}-k_0)\left(\frac{\int_\xi^\infty\Phi d\xi}{u\Psi_m}-1\right)^2\Phi+\gamma\frac{I_3}{I_2}\Phi^2=0 \quad (2.25)$$

where

$$I_2=\int_S\phi_0^2dS, I_3=\int_S\phi_0^3dS$$

Identifying the above equation with (2.14) taking into account (2.10) and setting

$$\rho_{max}=k_{max}-k_{\mathcal{B}}, \delta=k_{max}-k_0, \gamma_0=\gamma I_3/I_2, \psi_m=\Psi_m \quad (2.26)$$

we obtain the solution as following

$$\Phi=\Phi_m\sec h^2(\alpha\xi) \quad (2.27)$$

where

$$\phi_m=\frac{\delta-3\rho_{max}}{\gamma_0}, \alpha=\frac{\sqrt{\delta-\rho_{max}}}{2L}, u=\frac{1}{\alpha}\frac{\Phi_m}{\Psi_{max}} \quad (2.28)$$

From (2.28) follows existence condition for autowave in $3D$ case

$$k_{max}-k_0>\frac{3}{2}(k_{\mathcal{B}}-k_0)>0 \quad (2.29)$$

that for $k_{\mathcal{B}}=1$ turns into analogous existence condition for $1D$ case (2.13).

Evidently, from the point of view of inherent safety according to Feoktistiv, this is a required, but not sufficient, since the feedback dynamics is defined ˝manually˝and not according to any physical law, which should naturally prevent explosive development of chain reaction [1].

In order to estimate an influence of the found parameters on stability dynamics of the soliton-like nuclear burning wave, we shall use an informational-probabilistic approach developed by Seifritz [43].

We can write an expression for mean entropy of the process in question

$$S=-k_{\mathcal{B}}\int_{-\infty}^{\infty}p(x)\ln p(x)dx \quad (2.30)$$

where $p(x)$ is probability density w.r.t. $x$, $\ln(1/p(x))$ is a mean entropy, and $k_{\mathcal{B}}$ is Boltzmann constant.

By direct substitution of soliton-like solution (2.7) into equation (2.30) we obtain

$$\begin{aligned} S &= -2k_{\mathcal{B}} \int_0^{\infty} \sec h^2(\alpha\xi) \ln\left[\sec h^2(\alpha\xi)\right] d\left(\frac{1}{\mid \gamma \mid \phi_m L} x\right) \\ &= 4k_{\mathcal{B}} \int_0^{\infty} \frac{\ln \cos h(\beta y)}{cosh^2(\beta y)} dy \end{aligned} \tag{2.31}$$

The integration of (2.31) leads to to the following expression for the entropy

$$\begin{aligned} S &= \frac{4(1-\ln 2)}{\beta} = \frac{2(1-ln2)}{3} \alpha \left(\mid \gamma \mid \sum\nolimits_a \phi_m\right) k_{\mathcal{B}} \\ &= k_{\mathcal{B}} \frac{2(1-\ln 2)}{3} \frac{\sum\nolimits_a}{L} \left(2k_{max} + k_0 - 3\right) \sqrt{1-k_0} \end{aligned} \tag{2.32}$$

which in the case of isoentropic soliton transportation of soliton (2.2), i.e.

$$S \backsim \frac{\Sigma_a}{L} \left(2k_{max} + k_0 - 3\right) \sqrt{1-k_0} = const \tag{2.33}$$

shows, that the ratio $k_{max}/k_0$ w.r.t. condition $k_0 < 1,\ 2k_{max} + k_0 > 3\ k_{max} - 1 < \varepsilon$ has to have a constant mean $\langle k_{max}/k_0 \rangle = const$.

It is worth to mention here that if width $\Delta_{1/2} \to 0$, then by isoentropy (2.32) the shape of soliton becomes similar to so-called Dirac $\delta$-function. If we introduce two different sizes or scales of length $l_1 = \gamma\phi_m L$ and $l_2 = 1/\alpha$, then we could see that the first one gets bigger when the other is small, and vice versa. It happens because the area $S_{area}$ (2.9) under the soliton has to remain constant, because $S_{area} \infty l_1 l_2$. In this case the entropy of soliton tends to zero, since the entropy is proportional to the ratio of these two values $S_{area} \infty l_1/l_2 \to 0$. These properties are an implication of the fact that $l_1$ is a soliton non-linearity characteristic, and $l_2$ is a soliton dispersion characteristic. If $l_1 \gg l_2$, then the process has weak dispersion, and with $l_1 \ll l_2$ it has strong dispersion.

In the latter case the amplitude of soliton is big. And, finally, if $l_1 = l_2$, then the soliton velocity is $u \infty (l_1^2 l_2^2)^{1/2}$, see equation (2.12) that is, it is proportional to geometrical mean of dispersion and non-linearity parameter.

## 2.2 Chaos and integrability in non-linear dynamic of the reactor core.

It is necessary to note here that due to the simplification of reactor equation (2.1) the phase velocity of soliton-like nuclear burning wave is quite idealized, and does not reflect some substantial physical processes that take place in reality. For example, it does not consider the effective nucleus life-time $\tau_\beta$ for ${}^{239}_{92}U$ w.r.t. two $\beta$-decay of ${}^{239}_{92}$ and ${}^{239}_{93}Np$, which is a delay of plutonium nuclei generation in the chain (1.2).

In this regard one very important and fundamental results of Feoktistov, table 1.2, has to be recalled

$$\Lambda(a) = \frac{u\tau_\beta}{L} \tag{2.34}$$

where $\tau_\beta$ is a delay, caused, for instance, by active (fissionable) isotope birth, $\tau_\beta$ is equal to cumulative $\beta$-decay period compound nuclei either in $Uranium - Putonium$ Feoktistov chain (1.2) or in $Thorium - Uranium$ Teller chain (1.33), $a$ is a breadth of allowed region in the Bohr-Sommerfeld quantization condition (1.31), and $\Lambda(a)$ is a dimensionless coefficient, which appears in the Feoktisov simplified reactor diffusion model (1.24)-(1.26).

Obviously, due to its physical meaning, the equation (2.34) is a key factor which predetermines the value of phase velocity of the soliton-like burning wave. Therefore, this equation exists regardless of abstraction degree and approximation level of the model of reactor core, and should appear implicitly or explicitly in any model whose system of kinetics equation for nuclei and neutrons has a soliton-like solutions for neutrons. At the same moment, due to the fact that soliton wave average breadth has an order of $2L$ (see (2.8)), maximum values of dimensionless coeffitient $\Lambda(a)$ and velocity $u$ are define be the following approximate equality

$$\frac{1}{b}\Lambda_{max}(a) = \frac{u_{max}\tau_\beta}{bL} = 1, \tag{2.35}$$

where coefficient $b \sim 2$.

From the analysis of (2.35) it follows that the velocity of stable propagation of soliton-like wave is not necessarily equal to diffusion velocity, i.e. to $u = L/\tau_{/beta}$, and can be considerably slower or faster, which is an implication of a very strong domination of either non-linearity or dispersion parameter, respectively. These parameters in their turn are induced by peculiarities of nuclear transmutation members' birth and death kinetics, for example in chain (1.2) or (1.33). In practice they appear as higher or lower fuel burn-up degree, respectively.

In other words, when the wave velocity and, consequently, the fuel burn-up rate are low, then the wave stops due to the following reasons. First, neutrons from external source burn plutonium on the medium border, and simultaneously transmute uranium into neptunium-239 ($Ne_{239}$). $Ne_{239}$ starts to produce plutonium after a while, but could not create the required concentration fast enough, while the production rate of $Pu_{239}$ drops due to uranium burnup. A new layer without both $^{238}U$ and $^{239}Pu$ grows thicker and thicker at the medium border. Neutron diffusion through this layer does not suffice to increase plutonium concentration in sequent layers, and the wave does not appear even when $n_{Pu}(x, 0) = n_{crit}$.

Conversely, when the wave velocity and fuel burn-up rate are high, the wave stops due to insufficient (or, to be more precise, too delayed) plutonium production. This situation is similar to the fire in the woods under strong wind, when only the tops of tree crowns burn. When the wind speed increases, it could extinguish the fire altogether. In our case, there exists a velocity, for which, in the early stage $x = 0$ the front of neutron soliton wave leaves behind the front of plutonium production wave, and when the lag exceeds the neutron diffusion length, the neutron wave stops. It is interesting to note that this case is not studied in the literature (apart from [47]), but it is possible to postulate that it corresponds to some hypothetical situation where the nuclear burning wave appears under the conditions of highly-enriched fuel, which can be characterized by ultra-low critical concentration of the fuels active component.

Thus, lag (see figure 1.7(a)) or lead of neutron wave front relative to plutonium wave front for a distance exceeding the neutron diffusion length will leads to a full stop and degradation of wave. This means that the degradation of wave with very low or very high initial phase velocity, i.e. with very low or very high value of $a$, causes the expression (2.34) will tends to zero. Therefore, considering (2.35), we can conclude that (2.34) is correct for $0 \leq (1/b)\Lambda(a) \leq 1$. Based on this generalization, we can make an important assumption that the expression $(1/b)\Lambda(a)$ means the probability density distribution $p(a)$ w.r.t. $a$

$$\frac{u\tau_\beta}{bL} = p(a) \tag{2.36}$$

Let us consider and justify the type and main properties of such a statistics, and also show the results of its verification based on the known computational experiments in modelling a nuclear burning wave in $U - Pu$ (1.2) and $Th - U$ (1.33) fuel cycles.

In order to solve the posed problem let us use a known analogy between neutron diffusion equation and stationary Schrödinger equation in its qua-

siclassical approximation. Let us recall that this analogy was used earlier to solve the kinetics equation system for neutrons and nuclei (1.24)-(1.26) taking part in transformations of $U - Pu$ fuel cycle. Since equations system for neutrons and nuclei for $Th - U$ fuel cycle (1.33) is structurally identical to equation system for $U - Pu$ fuel cycle (1.2), then the ˝quantum mechanical˝solution will be common for both fuel cycles, except for a few details.

Now, let us recall that earlier, we have used the Bohr-Sommerfeld quantisation condition, which in the case of one-dimensional systems explicitly defines the energy eigenvalues $E_n$

$$\oint p(x)dx = \oint \sqrt{2m(E_n - V(x)}dx = 2\pi\hbar \left(n + \frac{1}{2}\right),\ n = 0, 1, 2, ... \quad (2.37)$$

where $m$ and $p(x)$ are the mass and particle momentum for the particle in the field of some smooth potential $V(x)$, respectively.

For an almost integrable Feoktistov system of equations (1.24)-(1.26) or anologous Teller system of equations, for which it is assumed that $m = 1/2$. $V(x) = 1$, and $n = 0$ this condition is applied as follows

$$\int_0^a \sqrt{E_0 - 1}dx = \frac{\pi}{2},\ E_0 = \frac{n_{fis}}{n_{crit}^{fis}} \quad (2.38)$$

where the index $fis$ denotes the fissionable isotope, for example $^{239}Pu$ in Feoktistov $U - Pu$ fuel cycle (1.2) and $^{233}U$in the Teller $Th - U$ fuel cycle (1.33).

In general case of description of fast reactor core evolution, however, respective equation systems for neutrons and nuclei are almost without exclusions nonintegrable. This, in turn, means that according to Kolmogorov-Arnold-Moser theorem [28]-[30] it is impossible to use quasiclassical quantization formulas in phase space[2], where movement not limited by multidimentional toruses. This is stidulated by the fact that in the case of nonintegrable hamiltonia systems a big amount of toruses collapse as the disturbance (non-integrability) grows, which leads to majority of bound states trajectories become entangled, the movement becomes mostly chaotic, and bound states themselves, as well as their energies, could not be described by the rules of quasiclassical quiantization, such as Einstein-Brillouin-Keller

[2]It is interesting to note that exactly due to this reason Einstein in his famous work [31] denied the quasiclassical approach altogether. Only half a century later Gutzwiller [32] could surmount the difficulties arising from the quantization of non-integrable systems, and has obtained an expression which can be viewed as a generalized Wentzel-Kramers-Brillouin (WKB) approximation.

(EBK) quantization rule for multidimentional case [33], which generalizes the Bohr-Sommerfeld quiantization rule.

The significance of these difficulties was first in full assessed by Persival [34], who proposed to separate the energy spectrum of the bounded state at the quasiclassical limit $\hbar \to 0$ into two parts:

- regular energy spectrum, which corresponds to the integrated movement mode in which all states can be quantized according to EBK quantization rules;
- irregular energy spectrum, which corresponds to mostly chaotic movement mode, for which the EBK quantization rules cannot be applied.

The notion of irregular spectrum is of great interest, since in a certain sense it implies that at the limit of $\hbar \to 0$ the ˝underlying˝classical chaos will manifest itself in quantum-mechanical properties of the system [33]. In the future this possibility served as a basis for introduction of ˝quantum chaos˝notion, which, as Tabor precisely notes, does not always associate with the limit $\hbar \to 0$. We shall also note that nowadays the ˝quantum chaos˝notion unite a number of problems connected with quantum-mechanical description of systems that behave chaotically in classical terms [35].

Since we will use a random matrices theory results in the research of chaotic properties of our statistics (2.36), let us first give an overview of the main concepts of this theory.

First, following [35], let us cinsoder shortly a nature of so-called universality classes and Gauss ensemble types. As is known, Hamilton operator matrix posessin any kind of symmetry can be reduced to block-diagonal form, where the matrix elements in each block are defined by a specific set of quantum numbers.

For the sake of simplicity we will assume that Schrödinger equation

$$i\hbar\frac{\partial\Psi}{\partial t} = \widehat{H}\Psi \tag{2.39}$$

is expressed for the states belonging to one single block. Here, the operator $\widehat{H}$ matrix dimension is finite and is an integer number.

Let us consider now the role of the symmetry with respect to the sign invertion – the time inversion. For this purpose let us introduce an operator $T$ which inverts the time sign

$$Tf(t) = f(-t) \tag{2.40}$$

Obviously, the exchange of $t$ for $-t$ in the $\partial/\partial t$ differential operator which is a part of non-stationary Schrödinger's equation (2.39) can be compensated

by exchanging $i$ for $-i$. Mathematically this can be expressed by considering the following commutative correlation

$$\left[CT, i\hbar\frac{\partial}{\partial t}\right] = 0, \tag{2.41}$$

where $C$ is a complex conjugation operator

$$CA = A^* \tag{2.42}$$

Now we have to find out if the Hamiltonian operator $\widehat{H}$ commutates with operator $CT$. It is easy to show that in the case of conservative systems $\widehat{H}$ commutates with $T$. So it will be enough then to establish how the $C$ operator affect the Hamiltonian operator $\widehat{H}$. Three different situations are possible here, and each of them defines a class of universality.

As shown in [35], these universality classes separate physical systems into groups according to their relation to orthogonal, unitary or simplectic transformation, which leave the $\widehat{H}$ matrix invariant. In other words, it is postulated in [35] that:

- the Hamiltonian of spinless system symmetrical w.r.t. time inversion is invariant w.r.t. orthogonal transformations and could be represented by real matrix;
- the Hamiltonian, which is asymmetrical w.r.t. time inversion, is invariant w.r.t. unitary transformations and could be represented by Hermitian matrix;
- the Hamiltonian of the system with spin 1/2 , symmetrical w.r.t. time inversion, is invariant w.r.t. simplectic transformations and could be represented by quaternion real matrix.

Now let us talk about Gaussian ensembles. If the matrix element distribution function is invariant with respect to one of the mentioned transformations, this means that the sets of all matrices with elements described by given distribution functions form, form a Gauss orthogonal ensemble (GOE), Gauss unitary ensemble (GUE), and Gauss simplectic ensemle (GSE), respectively.

We have to note at the same time one very substantial detail. The matrix element distribution function of Gauss ensembles could not be measured directly, since our experiment can only give us the information on the energy levels of the quantum-mechanical system in question. In other words, the energy eigenvalues distribution function is the most interesting from the practical point of view.

The quation derivation process for the ensembles show above can be found in [36]. Here, it appears that the energy eigenvalues correlated distribution function for all ensemble types can be respresented in a unified form

$$P(E_1, ...E_N) \sim \prod_{n>m} (E_n - E_m)^\nu \exp(-A \sum_n E_n^2), \tag{2.43}$$

where $\nu$ is an universality index, equals to 1, 2 and 4 for GOE, GUE and GSE statistics, respectively. In the case when $\nu = 0$ the energy eigenvalues are not correlated, and the interlevel distance distribution function can be described by Poisson statistics, and the matrix ensemble itself is called Poisson ensemble.

Due to the fact that interlevel distance distribution function is a most well-researched property of the chaotical systems, below, following [35], we shall only show a calculation of relatively simple case of gaussian $2 \times 2$ matrix ensemble. Let us calculate the interlevel distance distribution function $p(s)$ by substitution of function $P(E_1, E_2)$ in expression (2.43)

$$\begin{aligned} p(s) &= \int_{-\infty}^{\infty} dE_1 \int_{-\infty}^{\infty} dE_2 P(E_1, E_2) \delta(s - |E_1 - E_2|) \\ &= C \int_{-\infty}^{\infty} dE_1 \int_{-\infty}^{\infty} dE_2 |E_1 - E_2|^\nu \exp(-A \sum_n E_n^2) \delta(s - |E_1 - E_2|). \end{aligned} \tag{2.44}$$

Constants $A$ and $C$ are defined by two normalization conditions

$$\int_0^{\infty} p(s) ds = 1, \tag{2.45}$$

$$\int_0^{\infty} sp(s) ds = 1. \tag{2.46}$$

Here, the first condition is a normalization of total probability, and the second is a unit-norm normalization of average interlevel distance. Integration of (2.44) gives us the folowing so-called Wigner interlevel distance distribution function, which correspond to different gaussian ensembles

$$p(s) = \begin{cases} \frac{\pi}{2} s \exp(-\frac{\pi}{4} s^2), & \nu = 1(GOE), \\ \frac{32}{\pi} s^2 \exp(-\frac{\pi}{4} s^2) & \nu = 2(GUE), \\ \left(\frac{8}{3\sqrt{\pi}}\right)^6 s^4 \exp(-\frac{64}{9\pi} s^2) & \nu = 4(GSE) \end{cases} \tag{2.47}$$

Despite the fact that these functions were obtained for gaussian $2 \times 2$ matrix ensembles, they describe with sufficient precision the spectrums of arbitrary size matrices [35].

It is worthy to note that even if the random matrix theory was concieved in order to find regularities in heavy nuclei energy spectrums [36], the interest towards it grew after Bohigas, Giannoni and Schmit concluded [38] that it can be applied to ANY chaotic system.

Indeed, Wigner interlevel distance distributions (which mostly concerns GOE) were found in numerous completely different physical systems – from atomic nuclei to macroscopic billiards. Here, quite often it was impossible to tell the difference between the statistics of atomic nuclei spectrum and statistics of billiard spectrum. The same could be said about other spetrum correlational properties, some of which were discussed above. This fact, without any doubt, can be an indication that the nature of interactions in a particular physical system does not play a definitive role as long as the system behaves chaotically. On the other hard, however, exactly this property gives us a chance to use the same mathematical apparatus for the description of different chaotic systems, including nuclei, microwave billiardsa and mesoscopic systems, such as quantum points and quantum wells.

Going back to our problem of determining the statistics type of $p(a)$ (2.36), let us try to use the discussed properties of gaussian ensembles.

## 2.3 Wigner distribution and conditions of nuclear burning wave origin in fast reactors

Now, in the framework of almost integrable system, to which the system equation of Feoktistov $U - Pu$ fuel cycle (1.2) or Taylor $Th - U$ fuel cycle (1.33) nucler burning kinetics belongs, let us formally introduce the stationary state energy eigenvalue as $\tilde{n}_{fis}/n_{crit}^{fis} = E_0$, and quasistationary state energy eigenvalue $n_{fis}^{semi}/n_{crit}^{fis} = E_{semi}$, where $E_0 > E_{semi}$, and $n$ is a current equiliblium main isotope concentration, limited from above by the value of initial equilibrium main isotope concentration. In general case, to describe the wave nuclear burning mode, which is the mode the reactor is maintained in to remain near-critical, we can assume $E_{semi} \to 1$. Then, in the framework of quiantum-mechanicall analogy, the latter means that the burn process energy spectrum evolution in the allowed region can be described by some quasi-equvalent two-stage scheme, as show on figure 2.2.

Then, for almost-integrable system which describes the nuclei transmutatuin kinetics for Feoktistov $U - Pu$ fuel cycle (1.2) or for Taylor $Th - U$ fuel

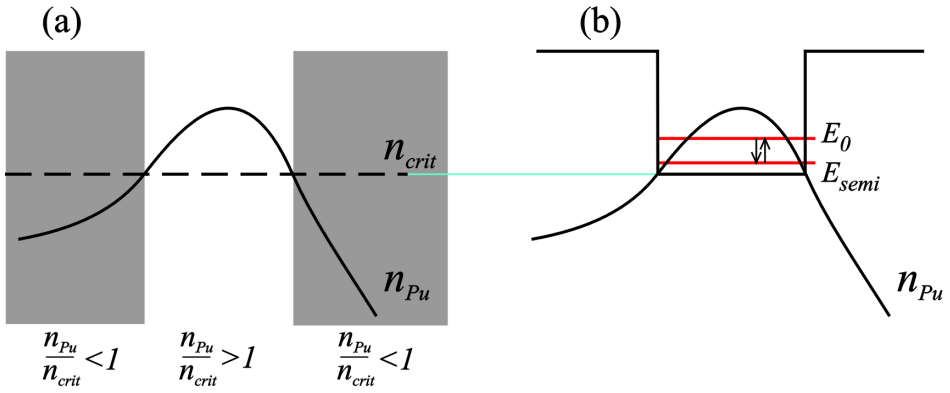


Figure 2.2: The schematic view of allowed and subbarier region boundaries in the Bohr-Sommerfeld quantization condition (a) and the corresponding quasi-equvalent two-stage energy scheme (b).

cycle (1.33) in the general case we can use an approximate Bohr-Sommerfeld condition as follows

$$\int_0^a \sqrt{\frac{n_{fis}}{n_{crit}^{fis}-1}}dz \approx \int_0^a \sqrt{E_0 - E_{semi}}dz \approx a\sqrt{E_0 - E_{semi}} \sim \frac{\pi}{2}. \qquad (2.48)$$

From here we can postulate one obvious and important assertion: due to Bohr-Sommerfled condition (2.48) the Wigner interlevel distance statistics type unambiguously predefines an analogous statistics type of parameter $a$, which characterizes the wave front width of the active (fissioning) material.

Here we have to note that before the experiment nothing is know about the value of energy $E_0$, but we can assume that $E_{semi} = 1$. If one adds that in the stationary mode all kinetic parameters of the wave are predefined by the values of initial equilibrium $\tilde{n}_{fis}$ and critical $n_{crit}^{fis}$ concentration of active (fissioning) isotope, then we notice the physical meaning and the necessity of the following substitution

$$a\sqrt{E_0 - E_{semi}} = a_*\sqrt{\frac{\tilde{n}_{fis}}{n_{crit}^{fis}} - 1}. \qquad (2.49)$$

Obviously, the conditions (2.48) and (2.49) let us obtain the expression for the assessment of a value of parameter $a_*$

$$a_*^2 \sim \frac{\pi^2}{4}\frac{n_{crit}}{\tilde{n}_{Pu} - n_{crit}}. \tag{2.50}$$

The next step for determining the $p(a_*)$ statistics type (2.36) is predefined by the necessity of verification of the suggested hypothesis using experimental data. Therefore we have conducted the comparison of gaussian ensemble statistics (2.47) with the results of calculation experiments [8], [19], [22]-[27], and this comparison showed a good accordance of calculation data with theoretical dependency, which is described by gaussian simplectic ensemble (GSE) statistics. The comparison results are presented in the table 2.1 and on figure 10, where we have also showed Feoktistivs analytical estimations (see table 1.2) from [8].

Table 2.1: The parameters of nuclear burning wave.

| Parameter | U-Pu cycle | | | | | | Th-U cycle | |
|---|---|---|---|---|---|---|---|---|
| | Rusov [69] | Sekimoto [23] | Fomin [26] | Fomin [26] | Fomin [26] | Ershov [19] | Teller [21] | Rusov |
| $\frac{\tilde{n}_{equil}^{fis}}{n_{crit}^{fis}}$ | $\frac{0.100}{0.056}$ | $\frac{2.585}{1.750}$ | $\frac{0.145}{0.080}$ | $\frac{0.024}{0.015}$ | $\frac{0.240}{0.105}$ | $\frac{0.10}{0.05}$ | $\frac{0.071}{0.032}$ | $\frac{0.070}{0.035}$ |
| $a_*$ | 1.772 | 2.274 | 1.743 | 2.028 | 1.385 | 1.571 | 1.423 | 1.571 |
| $\frac{u_{theor}}{u_{mod}}$ | $\frac{105}{106}$ | $\frac{2.9}{3.1}$ | $\frac{125}{130}$ | $\frac{21}{22}$ | $\frac{622}{620}$ | $\frac{293}{331}$ | $\frac{46}{\sim 50}$ | 25 |

Thus, we can conclude that the wave valocity values $u$ (2.36) are defined by the following approximate equality

$$\frac{u\tau_{beta}}{2L} \cong \left(\frac{8}{3\sqrt{\pi}}\right) a_*^4 \exp\left(-\frac{64}{9\pi}a_*^2\right),\ a_*^2 \cong \frac{\pi^2}{4}\cdot\frac{n_{crit}^{Pu}}{\tilde{n}_{Pu} - n_{crit}^{Pu}}, \tag{2.51}$$

where coefficient $b = 2$ (see 2.36), $\tau_\beta$ is a delay, caused, for instance, by active (fissionable) isotope birth, $\tau_\beta$ is equal to cumulative $\beta$-decay period compound nuclei either in uranium-plutonium Feoktistov chain (1.2) or in

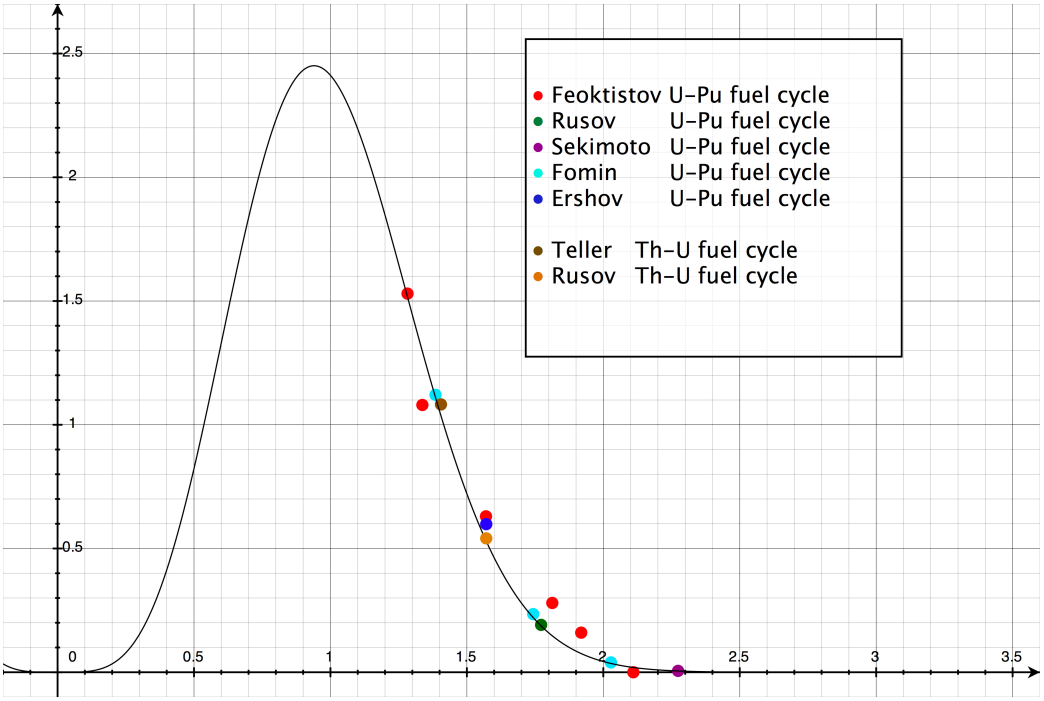


Figure 2.3: Theoretical (the black curve) and experimental (colored points) dependencies of $\Lambda(a_*)$ from the parameter $a_*$.

thorium-uranium Teller chain (1.33). $L \sim 5\,cm$ $\tau_\beta = 3.3\,days$ for $U - Pu$ and $\tau_\beta = 39.5\,days$ for $Th - U$ fuel cycle, respectively.

As computational experiments show (chapter 3), the wave lock-out conditions that characterize the process of its degradation and stop are predetermined by the degree with which the neutrons from the external source (at the initial stage of the process) burn up the main nonfissionable and active (fissionable) components of the fuel ahead of the wave front. This process is very important, since the high burn-up rate of the region ahead of the wave will prevent the wave from crossing this region, just like the fire in the steppe cannot cross the stripe of the plowed land. It is obvious that the fuel burn-up rate in the initial stage in defined mostly by the energy spectrum and intensivity of the external source neutrons, and by nuclear characteristics of the fuel. The most important of these characteristics is the delay time $\tau_\beta$, which equals to effective $\beta$-decay period of the intermediate nuclei in $U - Pu$ Feoktistov fuel cycle (1.2) or $Th - U$ Taylor fuel cycle (1.33). As a result, the higher these parameters are, the high is the probability of the wave lock-out and eventual extinction. Moreover, the following peculiarity can be observed during the formation of fast initial wave: in the case of tran-

sition to stationary wave mode the velocity of the wave will sharply drop, since the wave front of the neutron wave from the fast spectrum part will lead the plutonium wave front, which eventually leads to the extinction and full degradation of the fast component of the neutron wave.

In spite of the general understanding of physics of the nuclear burnung wave lock-out process, it is obvious that the process description difficulties outlined above only indicate that the problem we are trying to solve is far from trivial. Unfortunately, the scope from the problem exceeds the scope or this work, but it will be a subject of future research.

Despite the outlined difficulties it is show empirically (by computational experiments) that the expression for certain range of values of $a_*$, which correspond to existing concentration wave of nuclear fuel burning with nonzero velocity will look like this

$$0.05 \leq a_* \equiv \frac{\xi_a}{L} < 2.5 \tag{2.52}$$

where $\xi_a$ is an autovawe coordinate of $a_*$.

Thus, based on the verification of (2.51) we can make a conclusion that generalizes the physical conditions of Feoktistov wave mode: the soliton-like wave propagation velocity in the neutron-multiplicating medium is generally defined by two conditions, one of them the necessary one is predetermined by ratio of equilibrium plutonium concentration and critical plutonium concentration $n_{pu}/n_{crit} > 1$ see (1.1), or, to be more precise, Bohr-Sommerfeld quantization condition see (1.31), and the other the sufficient one is determined by the gaussian simplectic ensemble (GSE) sattistics with respect to parameter $a$, which characterizes the concentration wavefront width of the active component of nuclear fuel.

# Chapter 3

# The Simulation of Soliton-Like Criticality Wave

In this chapter in section 3.1 the simplified one-dimentional model of Pu accumulation and U burnup kinetics is proposed. In the section 3.2 taking into account delayed neutrons three-dimentional model for one-group diffusion approximation is offered. The numerical solution using the method of mesh points in the implicit form is obtained. Finally, in section 3.3 the simulation results and its verification w.r.t. obtained in the chapter 2 necessary and suffycient conditions of nuclear burning wave origin are given.

## 3.1 One-dimentional model

Let us consider an ingot of uranium-238 ($U_{238}$). In each cubic centimeter of ingot there are $5 \cdot 10^{22}$ atoms of $U_{238}$. An external neutron source is located left of an uranium-238 ingot and emits neutrons. In the suggested design a nuclear burning wave is ignited and propagates slowly in axial direction. Feoktistov uranium-plutonium fuel cycle (1.2) is used for soliton-like wave simulation

$$^{238}_{92}U(n,\gamma) \rightarrow ^{239}_{92}U \xrightarrow{\beta^-} ^{239}_{92}Np \xrightarrow{\beta^-} ^{239}_{92}Pu(n, fission)$$

The reactor contains a cylindrical core comprised of a nuclear ignitor, which is critical at the beginning, and a much longer nuclear burning wave-propagating region, which is subcritical in the initial state. In the front region $Pu_{239}$ is built up, because $U_{238}$ in the natural uranium is transformed into $Pu_{239}$ and local reactivity increases. Meanwhile in the tail region fission products (FPs) accumulate and local reactivity decreases. Consequently, the burning region drifts in axial direction.

The simplified model of Pu accumulation and U burnup kinetics is proposed as follows. A one-dimensional semi-infinite $U-Pu$ medium irradiated from the end of the cylinder by an external neutron source is considered in the diffusion one-group approximation (neutrons energy is $\sim 1MeV$). Then, taking into account delayed neutrons, the respective system of differential equations, which describes the kinetics of Feoktistov uranium-plutonium fuel cycle, i.e., the kinetics of initiation and propagation of neutron fission wave $n(x,t)$, is as follows

$$\frac{\partial n(x,t)}{\partial t} = D\Delta n(x,t) + q(x,t) \tag{3.1}$$

where

$$q(x,t) = [\nu(1-p)-1]\, n(x,t)\upsilon_n \sigma_f^{Pu} N_{Pu}(x,t) + \sum_{i=1}^{6} \frac{\tilde{N}_i \ln 2}{T_{1/2}^i} \tag{3.2}$$

$$-n(x,t)\upsilon_n \left[ \sum_{8,9,Pu} \sigma_a^i N_i(x,t) + \sum_{i=1}^{6} \sigma_a^i \tilde{N}_i(x,t) + \sum_{i=fragments} \sigma_a^i \overline{N}_i(x,t) \right]$$

$$\frac{\partial N_8(x,t)}{\partial t} = -\upsilon_n n(x,t)\sigma_a^8 N_8(x,t) \tag{3.3}$$

$$\frac{\partial N_9(x,t)}{\partial t} = \upsilon_n n(x,t)\sigma_a^8 N_8(x,t) - \frac{1}{\tau_\beta} N_9(x,t) \tag{3.4}$$

$$\frac{\partial N_{Pu}(x,t)}{\partial t} = \frac{1}{\tau_\beta} N_9(x,t) - \upsilon_n n(x,t)(\sigma_a^{Pu} + \sigma_f^{Pu}) N_{Pu}(x,t) \tag{3.5}$$

$$\frac{\partial \tilde{N}_i(x,t)}{\partial t} = p_i \upsilon_n n(x,t)\sigma_f^{Pu} N_{Pu}(x,t) - \frac{\ln 2 \tilde{N}_i}{T_{1/2}^i} \tag{3.6}$$

To determine the last term on the right-hand side of $q(x,t)$, the effective additional neutron absorber approximation was used

$$n(x,t)\upsilon_n \sum_{i=fragments} \sigma_a^i \overline{N}_i(x,t) = n(x,t)\upsilon_n \sigma_a^{eff} \overline{N}(x,t) \tag{3.7}$$

Taking into account the fact that fission with two fragment formation is most probable, the kinetic equation for $\overline{N}(x,t)$ becomes

$$\frac{\partial \overline{N}(x,t)}{\partial t} = 2\left(1 - \sum_{i=1}^{6} p_i\right) n(x,t)\upsilon_n \sigma_f^{Pu} N_{Pu}(x,t) + \sum_{i=1}^{6} \frac{\tilde{N}_i \ln 2}{T_{1/2}^i} \tag{3.8}$$

where $n(x,t)$ is the neutron density, $D$ is the diffusion constant of neutrons, $\upsilon_n$ is the neutron velocity ($E_n = 1MeV$ in one-group approximation), $\tilde{N}_i$ are the concentrations of the neutron-rich fission fragments of $^{239}Pu$ nuclei, $N_8$, $N_9$, $N_{Pu}$ are the $^{238}U$, $^{239}U$, $^{239}Pu$ concentrations, respectively, $\overline{N}_i$ are the concentrations of the rest fission fragments of $^{239}Pu$ nuclei, $\sigma_a$ is the neutron absorption micro cross-section, $\sigma_f$ is the neutron fission micro cross-section, $\tau_\beta$ is the nucleus life time w.r.t $\beta$-decay, $p_i$ ($p = \sum_{i=1}^{6} p_i$) are the parameters characterizing the dekayed neutrons groups for the main fuel fissionable nuclides.

The boundary conditions for the system of differential equations (3.1) - (3.6) are

$$n(x,t)|_{z=0} = \Phi_0/\upsilon_n,\ n(x,t)|_{z=l} = 0 \tag{3.9}$$

where $\Phi_0$ is the neutron density of the plane diffusion source of neutrons which is located on the boundary $z = 0$; $l$ is the uranium ingot length.

An estimation of the neutron flux density from the source on the boundary $\Phi_0$ can be obtained from an estimation of the $Pu$ critical concentration which is of order of 10%

$$4\tau_\beta \Phi_0 \sigma_a^8 N_8(x,t)|_{t=0} = 0.1 N_8(x,t)|_{t=0}$$

and therefore

$$\Phi_0 \approx 0.1/4\tau_\beta \sigma_a^8 \tag{3.10}$$

It's important to note here that (3.10) is only an estimation of $\Phi_0$. The results of the computational experiment show that it can be substantially smaller in reality.

In general, different boundary conditions can be used, depending on the physical conditions under which nuclear burning is initiated by the source neutrons, for example, the Dirichlet condition of (3.9) type, a Neumann condition or a so-called third-kind boundary condition, which summarizes first two conditions. The use of the third-kind boundary condition is recommended in neutron transport theory [50]. Here we use this condition in the simple case which is known as Milnes problem, or more precisely, it is a linear combination of the neutron concentration $n(x,t)$ and its spatial derivative $\partial n/\partial x(x,t)$ on the boundary

$$n(0,t) - 0.7104\lambda n^{(1,0)}(0,t) = 0, \tag{3.11}$$

where $\lambda$ is the range of neutrons and $n^{(1,0)}(0,t) \equiv \partial n/\partial x(0,t)$.

Although the behavior of the "neutron source - nuclear fuel"system depends on the boundary conditions near the boundary, computational experiments show that in the active zone, i.e., far from the boundary, the system

is asymptotically independent of the boundary conditions. This confirms the independence of wave propagation in the reactor volume on the boundary conditions and on the way in which the nuclear burning is initiated. In this sense the problem of determining the optimum parameters of nuclear fuel system is a nontrivial and extraordinarily vital issue, which requires a separate examination.

The initial conditions for the system of differential equations (3.1) – (3.6) are

$$n(x,t)|_{z=0,t=0} = \Phi_0/V_n,\ n(x,t)|_{z\neq 0,t=0} = 0; \tag{3.12}$$

$$N_8(x,t)|_{t=0,z=0,l} = \frac{\rho_8}{\mu_8} \approx \frac{19}{238} N_A,\ N_8(x,t)|_{z\neq 0,t=0} = 0; \tag{3.13}$$

$$\begin{aligned} N_9(x,t)|_{t=0} &= 0, \\ N_{Pu}(x,t)|_{t=0} &= 0, \\ \tilde{N}_i(x,t)|_{t=0} &= 0, \\ \overline{N}(x,t)|_{t=0} &= 0. \end{aligned} \tag{3.14}$$

where $\rho$ is the density, which is expressed in the units of $g\ cm^{-3}$, $N_A$ is the Avogadro constant.

The simulation results for the one-dimensional model are presented in figure 3.1.

More simulation results for one-dimentional and three-dimentional models of Feoktistov safe reactor are presented in a section 3.3.

## 3.2 3-dimentional model

### 3.2.1 One-group diffusion approximation

Taking into account delayed neutrons, the respective system of differential equations, which describes the kinetics of Feoktistovs U-Pu fuel cycle, can be represented in the cylindrical coordinate system with a radial coordinate $r$ , vertical coordinate $z$ and the symmetry about an azimuth $\varphi$ as follows.

The neutrons balance equation is represented as

$$\int\limits_{\upsilon} \frac{\partial n(r,z,t)}{\partial t} d\upsilon = -\oint\limits_{\upsilon} \vec{j}_n(r,z,t) dS + \int\limits_{\upsilon} q(r,z,t) d\upsilon, \tag{3.15}$$

where $q(r,z,t)$ is a bulk density of neutron source, $\vec{j}_n(r,z,t)$ is a neutron flux density.

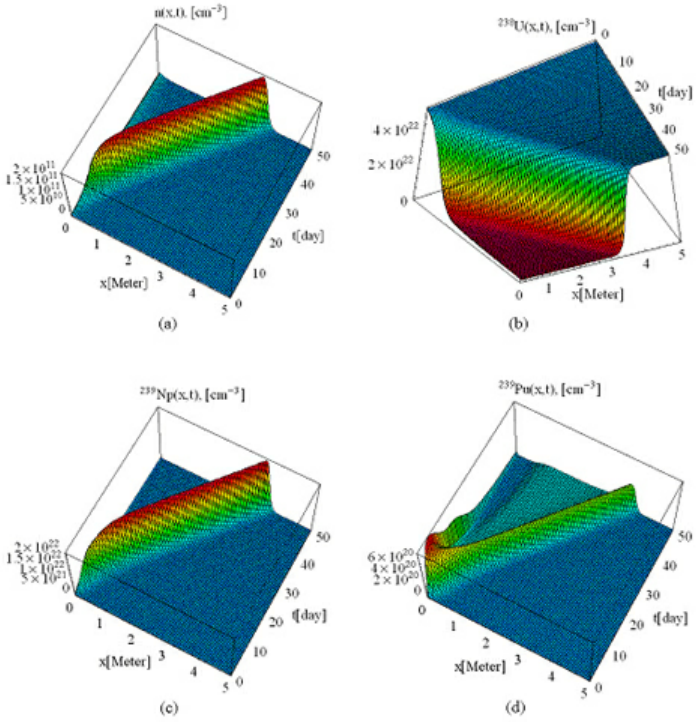


Figure 3.1: Concentration kinetics of (a) neutrons; (b) $^{238}U$; (c) $^{239}U$; (d) $^{239}Pu$ in the active zone of one- dimensional georeactor. Here $t$ is time axis, step is $\Delta t = 0.01s$; $x$ is spatial coordinate axis, step is $\Delta x = 1cm$; $z$ is a concentration axis, particles $cm^{-3}$, $\Phi_0 = 5 \times 10^{17} cm^{-2} s^{-1}$.

$$\int\limits_{\upsilon} \frac{\partial n(r,z,t)}{\partial t} d\upsilon = -\int\limits_{\upsilon} div\vec{j}_n(r,z,t)d\upsilon + \int\limits_{\upsilon} q(r,z,t)d\upsilon, \tag{3.16}$$

$$\frac{\partial n(r,z,t)}{\partial t} = -div\vec{j}_n(r,z,t) + q(r,z,t). \tag{3.17}$$

Let us consider the one-group approximation, with the given neutron energy $E_n \sim 1MeV$.

According to the Fick's first law of diffusion the diffusive flux

$$\vec{j}_n(r,z,t,E_n,T) = -D(r,z,t,E_n,T)\nabla n(r,z,t,E_n,T)$$

where the neutrons diffusion coefficient is as follows

$$D(r,z,t,E_n) = \frac{\upsilon_n \lambda_S(r,z,t,E_n,T)}{3} = \frac{\upsilon_n}{3\sum_S(r,z,t,E_n,T)} = \frac{\upsilon)n}{3\sum\limits_{i=8,9,Pu,Np,FP} \sigma_S^i(E_n,T)N_i(r,z,t,E_n,T)} \tag{3.18}$$

where $\lambda_S$ is the scattering mean free path of neutrons, $\sigma_S^i$ are the neutron scattering micro cross-section, $\upsilon_n$ is the neutron velocity (for the one energy group with the given energy $E_n \sim 1MeV$).

Then we can rewrite (3.15) as follows

$$\frac{\partial n(r,z,t,E_n)}{\partial t} = D(r,z,t,E_n,T)\Delta n(r,z,t,E_n) + \nabla D(r,z,t,E_n,T)\cdot\nabla n(r,z,t,E_n) + qD(r,z,t,E_n,T) \tag{3.19}$$

In this work the heat transfer (second summand) is not taken into account, therefore for one-energy-group approximation the neutrons balance equation (3.19) can be represented in the following way

$$\frac{\partial n(r,z,t)}{\partial t} = D\Delta n(r,z,t) + q(r,z,t) \tag{3.20}$$

where $n(r,z,t)$ is the neutron density, $D$ is the diffusion constant of neutrons, and a density of neutron source $q(r,z,t)$ is as follows

$$q(r,z,t) = [\nu(1-p)-1]\, n(r,z,t)\upsilon_n\sigma_f^{Pu}N_{Pu}(r,z,t) + \sum_{i=1}^{6}\frac{\tilde{N}_i \ln 2}{T^i_{1/2}} - n(r,z,t)\upsilon_n\left[\sum_{8,9,Pu}\sigma_a^i N_i(r,z,t) + \sum_{i=1}^{6}\sigma_a^i\tilde{N}_i(r,z,t) + \sum_{i=fragments}\sigma_a^i\overline{N}_i(r,z,t)\right] \tag{3.21}$$

where $\upsilon_n$ is the neutron velocity ($E_n = 1MeV$ in one-group approximation); $\nu$ is an average number of prompt neutrons per fission for $^{238}U$, $^{239}U$,$^{239}Np$, $^{239}Pu$; $\tilde{N}_i$ are the concentrations of the neutron-rich fission fragments of $^{239}Pu$ nuclei; $N_8$, $N_9$, $N_{Pu}$ are the $^{238}U$, $^{239}U$, $^{239}Pu$ concentrations, respectively; $\overline{N}_i$ are the concentrations of the rest fission fragments of $^{239}Pu$ nuclei; $\sigma_a$ is the neutron absorption micro cross-section; $\sigma_f$ is the neutron fission micro cross-section; $p_i$ ($p = \sum_{i=1}^{6} p_i$) and $T^i_{1/2}$ are the parameters characterizing the delayed neutrons groups for the main fuel fissionable nuclides.

To determine the last term on the right-hand side of $q(r,z,t)$, the effective additional neutron absorber approximation was used

$$n(r,z,t)\upsilon_n \sum_{i=fragments} \sigma_a^i \overline{N}_i(r,z,t) = n(r,z,t)\upsilon_n \sigma_a^{eff} \overline{N}(r,z,t) \tag{3.22}$$

The kinetic equations for $^{238}U$, $^{239}U$, $^{239}Pu$ nuclei and the neutron-rich fission fragments are as follows

$$\frac{\partial N_8(r,z,t)}{\partial t} = -\upsilon_n n(r,z,t)\sigma_a^8 N_8(r,z,t) \tag{3.23}$$

$$\frac{\partial N_9(r,z,t)}{\partial t} = \upsilon_n n(r,z,t)\sigma_a^8 N_8(r,z,t) - \frac{1}{\tau_\beta} N_9(r,z,t) \tag{3.24}$$

$$\frac{\partial N_{Pu}(r,z,t)}{\partial t} = \frac{1}{\tau_\beta} N_9(r,z,t) - \upsilon_n n(r,z,t)(\sigma_a^{Pu} + \sigma_f^{Pu}) N_{Pu}(r,z,t) \tag{3.25}$$

$$\frac{\partial \tilde{N}_i(r,z,t)}{\partial t} = p_i \upsilon_n n(r,z,t)\sigma_f^{Pu} N_{Pu}(r,z,t) - \frac{\ln 2 \tilde{N}_i}{T_{1/2}^i} \tag{3.26}$$

where $\upsilon_n$ is the neutron velocity ($E_n = 1MeV$ in one-group approximation), $\tilde{N}_i$ are the concentrations of the neutron-rich fission fragments of $^{239}Pu$ nuclei, $N_8$, $N_9$, $N_{Pu}$ are the $^{238}U$, $^{239}U$, $^{239}Pu$ concentrations, respectively, $\overline{N}_i$ are the concentrations of the rest fission fragments of $^{239}Pu$ nuclei, $\sigma_a$ is the neutron absorption micro cross-section, $\sigma_f$ is the neutron fission micro cross-section, $\tau_\beta$ is the nucleus life time w.r.t $\beta$-decay, $p_i$ ($p = \sum_{i=1}^6 p_i$) and $T_{1/2}^i$ are the parameters characterizing the delayed neutrons groups for the main fuel fissionable nuclides.

Taking into account the fact that fission with two fragment formation is most probable, the kinetic equation for $\overline{N}(r,z,t)$ becomes

$$\frac{\partial \overline{N}(r,z,t)}{\partial t} = 2\left(1 - \sum_{i=1}^6 p_i\right) n(r,z,t)\upsilon_n \sigma_f^{Pu} N_{Pu}(r,z,t) + \sum_{i=1}^6 \frac{\tilde{N}_i \ln 2}{T_{1/2}^i} \tag{3.27}$$

The boundary conditions for the system of differential equations (3.20) (3.26) are

$$n(r,z,t)|_{z=0} = \Phi_0/\upsilon_n,\ n(r,z,t)|_{z=l} = 0 \tag{3.28}$$

where $\Phi_0$ is the neutron density of the plane diffusion source of neutrons which is located on the boundary $z = 0$; $l$ is the uranium ingot length.

An estimation of the neutron flux density from the source on the boundary $\Phi_0$ can be obtained from an estimation of the $Pu$ critical concentration which is of order of 10%

$$4\tau_\beta \Phi_0 \sigma_a^8 N_8(r,z,t)|_{t=0} = 0.1 N_8(r,z,t)|_{t=0}$$

and therefore

$$\Phi_0 \approx 0.1/4\tau_\beta \sigma_a^8 \tag{3.29}$$

It's important to note here that (3.29) is only an estimation of $\Phi_0$. The results of the computational experiment show that it can be substantially smaller in reality.

The initial conditions for the system of differential equations (3.20) (3.26) are

$$n(r,z,t)|_{z=0,t=0} = \Phi_0/V_n,\ n(r,z,t)|_{z\neq 0,t=0} = 0, \tag{3.30}$$

$$N_8(r,z,t)|_{t=0,z=0,l} = \frac{\rho_8}{\mu_8} \approx \frac{19}{238} N_A,\ N_8(r,z,t)|_{z\neq 0,t=0} = 0, \tag{3.31}$$

$$\begin{aligned} N_9(r,z,t)|_{t=0} = 0,\ N_{Pu}(r,z,t)|_{t=0} = 0, \\ \tilde{N}_i(r,z,t)|_{t=0} = 0,\ \overline{N}(r,z,t)|_{t=0} = 0. \end{aligned} \tag{3.32}$$

where $\rho$ is the density, which is expressed in the units of $g\ cm^{-3}$, $N_A$ is the Avogadro constant.

### 3.2.2 The numerical solution. The mesh points method.

The cylinder-symmetric one-group neutron diffusion and nuclide transformation equations are solved numerically. For the numerical solution of the system of partial differential equations (3.20) – (3.26), which describe the neutron diffusion and time evolution of the nuclear reaction products concentration in cylindrical coordinates, the method of mesh points in the implicit form was used.

The main advantage of this method is that it does not require additional information about the type of the solution.

The differential equation, which describes the neutron diffusion with a source in a cylindrical coordinate system w.r.t. symmetry about angular coordinate, is as follows

$$\frac{\partial n(r,z,t)}{\partial t} = D\Delta n(r,z,t) + q(r,z,t) \tag{3.33}$$

where $\Delta n = \frac{\partial^2 n}{\partial r^2} + \frac{\partial^2 n}{\partial z^2} + \frac{1}{r}\frac{\partial n}{\partial r}$ is the Laplace operator, $n(r,z,t)$ is the neutrons concentration, $q(r,z,t)$ is the neutron source density, $r$, $z$ are the spatial coordinates, $t$ denotes time, $D$ is the diffusion coefficient (generally speaking $D$ is a function of the coordinates and time $D = D(r,z,t)$).

Let us consider $N_z$ is a number of steps over coordinate $z$, $N_r$ is a number of steps over coordinate $r$, $N_t$ is a number of steps over time. Here we consider the net function $n^k_{i,j}$, which approximates the desired function $n(r,z,t)$ in the points $r = r_i = ih_z,\ z = z_j = jh_r,\ t = t_k = kh_t$, where $i = \overline{0, N_z}$, $j = \overline{0, N_r}$, $k = \overline{0, N_t}$.

The points of mesh with $i = 0$ correspond to the left boundary of the cylinder, the points with $i = N_z$ correspond the right boundary of cylinder, $j = 0$ corresponds the cylinder axis, $j = N_r$ corresponds the cylinder surface, $k = 0$ corresponds the initial moment of time, $k = N_t$ corresponds the final moment of time, respectively.

The differential equation (3.33) for the points of admitted region for $r$, $z$, $t$ can be approximated by a difference quotient

$$\begin{aligned}\frac{n^{k+1}_{i,j} - n^k_{i,j}}{h_t} &= \sigma D \\ \cdot \left[\frac{n^{k+1}_{i,j-1} - 2n^{k+1}_{i,j} + n^{k+1}_{i,j+1}}{h_r^2} + \frac{1}{jh_r}\frac{n^{k+1}_{i,j+1} - n^{k+1}_{i,j-1}}{2h_r} + \frac{n^{k+1}_{i-1,j} - 2n^{k+1}_{i,j} + n^{k+1}_{i+1,j}}{2}\right] &\\ +(1-\sigma)D \\ \cdot \left[\frac{n^{k}_{i,j-1} - 2n^{k}_{i,j} + n^{k}_{i,j+1}}{h_r^2} + \frac{1}{jh_r}\frac{n^{k}_{i,j+1} - n^{k}_{i,j-1}}{2h_r} + \frac{n^{k}_{i-1,j} - 2n^{k}_{i,j} + n^{k}_{i+1,j}}{h_z^2}\right] &\\ +q^k_{i,j}\end{aligned} \tag{3.34}$$

where $i = \overline{1, N_z - 1}$, $j = \overline{1, N_r - 1}$, $k = \overline{0, N_t - 1}$. For $\sigma = 0$ there is an explicit scheme, for $0 < \sigma \leq 1$ there is an implicit scheme.

Taking into account symmetry about a cylinder axis (for $r = 0$) the diffusion equation (for $j = 0$) can be approximated by a difference quotient

$$\begin{aligned}\frac{n^{k+1}_{i,j} - n^k_{i,j}}{h_t} &= \sigma D\left[2\frac{n^{k+1}_{i,j} - n^{k+1}_{i,0}}{hr^2} + \frac{n^{k+1}_{i-1,j} - 2n^{k+1}_{i,j} + n^{k+1}_{i+1,j}}{h_z}\right] \\ &+(1-\sigma)D\left[2\frac{n^{k}_{i,j} - n^{k}_{i,0}}{hr^2} + \frac{n^{k}_{i-1,j} - 2n^{k}_{i,j} + n^{k}_{i+1,j}}{h_z^2}\right] + q^k_{i,j}\end{aligned} \tag{3.35}$$

where $q^k_{i,j}$ depends on fission products concentration $N_i$ for which the approximation by a difference quotient is as follows

$$\frac{N^{k+1}_{i,j} - N^k_{i,j}}{h_t} = f_N(N^k_{i,j}, n^k_{i,j}, ...) \tag{3.36}$$

The set of equations (3.34)-(3.36) is solved sequentially for each moment of time $k$ in the following way. From (3.36) we can write the fission products concentrations in the next moment of time $k+1$ for each $k = 0, 1, ..., N_t - 1$ as follows

$$N_{i,j}^{k+1} = h_t f_N(N_{i,j}^k, n_{i,j}^k, ...) + -N_{i,j}^k \tag{3.37}$$

Now we can solve the set of equations (3.34), (3.35) for the same moment of time using the matrix sweep method.

Let us consider the vector function $Y_i^k = \begin{bmatrix} n_{i,0}^k \\ ... \\ n_{i,n_r}^k \end{bmatrix}$ for each $i = \overline{0, N_z}$. Now we can rewrite (3.34), (3.35) for functions $Y_i^k$ for each $k = \overline{1, N_t - 1}$ as follows

$$\begin{aligned} C_0 y_0 - B_0 y_1 &= F_0, \\ -A_i y_{i-1} + C_i y_i - B_i y_{i+1} &= F_i,\ i = 1, 2, ..., N_z - 1, \\ -A_{N_z} y_{N_z - 1} + C_{N_z} y_{N_z} &= F_{N_z} \end{aligned} \tag{3.38}$$

Where vectors $Y_i^k$ are denoted by $y_i$, for each $i = \overline{0, N_y}$.

To solve the system (3.39) matrix sweep method was used. This method is well described in [47], [48], [49].

In compliance with the algorithm of matrix sweep method we are looking for the solution of the system in the following form

$$y_i = \alpha_{i+1} y_{i+1} + \beta_{i+1},\ i = 0, 1, ..., N - 1 \tag{3.39}$$

where $\alpha_{i+1}$ are square matrixes of the same degree $M$ as the matrixes $A_i$, $B_i$, $C_i$, and $\beta_{i+1}$ is a vector of lenth $M$.

Matrixes $\alpha_{i+1}$ and vectors $\beta_{i+1}$ are determined as follows recurrence equations

$$\begin{aligned} \alpha_{i+1} &= (C_i - A_i \alpha_i)^{-1} B_i, \\ \beta_{i+1} &= (C_i - A_i \alpha_i)^{-1} (A_i B_i + F_i) \end{aligned} \tag{3.40}$$

where $i = 1, 2, ..., N-$. The initial values $\alpha_1$ and $\beta_1$ are determined using $-C_0 y_0 + B_0 y_1 = -F_0$ as follows

$$\alpha_1 = C_0^{-1} B_0,\ \beta_1 = C_0^{-1} F_0. \tag{3.41}$$

When all the sweeping coefficient $\alpha_i$, $\beta_i$ are determined in the direct course of sweep, we have to determine vectors $y_i$, for $i = N-1, N-2, ..., 1, 0$. These

vectors $y_i$ are determined from equation (3.39) in the reverse course of sweep starting with $y_{N-1}$. Here we need the vector $y_N$, which is determined from

$$A_N y_{N-1} - C_N y_N = -F_N,\ y_{N-1} = \alpha_N y_N + \beta_N$$

From this we get

$$y_N = (C_N - A_N \alpha_N)^{-1}(A_N \beta_N + F_N) \tag{3.42}$$

Now, from (3.39)-(3.42) we get the following matrix sweep method algorithm for (3.39)

$$\alpha_{i+1} = (C_i - A_i \alpha_i)^{-1} B_i,\ i = 1, 2, ..., N-1,\ \alpha_1 = C_0^{-1} B_0, \tag{3.43}$$
$$\beta_{i+1} = (C_i - A_i \alpha_i)^{-1} (A_i B_i + F_i),\ i = 1, 2, ..., N-1\ \beta_1 = C_0^{-1} F_0, \tag{3.44}$$
$$y_i = \alpha_{i+1} y_{i+1} + \beta_{i+1},\ i = N-1, N-2, ..., 1, 0,\ y_N = \beta_{N+1} \tag{3.45}$$

The matrixes $C_i - A_i \alpha_i$ have to be invertible at the each step $i = 1, 2, ..., N-1$ of recursion.

Let us apply this matrix sweep method to the neutron diffusion equation (3.33)

$$\frac{\partial n(r,z,t)}{\partial t} = D\Delta n(r,z,t) + q(r,z,t), \tag{3.46}$$
$$\Delta n = \frac{\partial^2 n}{\partial r^2} + \frac{\partial^2 n}{\partial z^2} + \frac{1}{r}\frac{\partial n}{\partial r} \tag{3.47}$$
$$\tag{3.48}$$

We can approximate (3.46) by a difference quotient as follows

$$\frac{n_{i,j}^{k+1} - n_{i,j}^{k}}{h_t}$$

$$= D\left[\frac{n_{i,j-1}^{k+1} - 2n_{i,j}^{k+1} + n_{i,j+1}^{k+1}}{h_r^2} + \frac{1}{jh_r}\frac{n_{i,j+1}^{k+1} - n_{i,j-1}^{k+1}}{2h_r} + \frac{n_{i-1,j}^{k+1} - 2n_{i,j}^{k+1} + n_{i+1,j}^{k+1}}{hz^2}\right]$$

$$+q_{i,j}^{k},$$

$$i = \overline{1, N_z - 1},\ j = \overline{1, N_r - 1},\ k = \overline{0, N_t - 1}$$

where $N_z$ is a number of steps over coordinate $z$, $N_r$ is a number of steps over coordinate $r$, $N_t$ is a number of steps over time.

Now, moving all the summands with $k+1$ to the right-hand side, and all the summands with $k$ to the left-hand side we will get system (3.39) for (3.46) in the form

$$\begin{gathered} -C_0 n_{0,j} + B_0 n_{1,j} = -F_0, \\ A_i n_{i-1,j} - C_i n_{i,j} + B_i n_{i+1,j} = -F_i,\ i = 1, 2, ..., N_z - 1, \\ A_{N_z} n_{N_z-1,j} - C_{N_z} n_{N_z,j} = -F_N, \end{gathered} \tag{3.49}$$

where $C_0 = E_{N_r-1}$, $E_{N_r-1}$ is an identity matrix of size $N_r - 1$, $B_0 = 0$, $\vec{F}_0 = \vec{0}$ is a boundary condition, $A_{N_z} = 0$, $C_{N_z} = E_{N_r-1}$, $\vec{F}_{N_z} = \vec{0}$ is a boundary condition,

$$-A_i = \frac{ht \cdot D}{hz^2} E_{N_r-1},\ -B_i = \frac{ht \cdot D}{hz^2} E_{N_r-1},$$

$$C_i = \begin{bmatrix} -\left[1 + 2Dht\left(\frac{2}{hr^2} + \frac{1}{hz^2}\right)\right] & 4\frac{Dht}{hr^2} & 0 & 0 \\ \frac{Dht}{hr^2}\left[1 - \frac{1}{2j}\right] & -\left[1 + 2Dht\left(\frac{1}{hr^2} + \frac{1}{hz^2}\right)\right] & \frac{Dht}{hr^2}\left[1 + \frac{1}{2j}\right] & 0 \\ ... & ... & ... & ... \\ ... & ... & ... & ... \end{bmatrix} \begin{cases} j = 1 \\ j = 2 \\ ... \\ j = N_r - 1 \end{cases} \tag{3.50}$$

$$F_i = \begin{bmatrix} -n_{i,0}^k + ht \cdot q_{i,j}^k \\ -n_{i,j}^k \cdot q_{i,j}^k \\ -n_{i,j}^k - n_{i,N_r}^{k+1} \frac{Dht}{hr^2}\left[1 + \frac{1}{2j}\right] \cdot q_{i,j}^k \end{bmatrix} \begin{cases} j = 0 \\ j = \overline{1, N_r - 2} \\ j = N_r - 1 \end{cases}$$

## 3.3 The Simulation Parameters and Results

The system of equations (3.1) – (3.6) with boundary conditions (3.9), initial conditions (3.15) is solved numerically using the software package FORTRAN Power Station 4.0. For distributed parallel computation the MATLAB®7.4.0 was used. The source files and program listings can be found in Appendix.

The computer modeling allows to easily control the following parameters of reactor

$$\tau_n(x,t) = \frac{l_n(x,t)}{\upsilon_n} = \frac{1}{\upsilon_n \sum\limits_{i=8,9,Np,Pu,fr} (\sigma_S^i + \sigma_c^i + \sigma_f^i) N_i(x,t)} \quad (3.51)$$

$$k_{eff}(x,t) = \frac{n(x,t+\tau_n)}{n(x,t)} \quad (3.52)$$

$$\rho(x,t) = \frac{k_{eff}(x,t)-1}{k_{eff}(x,t)} \quad (3.53)$$

$$T = \frac{\tau_n(x,t)}{\rho(x,t)} \quad (3.54)$$

where $\tau_n(x,t)$ is the neutrons life time, $k_{eff}$ is the effective neutron multiplication rate, $\rho(x,t)$ is the reactivity, and $T$ is the reactor period.

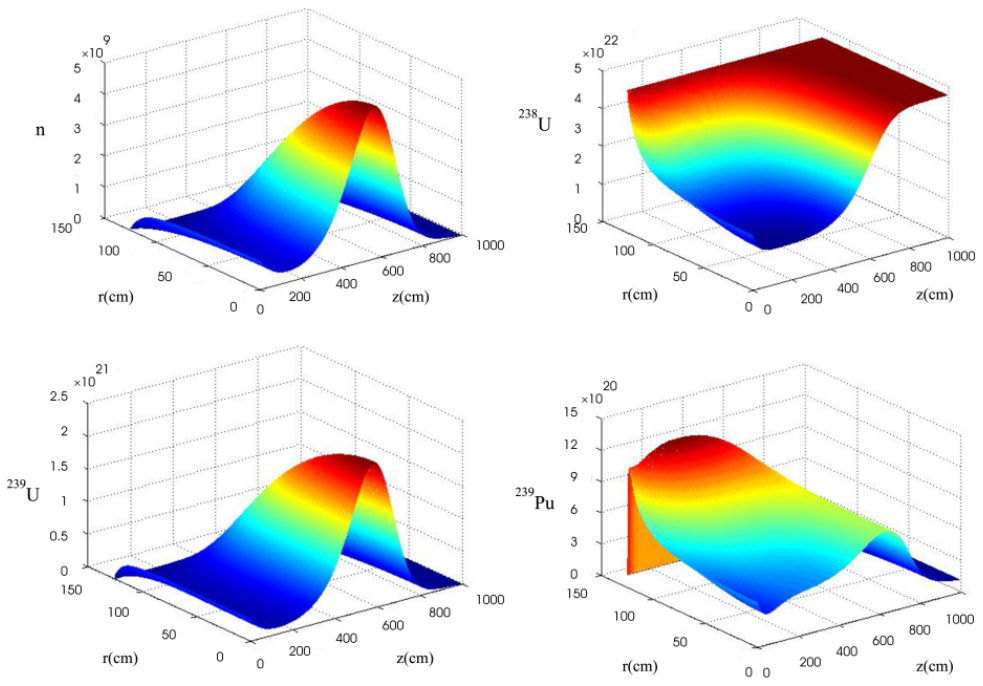


Figure 3.2: Concentration kinetics of neutrons, $^{238}U$, $^{239}U$, $^{239}Pu$ in the active zone of cylindrical reactor with radius of 125 cm and 1000 cm long at time moment of 240 days. Here $r$ is transverse spatial coordinate axis (cylinder radius), $z$ is longitudinal spatial coordinate axis (cylinder length).

The following values of constants were used for the simulation

$$\sigma_f^{Pu} = 2.0 \times 10^{-24} cm^2, \ \sigma_f^8 = 0.55 \times 10^{-24} cm^2, \quad (3.55)$$

$$\sigma_a^8 = \sigma_a^i = \sigma_a^{fragments} = 5.38 \times 10^{-26} cm^2, \qquad (3.56)$$
$$\sigma_a^9 = \sigma_a^{Pu} = 2.12 \times 10^{-26} cm^2,$$

$$\nu = 2.9,\ \tau_\beta \sim 3.3\ days,\ \upsilon_n \approx 10^9 cm\ s^{-1}, \qquad (3.57)$$
$$D \approx 2.8 \times 10^9 cm^2\ s^{-1}$$

The figure 3.2 shows the simulation data for the cylindrical reactor at the fixed moment of time of 240 days. Obviously, the spatial-temporal picture of the concentration distribution of neutrons and main nuclides in a radial half plane of a cylindrical reactor confirms the stable occurrence of self-regulating neutron fission wave.

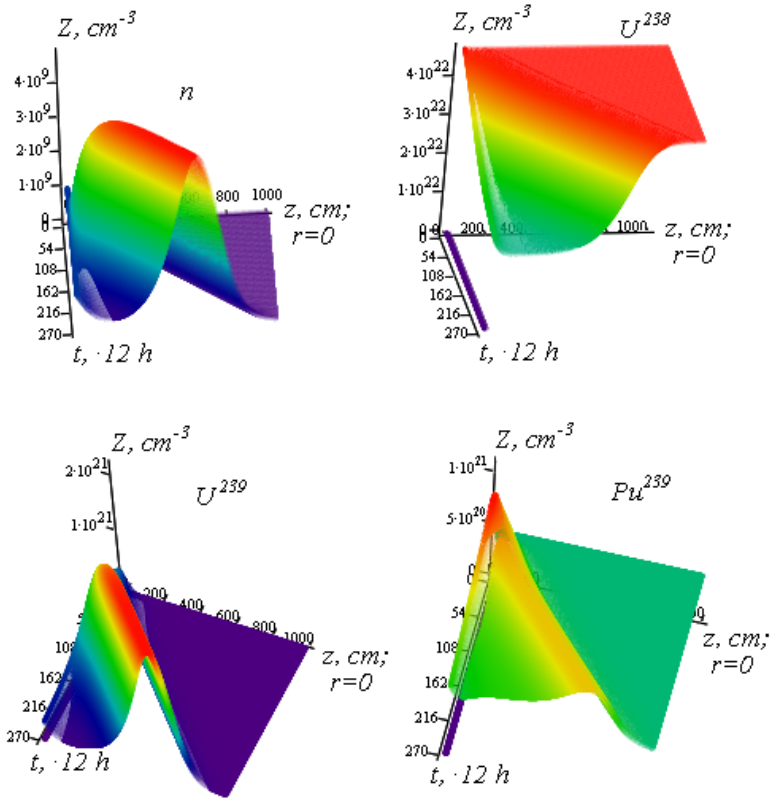


Figure 3.3: Kinetics of concentration $U_{238}$, $U_{239}$, $Pu_{239}$ and fission products on axis of the cylinder, with the initial conditions: $R = 125cm$, $Z = 1000m$, $\frac{N_{Pu}}{N_8} = \frac{1}{99}$ at the moment of time $t = 135$ days

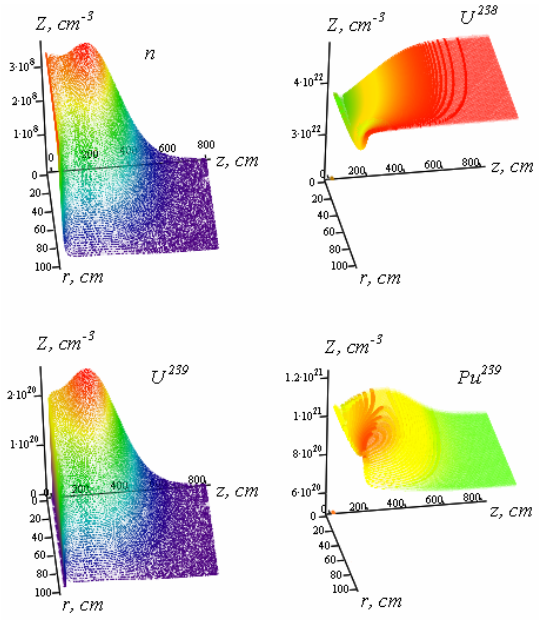


Figure 3.4: Kinetics of concentration $U_{238}$, $U_{239}$, $Pu-239$ and fission products in the cylinder, with the initial conditions: $R = 100cm$, $Z = 800m$, $\frac{N_{Pu}}{N_8} = \frac{2}{98}$, $t_1 = 110$ days and $t_2 = 210$ days

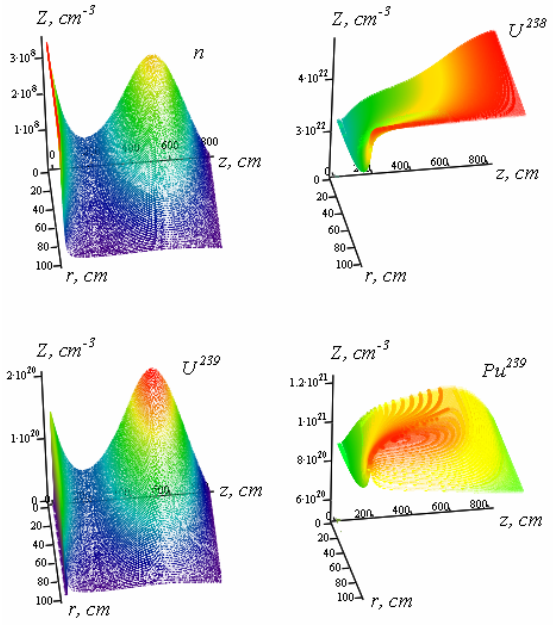


Figure 3.5: Kinetics of concentration $U_{238}$, $U_{239}$, $Pu-239$ and fission products in the cylinder, with the initial conditions: $R = 100cm$, $Z = 800m$, $\frac{N_{Pu}}{N_8} = \frac{2}{98}$, $t_2 = 210$ days

As we can see at the figures 3.1, 3.2, 3.3, 3.4 and 3.5 the simulation shows the appearance and propagating of the solitone-like nuclear burning wave in our reactor model.

Here a reasonable question inevitably comes to mind: "How did results obtained in the chapter 2 correspond to the simulation output, and how to apply in practice the conditions of nuclear burning wave origin obtained in chapter 2?"

The first of the conditions obtained in the chapter 2, the necessary one, is predetermined by ratio of equilibrium plutonium concentration and critical plutonium concentration $n_{pu}/n_{crit} > 1$ see (1.1), or, to be more precise, Bohr-Sommerfeld quantization condition see (1.31).

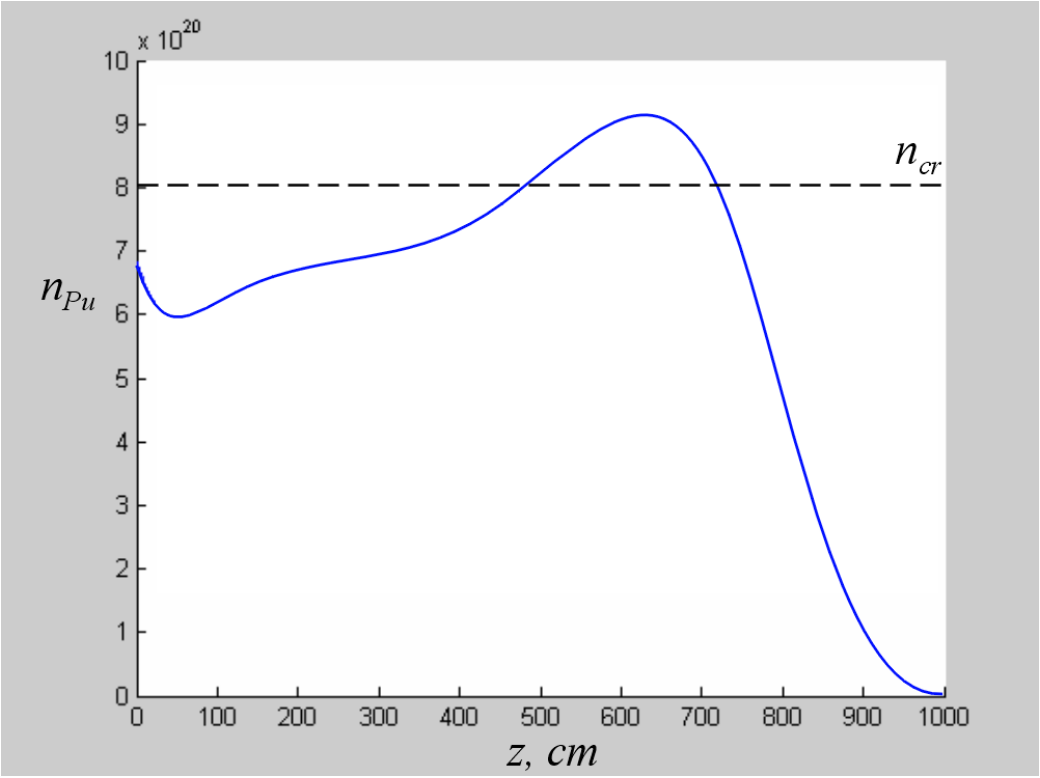


Figure 3.6: The $^{239}Pu$ concentration distribution at the cylinder axis for $n_{pu} = 0.1$ $n_{crit}^{Pu} = 0.0167$ see (1.11) at $t = 217\,days$.

Indeed, our calculations showed that in the steady-state regime, condition (1.31) is satised with accuracy up to several percent. There is no reason to expect higher accuracy because the quantization condition for the lower level is itself approximate. In figure 3.6 the plutonium concentration distribution, and plutonium critical concentration is shown. $n_{pu} = 0.1$ $n_{crit}^{Pu} = 0.0167$ are

the relative equilibrium concentration and relative critical concentration of plutonium, respectively, normalized w.r.t. $^{238}U$ (see (1.11)).

Let us check the second condition, the sufficient one, which is determined by the gaussian simplectic ensemble (GSE) statistics with respect to parameter $a_*$. For this purpose, let us analyze obtained simulation data.

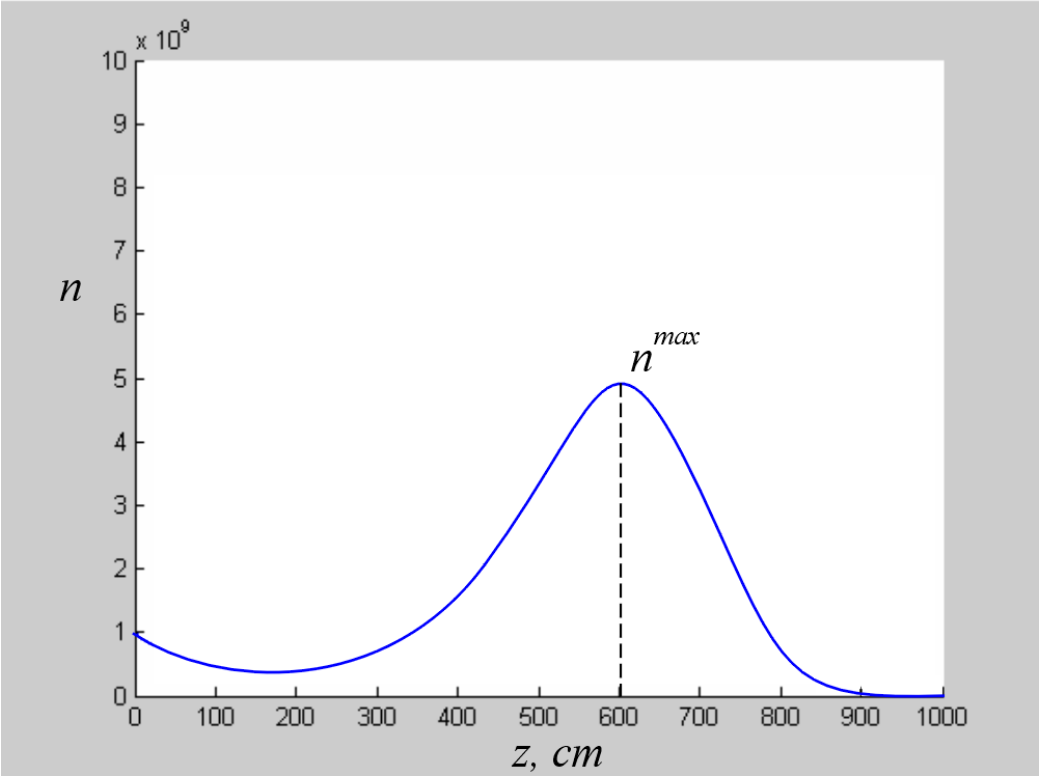


Figure 3.7: The neutrons concentration distribution at the cylinder axis at $t = 217\ days$. The wave velocity is $u_{simul} \approx 2.77$.

Figure 3.7 shows the neutrons concentration distribution at the moment of time $t = 217 days$. (The plot for 217th day was taken to simplify calculations. In this moment of time maximum concentration of neutrons – the wave crest – is in the about 600 $cm$ of cylinder length). Knowing that in 217 days the wave crest is at 600 cm of cylinder length, we can easily calculate the wave velocity

$$u_{simul} = 600\ cm/217\ days \approx 2.77\ cm\ day^{-1}.$$

Now, knowing the wave velocity and recalling an expression (2.34) we can find the value of dimensionless constant $\Lambda(a_*)$ for our wave. For $U - Pu$ fuel cycle diffusional absorption length of neutrons is $L = 5cm$, and $\tau = 3.3\ days$.

$$\Lambda(a_*) = \frac{u_{simul}\tau_\beta}{L} = \frac{2.77 \cdot 3.3}{5} = 1.8282 \tag{3.58}$$

Thus, the experimental value of parameter $\Lambda(a_*)$ obtained as a result of our computer simulation is 1.8282.

The other way to calculate the value of parameter $\Lambda(a_*)$ using the approximate equality (2.51) obtained in chapter 2, for $n_{pu} = 0.1$ $n^{Pu}_{crit} = 0.0167$ we will get

$$\Lambda(a) \sim 1.8638,$$

what corresponds to the wave velocity $u_{theor} = 2.82\, cm\, day^{-1}$.

The figure 3.8 shows theoretical (the black curve) and experimental (colored points) dependencies of $\Lambda(a_*)$ from the parameter $(a_*)$ including the result of our simulation.

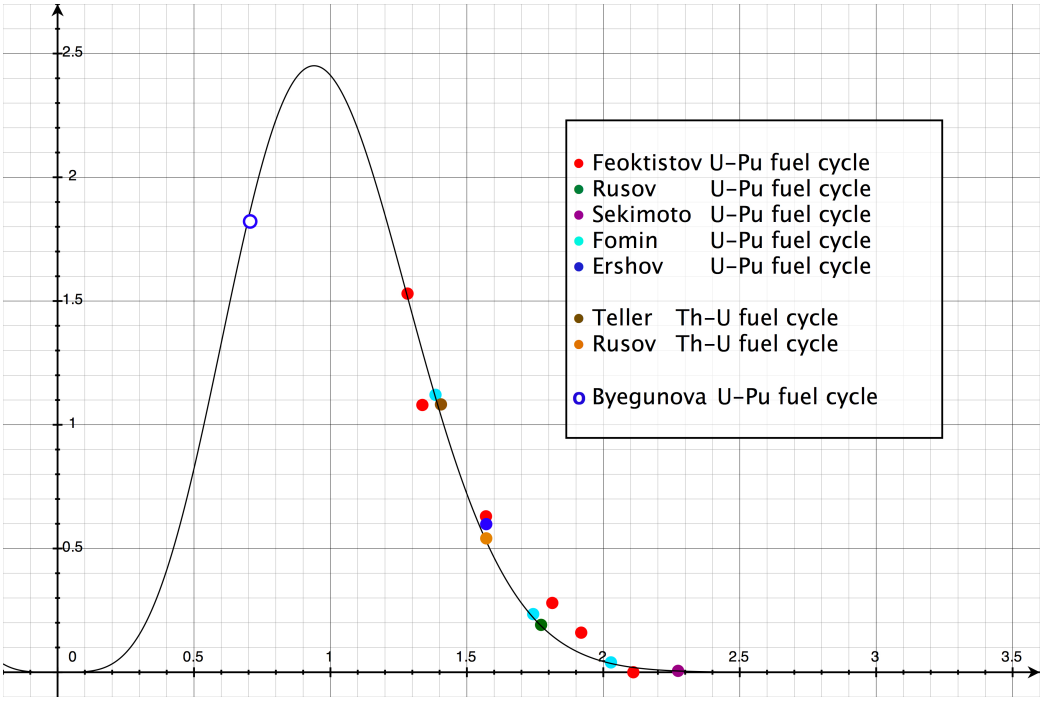


Figure 3.8: Theoretical (the black curve) and experimental (colored points) dependencies of $\Lambda(a_*)$ from the parameter $a_*$.

Thus, to test the computational scheme, we calculated the wave formation which corresponds to the formulation of Feoktistow [1] and satisfy with high accuracy both, necessary and sufficient conditions obtained in chapter 2 of this work. The simulation were done for the different initial and boundary

condition, with and without initial fuel enrichment. Critical concentration was varied. The calculated wave velocity was in good agreement with the condition (2.51).

# Chapter 4

# Nuclear georeactor of Feoktistov type

In this chapter an alternative description of the data produced in the KamLAND experiment is given. Assuming the existence of a natural nuclear reactor on the boundary of the liquid and solid phases of the Earth's core, a geoantineutrino spectrum is obtained. The assumed in chapter 3 model for the accumulation and burn-up kinetics in Feoktistov U-Pu fuel cycle is used for numerical simulations of neutron-fission wave in a two-phase $UO_2/Fe$ medium on the surface of the Earth's solid core. The $^3He/^4He$ distribution in the Earth's interior is calculated in section 4.2, which in turn can be used as a natural quantitative criterion of the georeactor thermal power. Finally, in the section 4.3 a tentative estimation of the geoantineutrino intensity and spectrum on the Earth's surface is given.

## 4.1 Hypothesis of existence of a natural nuclear reactor within the Earth's core

The problem of describing the geoantineutrino spectrum and the reactor antineutrino experimental spectrum in KamLAND [51] for antineutrino energy in the range of $\approx 2.8MeV$ makes it possible to consider the possible existence of additional energy sources in the interior of the Earth [52] to recover the geoantineutrino balance. Among such sources may be actinides, located deeper than the core-mantle (Gutenberg) boundary. While actinide concentration deep in the Earths interior during gravity differentiation has been suggested by a number of workers [53], [54], [55], [56]. The experimental results of Anisichkin et al. [57] seem the most developed in terms of providing a mechanism for formation of an actinide shell within the Earth's core.

According to these results, the chemically stable high-density actinide compounds (particularly uranium carbides and uranium dioxides) lose most of their lithophilic properties at high pressure, sink together with melted iron and concentrate in the Earth's core consequent to the initial gravitational differentiation of the planet [58]. The concentration of actinides on the surface of the Earths solidifying inner core could have taken place subsequently, i.e., from 4 to $4.5 \times 10^9$ years ago.

Self-propagating waves of nuclear burning in $^{238}U$ and/or $^{232}Th$ media could be a natural physical result of the existence of such an actinide shell in the Earths core.

Let us consider the nuclear-geophysical aspects of the initiation of the progressing wave of nuclear burning in a real $^{238}U$-medium. The two-phase $UO_2/Fe$ layer on the surface of the Earth's solid core is a natural medium for the neutron-fission wave development. Since in such a wave even depleted U can react, let us estimate the real possibility of a wave process. The critical concentration of the pure $^{239}Pu$ in the infinite $^{238}U$ medium which was calculated using the octa-group constants is about 3.7% [55], [57]. Dilution by oxygen leading to the formation of $UO_2/PuO_2$ increases the critical concentration up to $n_{crit} \sim 6.4\%$. The presence of iron in nuclear fuel pores (with typical poured concentration about 60%) will also increase the critical concentration of $^{239}Pu$ up to $n_{crit} \sim 8.2\%$ ($\rho \sim 19.5\ g/cm^3$ for $UO_2/PuO_2$ and $\rho \sim 12\ g/cm^3$ for $Fe$ were used for calculations) [19]. Non-trivial thermodynamic conditions, i.e., high temperature and pressure, might increase the critical concentration of $Pu$ up to $n_{crit} \sim 10\%$. This means that the model system of equations (3.20)-(3.26) described in Chapter 3 reflects well the main properties of a real breeding medium. Indeed, the addition of oxygen and Fe practically does not change the solutions because their neutron-absorption cross-sections are at least an order of magnitude smaller than the actinides' cross-sections.

Here a natural question arises: Why does gravitational instability not lead to the sinking of a $UO_2/Fe$ actinide mat ($\rho \sim 15\ g/cm^3$) located on the boundary of the liquid and solid phases of the Earth's core to the center of the inner core ($\rho = 12.76 - 13.09\ g/cm^3$ [60])?

This can be caused by following reasons:

1. Despite the fact that the Earth's inner core was discovered 60 years ago, some seismologists, analyzing waves penetrating the inner core, are still not sure, whether it is solid or liquid, or whether it is ″a matter with new properties″which are needed for its description [62]. They are practically convinced that the inner core (also called G-core) is solid; to prove this they register shear-waves (so called PKJKP-

waves) which penetrate into the G-core. The only paper [63] on the detection of these PKJKP-waves has not been widely acknowledged by seismologists. Tromp [68] noted that PKJKP has become something of a "Holy Grail"of the body-wave seismology community.

As long as PKJKP-wave existence, and consequently, the experimental value of the inner core density do not have a convincing proof, it can be assumed that the model values of the actinide medium ($\rho \sim 15\ g/cm^3$) and the inner core ($12.76 - 13.09\ g/cm^3$ [61]) are equal within an error of 20%.

2. Recently, a large number of seismic traces (310,000 [64]) passing through the core have been analyzed and as a result new interesting properties of the core have been found:

   The first concerns the discovery of inner core anisotropy, or that the velocity of PKiKP-waves crossing the core is somewhat higher along the Earth's rotation axis than in the equatorial plane. Most researchers consider this anisotropy is due to a relatively thin layer near the inner core boundary [62]. By using travel-time data of 313,422 traces of PKiKP-waves (registered by 2335 seismic stations from 26377 earthquakes), Su and Dziewonski [64] obtained a three-dimensional image of the region generating the inner core anisotropy. They found this region constitutes only a few percent of the inner core volume, is concentrated in a layer at the inner-outer core boundary, and is about 200-300 km thick. Later Russian geophysicists [65], [66] found, based on the information of the PKiKP-wave registration from the nuclear explosions at small epicentral distances, that the actual layer thickness is much less perhaps in the range 2-4 km. As they showed, other characteristics of the inner core are also significant. For example, the seismic data are best explained by a mosaic structure of the inner cores surface. Such a mosaic can be composed of patches, in which the transition from the solid inner to the liquid outer core includes a thin partially liquid layer interspersed with patches containing a sharp transition. Moreover the density of 2.2 km thick layer corresponds to the bottom of the outer core ($12.1663\ g/cm^3$) and the top of the inner core ($12.7636\ g/cm^3$) for liquid and solid layers respectively, while P-wave velocity is $12\ km\, s^{-1}$. See figure 4.1.

   Such a layer of increased density, if its existence is confirmed, might be considered as a platform for actinide concentration (in particular, for carbides and dioxides of U and Th). In this case, the actinide shell constituting a two-phase $UO_2/Fe$ layer on the surface of the solid

(iron) core in which iron ($\rho \sim 12.0\ g/cm^3$) is located in the pores of the nuclear fuel ($\rho \sim 19.5\ g/cm^3$) at "poured"concentration of about 90%, does not sink to the center of the inner core ($\rho = 12.76 - 13.09\ g/cm^3$ [60]), since it has a density $\rho \sim 12.75\ g/cm^3$. This in turn leads to an increase of the critical concentration up to $n_{crit} \sim 10 - 12\%$. Obviously, such a modification of the two-phase layer density and of the critical concentration does not change our previous simulation results on Feoktistov's neutron-fission wave.

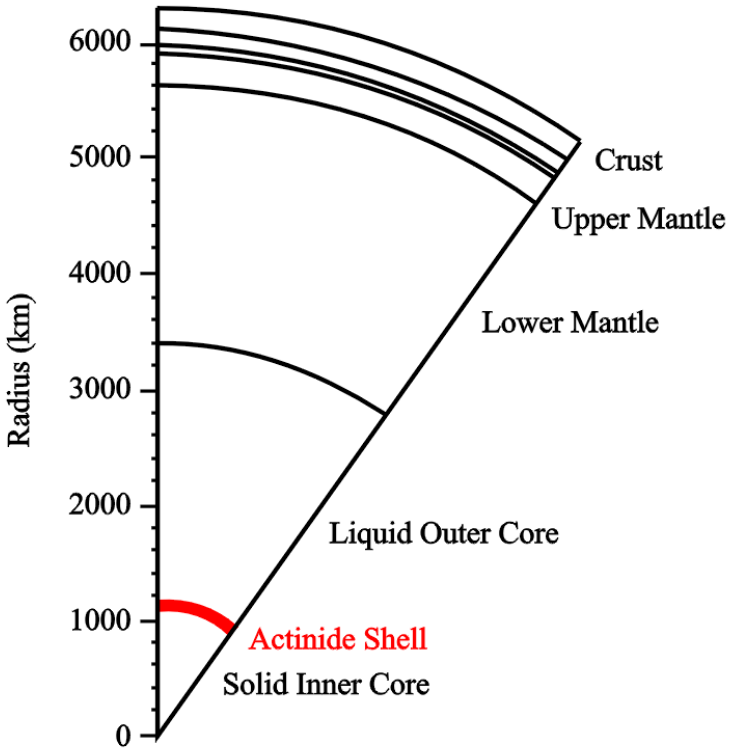


Figure 4.1: Schematic representation of internal structure of the Earth as a whole with the actinide shell on the boundary of the liquid and solid phases of the Earths core, where a natural nuclear reactor of Feoktistov or/and Teller type may exist.

A question of no lesser importance is the following: Where do the neutrons for the initiation of the chain reaction come from?

In spite of active discussions of the possibility of chain nuclear reactions

in the interior of the Earth and other planets in numerous papers (starting with Kuroda [67] and including Driscoll [53], Herndon [54], and Anisichkin et al. [55]), the question of natural external neutron sources which might locally start the mechanism of nuclear burning remains open and requires serious joint efforts of theorists. However, taking into account the difficulties concerning the explanation of the mechanism of neutron-fission wave initiation, it is possible to take an alternative route and to try to find geophysical events in the thermal history of the Earth which directly or indirectly demonstrate the existence of slow nuclear burning. Note that these events should be quite recent so that at the present time they are characterized by a lowered, i.e., subcritical concentration of odd isotopes of U and Pu. Let us consider below an example of such a geophysicochemical paleoevent.

Thus, in the thermal history of the Earth, some physicochemical signals should be detectable which would confirm the existence of spontaneous reactor-like reactions of the Feoktistov uranium-plutonium fuel-cycle-type and/or Teller thorium-uranium fuel-cycle-type on the boundary of liquid and solid phases of the Earth's core.

The anomalous $^3He/^4He$ ratio distributions in the Earth's interior are good candidates for such signals.

## 4.2 $^3He/^4He$ distribution in the Earth's interior as a quantitative criterion of georeactor thermal power.

Fundamental models of the origin of the anomalous $^3He$ concentration and $^3He/^4He$ ratio distribution in the Earths interior have serious contradictions. For example, D. L. Anderson et al. [60] has pointed out: "The model whereby high $^3He/^4He$ is attributed to a lower-mantle source, and is thus effectively an indicator of plumes from the lower mantle, is becoming increasingly untenable as evidence for a shallow origin for many high-$^3He/^4He$ hotspots accumulates. Shallow, low-$^4He$ models for high-$^3He/^4He$ are logically reasonable, cannot be ruled out, and need to be rigorously tested if we are to understand the full implications of this important geochemical tracer".

Let us assume that $^3He$ is produced by a natural reactor located on the boundary of the liquid and solid phases of the Earths core. At the same time, $^4He$ is produced both by the georeactor and due to the decay of $^{238}U$ and $^{232}Th$ in the crust, in the upper (depleted) and in the lower mantle of the Earth.

To determine the $^4He$ accumulation rate, the total and partial radiogenic

heat production rates of uranium $H_U$ and thorium $H_{Th}$ in the crust, in the upper (depleted) mantle and directly in the mantle is used. These rates have been obtained in [69] in the framework of the O'Nions geochemical evolution model [87].

It is obvious that the difference between the real heat (which is produced now in the Earth) and the calculated radiogenic heat [70] is very significant even with allowance for the high thermal inertia of the Earth $\tau_E \approx 10^9 years$ [71]. D. L. Anderson refers to this difference as the missing heat source problem and summarizes the situation in the following words: Global heat flow estimates range from 30 to $44TW$. . . Estimates of the radiogenic contribution (from the decay of $U$, $Th$ and $K$ in the mantle), based on cosmochemical considerations, vary from 19 to 31 TW. Thus there is either a good balance between current input and output. . . or there is a serious missing heat source problem, up to a deficit of 25 TW. . . [60]. In any case, the decisive argument in favor of one or the other paradigm can be only experimental (trivial as it may seem). Since the radiogenic component is essentially based on cosmochemical considerations which, as it is well known, are quite uncertain, only a direct determination such as the geoneutrino detection or the indirect determination of $^3He/^4He$ ratio depth distribution are significant. In other words, if the amount of radioactive elements can be determined by means of geoneutrinos and/or the $^3He/^4He$ ratio, an important ingredient of the Earths energetics will be established [72].

A source of additional thermal power (designated as $H_f$) can be provided by nuclear burning of an actinide shell which consists of chemically stable and highdensity actinide compounds. Obviously, if the additional thermal power $H_f$ is generated only by the radiogenic heat $H_\alpha$, there will be no contribution of the actinide shell to the geoantineutrino integral intensity. In order to obtain the actual contribution of the actinide shell we assume that the energy release power $H_f$ of the actinide shell (as a nuclear energy source) is substantially higher than the partial power of the radiogenic heat $H_\alpha$, produced by $^{238}U$ and $^{232}Th$ radioactive chains, i.e., $H_\alpha \ll H_f$.

For simplicity, let us consider the actinide shell as a $UO_2/Fe$ two-phase layer on the surface of the solid (iron) core. Iron ($\rho \approx 12.0\ g\ cm^3$ ) with poured concentration of $\sim 90\%$ is contained in the pores of the nuclear fuel ($\rho \approx 19.5\ g\ cm^3$) and decreases the density of the two-phase layer down to $\rho \approx 12.75\ g\ cm^3$. Let us assume that $H_\alpha \sim 0.1 \div 0.5\ TW$. If the two-phase actinide medium with the total mass of natural uranium

$$M(U) = \frac{H_\alpha}{\epsilon(U)} \sim 10^{15} kg, \tag{4.1}$$

where $\epsilon(U) \cong 0.95 \times 10^{15} kg^{-1}$represents a continuous homogeneous shell

on the surface of the Earth's solid core, its thickness will be $\sim 1 - -5cm$. Apparently, it is more correct to picture such a two-phase actinide medium as an inhomogeneous shell which represents a stochastic web of actinide rivers and lakes located in the valleys of rough surface [60], [66] of the Earth's solid core.

Below we consider a georeactor model of the origin of $^3He$ anomalous concentrations and the $^3He/^4He$ ratio distribution in the Earth's interior. Pending an experimental confirmation of the existence of a georeactor, this model naturally explains the so-called helium paradoxes [60].

Let us assume that the reactor power is P = 30 TW. Further calculations in the framework of georeactor model will show that this value is the most adequate estimation of the reactor power. In this case, the constancy of the anomalous isotopic composition of the mantle $He$ is explained by the properties of the fast ($\sim 1MeV$) neutroninduced fission of $^{239}Pu$ in the neutron fission wavefront. The $^3He$ production probability is mainly determined by the probability of $^3H$ production as a fission fragment of $^{239}Pu$ triple fission. This probability is about $\sim 1.6\times10^{-4}$ [73]. Hence the total accumulation rate of $^3He$ produced due to tritium $\beta$-decay ($T_{1/2} \sim 12.3\ years$) is approximately

$$N_{fB}^{30}(^3He) \sim 1.6 \times 10^{-4} n_f \approx 1.6 \times 10^{-4} \frac{P}{E_f} = 14.8 \times 10^{19} s^{-1}, \qquad (4.2)$$

where $E_f = 210.3MeV$ is the average energy per $^{239}Pu$ fission.

On the other hand, $^4He$ accumulation rate due to the $^{238}U$ radioactive decay in the $UO_2/Fe$ actinide web (by hypothesis of $H_\alpha^U \approx 0.1/0.5TW$) has the form

$$N_{fB}(^4He) \sim 8\frac{H_\alpha^U}{Q_\alpha^U} = 8\frac{(0.1-0.5)\times10^{15}}{51.7\times1.6\times10^{-13}} \approx (9.7-48.5)\times1022s^{-1}. \quad (4.3)$$

Therefore the helium ratio $R_{fB}$ in the $UO_2/Fe$ actinide web (located on the boundary of solid and liquid phase of the Earths core) is

$$R_{fB}^{30} = \frac{N_{fB}^{30}(^3He)}{N_{fB}(^4He)} \approx (0.3-1.6)\times10^{-3} \qquad (4.4)$$

Here a number of physical assumptions which allow us (without loss of generality) to get rough estimations of the helium ratio $R$ for different geospheres of the Earth are used. A simplified consideration of helium isotopes transport is connected with the assumption of the radial drift dominating over the diffusion; at the same time the average radial drift speeds of $^3He$ and $^4He$ areapproximately equal in the gravity fields of different geospheres

of the Earth. The average cross sections (or probabilities) for these isotopes to be captured by different traps in the Earth are also approximately equal but are so small that we can neglect the decrease of these isotopes' flows in the direction of radial drift.

Now we can estimate the ratio $R$ in the mantle and in the crust. The $^4He$ accumulation rate due to $^{238}U$ and $^{232}Th$ radioactive decay in the mantle (minus the depleted upper mantle) [69] is approximately

$$N_{M-UM}(^4He) \sim 8\frac{H_U}{Q_\alpha^U} + 6\frac{H_{Th}}{Q_\alpha^{Th}} \approx 9.93 \times 10^{24} s^{-1} \tag{4.5}$$

where $Q_\alpha^U = 51.7\ MeV$ and $Q_\alpha^{Th} = 42.8\ MeV$ are the decay energies

$$^{238}U \rightarrow {}^{206}Pb + 8^4He + 6e + 6\tilde{\nu} \tag{4.6}$$

$$^{232}Th \rightarrow {}^{208}Pb + 6^4He + 4e + 4\tilde{\nu} \tag{4.7}$$

Thus, taking into account (4.2), (4.3), and (4.5), the $^3He/^4He$ in the mantle (minus the depleted upper mantle) $R_{M-DUM}$ due to Feoktistov fuel-cycle georeactor ($P = 30TW$) is approximately

$$R_{M-DUM}^{30} = \frac{N_{fB}^{30}(^3He)}{N_{M-DUM}(^4He) + N_{fB}(^4He)} \cong \frac{N_{fB}^{30}(^3He)}{N_{M-DUM}(^4He)} \approx 11.15R_a \tag{4.8}$$

where $Ra = 1.38 \times 10^{-6}$ is the atmospheric $^3He/^4He$ ratio.

In a similar manner, the average values of $^3He/^4He$ for the upper (depleted) mantle $R_{DUM}$ and for the crust $R_{crust}$ are respectively

$$R_{DUM}^{30} = \frac{N_{fB}^{30}(^3He)}{N_{DUM}(^4He) + N_{M-DUM}(^4He) + N_{fB}(^4He)} \approx 9.05R_a, \tag{4.9}$$

$$R_{crust}^{30} = \frac{N_{fB}^{30}(^3He)}{N_{crust}(^4He) + N_{DUM}(^4He) + N_{M-DUM}(^4He) + N_{fB}(^4He)} \tag{4.10}$$

At the same time the statistical analysis of the depth distribution of helium isotopes made on t he basis of numerous experimental data has shown that the average value of $^3He/^4He$ for the crust $R_{crust}$ and for the upper mantle $R_{DUM}$ are equal $R_{crust} = (7.47 \pm 1.95)R_a$ and $R_{DUM} = (9.14 \pm 3.59)R_a$, whereas values $R_{M-UM} = (11 - 15)R_a$ are commonly attributed to deep mantle plumes and are "indicative of lower mantle involvement"[61]. It is obvious, that theoretical estimates (26) (28) practically coincide with the experimental data.

Thus, if georeactor power is 30 $TW$, the average values of $^3He/^4He$ for crust, the upper mantle, the mantle (minus the depleted upper mantle) and the thin layer on the boundary of liquid and solid of the Earth's core $R_{fB}$ become

$$\begin{array}{lcl} R^{30}_{crust} & \approx & 7.6R_a,\ R^{30}_{DUM} \approx 9.1R_a,\ R^{30}_{M-DUM} \approx 11.2R_a, \\ R^{30}_{fB} & \approx & (220 - 1160)R_a \end{array} \tag{4.11}$$

which are in close agreement with the corresponding average values of the experimental helium ratios [61]. Finally, we consider some lower layers of the undepleted mantle ($M - DUM$) which we call the lower mantle ($LM$) and which are defined as its lower part with characteristic volume of

$$V_{LM} \cong (0.2 - 0.3)V_{M-DUM}.$$

Now it is possible to obtain the average value of $^3He/^4He$ RLM for the lower mantle

$$R^{30}_{LM} = \frac{V_{M-DUM}}{V_{LM}} R^{30}_{M_DUM} = (30 \div 50)R_a, \tag{4.12}$$

which agrees with the well known experimental data by [74] and [76]. Thus, if $^3He$ indeed has a georeactor origin, the $^3He/^4He$ ratio distribution in the Earth's interior is a natural quantitative criterion of the georeactor thermal power. Moreover, if the georeactor exists, the corresponding $^3He/^4He$ ratio distribution is predetermined not only by the georeactor thermal power but also by the corresponding distribution of $^{238}U$ and $^{232}Th$ in the crust and in the mantle [69].

## 4.3 Contribution of georeactor antineutrinos to the antineutrino spectrum of the Earth. Comparison with KamLAND experimental data.

Obviously, the geoneutrino spectrum is an unambiguous test for the existence of a georeactor in the Earth's interior (especially at energies $> 3.272\ MeV$, where only fission geoneutrinos are detected, i.e., geoneutrinos produced due to the actinide fission). In this sense, the idea of a georeactor is fruitful not only for the understanding of the physical essence of the so-called helium paradoxes [60], but at the same time, it effectively solves the problem of describing the geoantineutrino spectrum and the reactor antineutrino

experimental spectrum in KamLAND in the range of antineutrino energy $\sim 2.8\ MeV$.

The $^{239}Pu$ fission rate in neutron-fission wave front is

$$\eta_f = P/E_f \approx 8.9 \times 10^{-23}\ fission\ s^{-1} \tag{4.13}$$

where $E_f = 210.3\ MeV$ is the average energy per $^{239}Pu$ fission.

Hence, a crude estimation of the contributions to the total antineutrino integral intensity on the Earths surface which from two diametrically opposite points on the boundary of liquid and solid of the Earths core and which are produced by the burning wave front in the $UO_2/Fe$ actinides web has the form

$$\Phi_{\overline{\nu}} = \frac{1}{4\pi(R_\oplus \pm r_N)^2}\eta_f \mu_{\overline{\nu}} \tag{4.14}$$

$$= \begin{cases} 0.72 \times 10^6\ cm^{-2}s^{-1}, & if\ R_\oplus + r_N, \\ 1.56 \times 10^6\ cm^{-2}s^{-1}, & if\ R_\oplus - r_N \end{cases} \tag{4.15}$$

where $\mu \approx 5.37$ is the number of antineutrinos per $^{239}Pu$ fission; $R_\oplus \approx 6400\ km$; $r_N$ $1200\ km$.

Using the method of calculation of partial and total $\beta$, $\tilde{\nu}$ energy-spectra of radioactive nuclides explained in detail in [69], the partial $d\Phi_{\tilde{\nu}}/dE(^{238}U)$, $d\Phi_{\tilde{\nu}}/dE(^{232}Th)$, $d\Phi_{\tilde{\nu}}/dE(^{40}K)$ (Figure 4.2) were constructed, $d\Phi_{\tilde{\nu}}/dE(^{239}U)$ (Figure 4.3) [75] and total antineutrino energy spectra (without oscillations) of the Earth $d\Phi_{\tilde{\nu}}/dE(^{238}U{+}^{232}Th{+}^{40}K{+}^{239}Pu)$ [75] (Figure 4.4). The partial contributions were previously normalized to the corresponding geoantineutrino integral intensity on the Earth's surface [69], [75]

The theoretical form of measured total energy spectrum $dn_{\tilde{\nu}}/dE$ is

$$\frac{dn_{\tilde{\nu}}}{dE} = \varepsilon N_p \sum_i p_i(E_{\tilde{\nu}}, L)\frac{d\lambda^i_{\tilde{\nu}}}{dE}\sigma_{\nu p}(E_{\tilde{\nu}})\Delta t,\ MeV^{-1}, \tag{4.16}$$

where the probability of neutrino oscillation can be written for two neutrino flavours as follows

$$p(E_{\tilde{\nu}}, L) \cong 1 - sin^2 2\theta_{12} \sin^2\left(\frac{1.27\Delta m^2_{12}[eV^2]L[m]}{E_{\tilde{\nu}}[MeV}\right), \tag{4.17}$$

where $d\lambda_{\tilde{\nu}}/dE \equiv d\Phi_{\tilde{\nu}}/dE$ at $E_{\tilde{\nu}} \geq 1.804\ MeV$, $\sigma_{\nu p}$ is the antineutrino-proton interaction cross-section for the inverse $\beta$-decay reaction with the corresponding radiation corrections; $L$ is the distance between the source

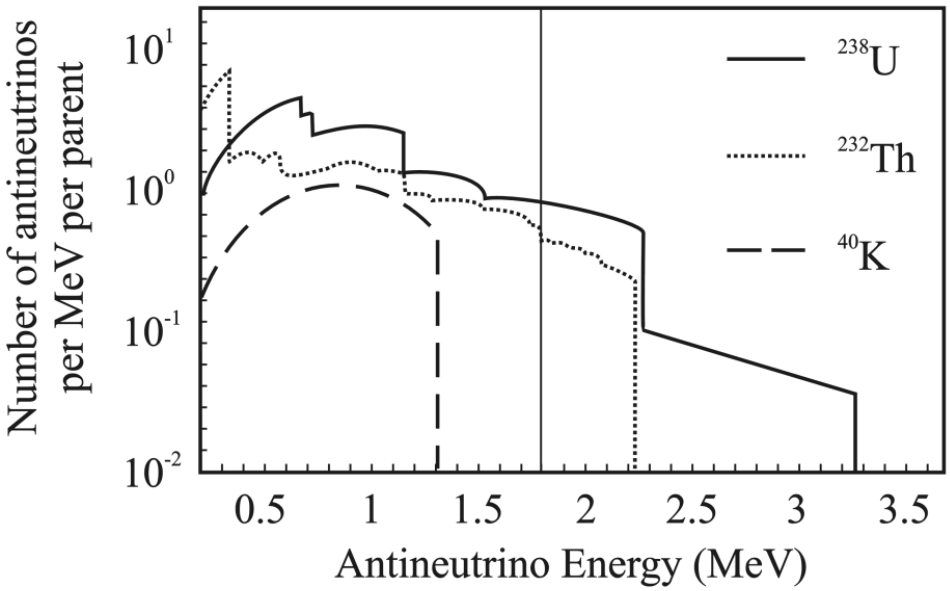


Figure 4.2: Expected $^{238}U$,$^{232}Th$, and $^{40}K$ decay chain electron antineutrino energy distributions. KamLAND detector can only detect electron antineutrinos to the right of the vertical dotted line.

and the detector; $\Delta m^2_{12} \equiv |m^2_2 - m^2_1|$ is the mass squared difference, $\theta$ is the mixing angle.

It is clear that the standard calculations of the true antineutrino spectrum and of the oscillation parameters $(\Delta m^2_{12}, \sin^2 2\theta_{12})$ in the KamLAND-experiment have to be recalibrated, since the reactor geoantineutrinos are in the spectral region of prompt energy above 2.6 $MeV$. In other words, the standard methods of obtaining consistent estimates (e.g., the maximum-likelihood method) normally used for the determination of the oscillation parameters $(\Delta m^2_{12}, \sin^2 2\theta_{12})$ must take into account one more reactor, or, more specifically, account for the antineutrino spectrum of georeactor with the power of 30 TW which is located at a depth of $L \sim 5.2 \times 10^6$ $m$. The results presented below show that the hypothesis of the existence of a georeactor with the power of 30 TW on the boundary of liquid and solid phases of the Earths core does not conflict with the experimental data.

Let us proceed as follows: If CPT invariance is assumed, the probabilities of the $\nu_e \to \nu_e$ and $\tilde{\nu}_e \to \tilde{\nu}_e$ oscillations should be equal at the same values $L/E_\nu$. At the average distance $L \sim 180$ $km$ of the Japan reactors from the KamLAND detector and at the typical energies of a few MeV of the reactor

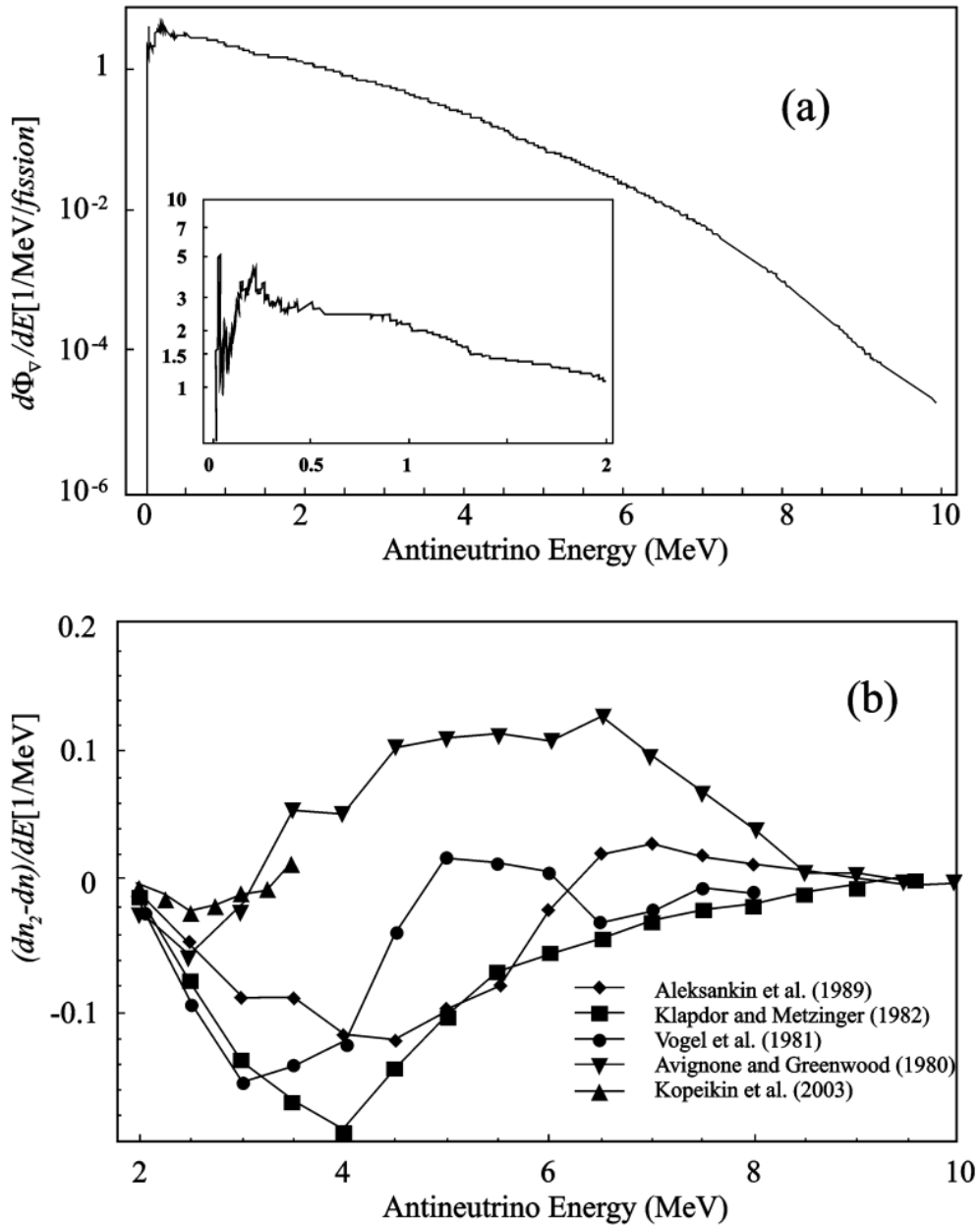


Figure 4.3: (a) Calculated partial antineutrino spectra of $^{239}Pu$ normalized to nuclear decay and (b) its deviation from theoretical spectra obtained by different authors in the energy range of $1.8 - 10.0\ MeV$.

$\tilde{\nu}_e$, the experiment has near optimal sensitivity to the $\Delta m^2$ value of the large mixing angle (LMA) solar solution [77]. Furthermore, it is known that the

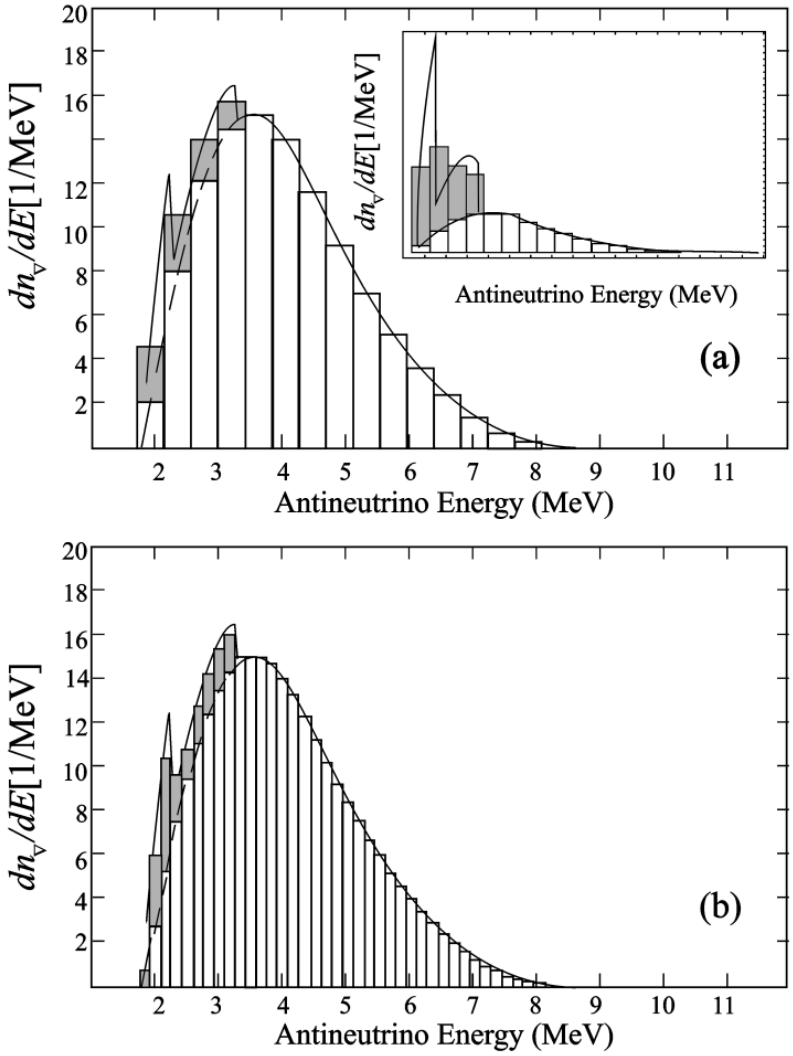


Figure 4.4: Calculated total geoantineutrino spectrum of the Earth (taking into account the reactor power of 30 TW) in KamLAND detector. Solid line is ideal spectrum, histogram is spectrum with the energy bin of (a) 0.425 MeV and (b) 0.17 MeV. Insert shows the same spectrum but for reactor power of 2.5 TW.

mass squared difference indicated by the solar neutrino data is $\sim 6\times10^{-5}\ eV^2$ and the mixing is large but not maximal, $tan^2\theta \sim 0.4$ [78].

Since the sensitivity in $\Delta m^2$ can be dominated by the spectral distortion in the antineutrino spectrum, whereas the solar neutrino data provide the best constraint on $\theta$, within the framework of further analysis, we can assume

(basing on CPT theorem) that the angle of mixing in KamLAND -experiment is determined by the "solar"equality $tan^2\theta_{12} = 0.4$ or $\sin^2 2\theta_{12} = 0.83$. Therefore, to calculate the integral intensity of the reactor geoneutrinos, the following approximation for survival probability $p_{i=Pu}$ in (4.17) was also used

$$p_{i=Pu}(E_{\tilde{\nu}|}, L) = 1 - 0.5\sin^2 2\theta_{12} \cong 0.59, \tag{4.18}$$

$$\tag{4.19}$$

$$L \gg L_{osc}[m] = \frac{2.48E_{\tilde{\nu}}[MeV]}{\Delta m^2_{12}[eV^2]}, \tag{4.20}$$

where $L_{osc}$ is the oscillation length, $L \sim 5.2 \times 10^6\ m$ is the distance apart the boundary of liquid and solid phases of the Earths core and detector.

Then, using equation (4.16), it is possible to show that in the first KamLAND [79] the integral intensity of the reactor geoantineutrinos ${}^{Pu}n_{\tilde{\nu}}$ on the Earth's surface, taking into account equation (4.20), is

$$\begin{aligned} {}^{Pu}n_{\tilde{\nu}} &= p_{i=Pu}\varepsilon N_p \Delta t \int\limits_{E=1.804}^{\infty} \frac{d\lambda_{\tilde{\nu}}(Pu)}{dE}\sigma_{\nu p}dE \\ &= p_{i=Pu}[12.72(Pu)|_{E_\nu \le 3.272} + 30.24(Pu)|_{E_\nu > 3.272}] \\ &= 7.50|_{E_{\tilde{\nu}} \le 3.272} + 17.84|_{E_{\tilde{\nu}} > 3.272}, \end{aligned} \tag{4.21}$$

where $\varepsilon \approx 0.783$ is the detection efficiency; $N_P = 3.46 \times 10^{31}$ is the number of protons in the detector sensitive volume; $\Delta t = 1.25 \times 10^7$ is the exposure time [79]; $\sigma_{\nu p}$ is the antineutrino-proton interaction cross-section of inverse the $\beta$-decay reaction with the corresponding radiation corrections [80].

In the domain of the prompt energies $E_{prompt} > 2.6\ MeV$ (see figure 4.5(a) the ratio of the "true"flux of the reactor antineutrinos $N_{obs}$ is determined, which is equal to the difference between the measured flux $N_{full}$ and the background flux caused by the $^{13}C(\alpha, n)^{16}O$ reaction [51], $N_C$ and the reactor geoneutrinos ${}^{Pu}n_{\tilde{\nu}}$ to expected flux $N_{expected}$ in KamLAND-experiment. Taking into account that in the first KamLAND-experiment $N_{ful}l = 54$, $N_{expected} = 86.8 \pm 5.6$ [79], $N_C \cong 2$ (see figure 4.5), ${}^{Pu}n_{\tilde{\nu}}$ $(E_{prompt} > 2.6\ MeV) = 17.84$ (see (4.21)), the ratio $\Re$ is

$$\begin{aligned} \Re &= \frac{N_{obs}}{N_{expected}} = \frac{N_{full} - N_C - {}^{Pu}n_{\tilde{\nu}}|_{E_{prompt}>2.6}}{N_{expected}} \\ &\cong 0.394 \pm 0.096(stsat) \pm 0.042(syst). \end{aligned} \tag{4.22}$$

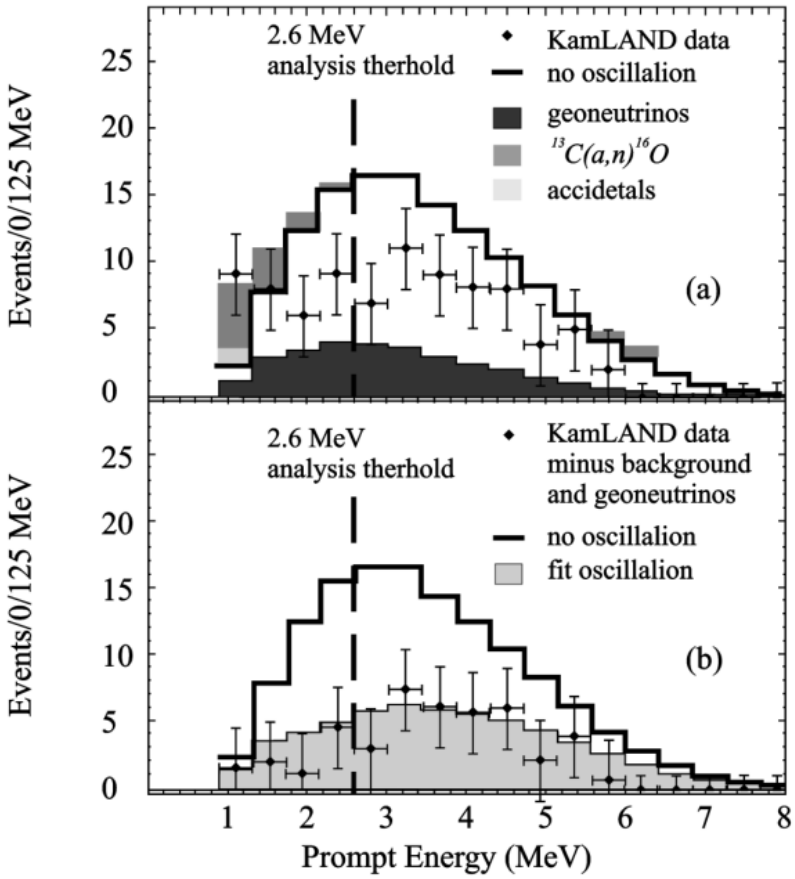


Figure 4.5: (a) Energy spectrum of the observed prompt events (solid black circles with error bars) [79], along with the expected no oscillation spectrum (histogram, with events from $^{13}C(a,n)^{16}O$ reactions and accidentals shown) and calculated total geoantineutrino oscillation spectrum in KamLAND detector (shaded histogram). (b) Energy spectrum of the observed prompt neutrinos (solid circles with error bars), which is equal to difference between the energy spectrum of the observed prompt events (solid black circles with error bars), background and total geoantineutrino (oscillation) spectrum (shaded histogram). Fit oscillation (lower shaded histogram) describing the expected oscillation spectrum from Japans reactor. Vertical dashed line corresponds to the analysis threshold at 2.6 MeV.

The probability that the KamLAND result is consistent with the no disappearance hypothesis is less than 0.05%. Figure 4.6 shows the ratio $\Re$ for KamLAND as well as for the previous reactor experiments as function of the average distance from source. On the same figure the shaded region indicates

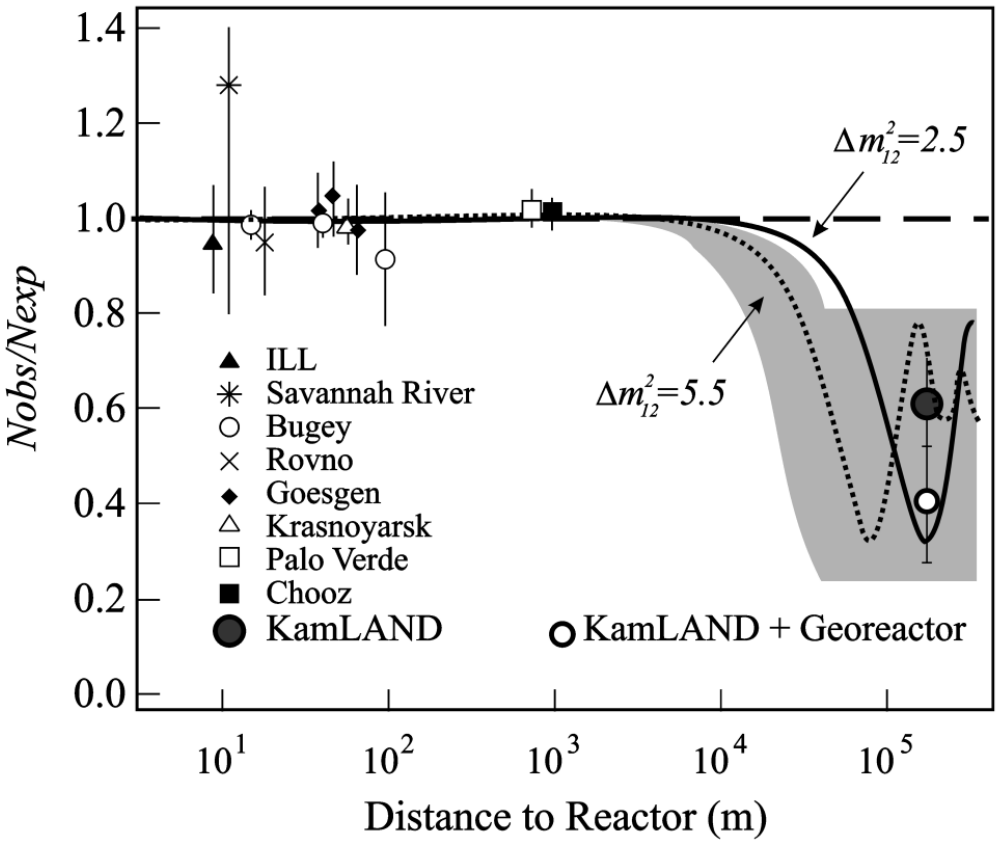


Figure 4.6: Ratio $\Re = N_{obs}/N_{expected}$ of measured to expected flux from reactor experiments [85]. The solid dot [79] and circle is the KamLAND point plotted at a flux-weighted average distance (the dot size and circle size is indicative of the spread in reactor distance). The shaded region indicates the range of flux predictions corresponding to the 95% CL LMA region found in a global analysis of a solar neutrino data [81]. The thick curve corresponds to $\sin^2 2\theta_{12} = 0.83$ and $\Delta m^2_{12} = 2.5 \times 10^5\, eV^2$. The dotted curve corresponds to $\sin^2 2\theta_{12} = 0.833$ and $\Delta m^2_{12} = 5.5 \times 10^5\, eV^2$ [81] and is representative of recent best-fit LMA predictions while the dashed curve shows the case of small mixing angle (or no oscillation). Adapted from [79].

the range of flux predictions corresponding to the 95% confidence level(CL). LMA region found in a global analysis of the solar neutrino data [81]. It turns out that only those values which are in interval $\Delta m^2_{12} \approx (2 \div 4) \times 10^{-5}\, eV^2$. Figure 4.7 are permitted for the given value of $\Re$ (4.23) and the fixed angle of mixing ($sin^2 2\theta_{12} = 0.83$). For the following calculations we chose the value

of $\Delta m^2_{12} = 2.5 \times 10^5\ eV^2$. The shape of the antineutrino spectrum for $\Re$ given by (4.23) (see the insert in figure 4.7) calculated for first KamLAND-experiment at the fixed angle of mixing and different $\Delta m^2_{12}$ from the interval $(2-4) \times 10^{-5}\ eV^2$ has been used as a rule of selection for this value.

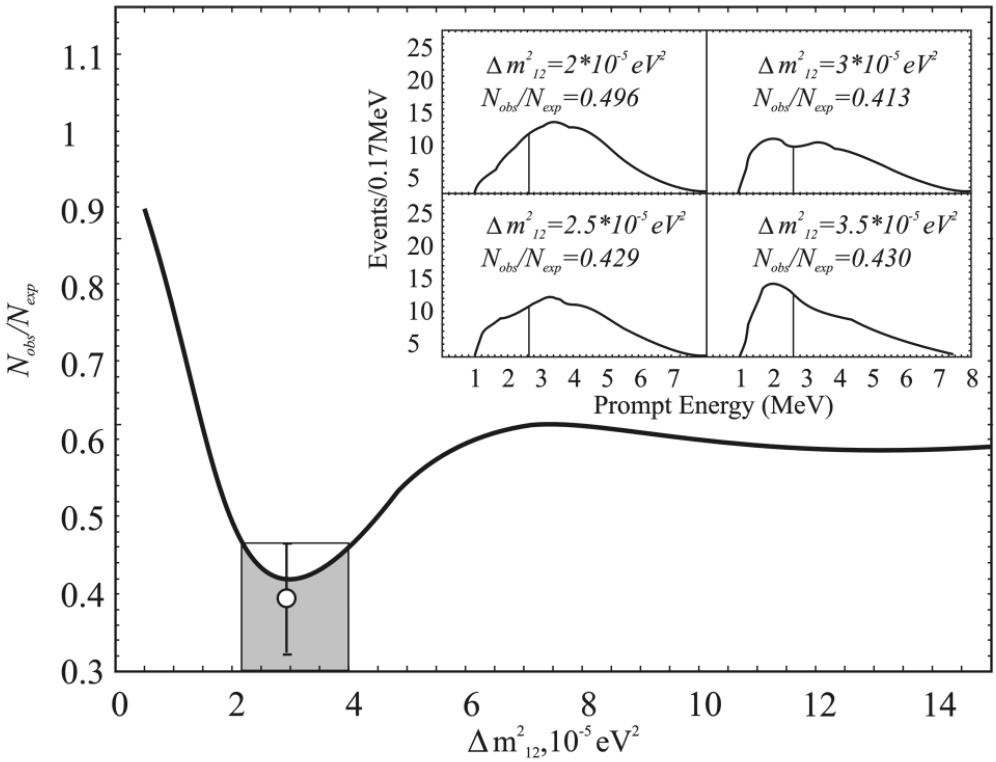


Figure 4.7: The ratio $\Re = N_{obs}/N_{expected}$ of measured to expected flux in KamLAND-experiment at fixed angle of mixing $\sin^2 2\theta_{12} = 0.83$ but at the different mass squared differences. The insert: theoretical antineutrino spectrums in KamLAND experiment at at fixed angle of mixing $\sin^2 2\theta_{12} = 0.83$ and the different mass squared difference $\Delta m^2_{12} \approx (2 \div 4) \times 10^{-5}\, eV^2$. Vertical line corresponds to the analysis threshold at 2.6 MeV. The green curve corresponding to theoretical antineutrino spectrum in KamLAND experiment at $\Delta m^2_{12} = 2.5 \times 10^{-5} eV^2$ is selected on two correlated signs (the spectrum shape and value of $\Re = 0.429$ for the KamLAND experimental data description.

Calculations of theoretical antineutrino spectra for the given oscillation parameters (see the insert in figure 4.7 and figure 4.5(b)) is made by using equations (4.16)-(4.17). The necessary parameters characterizing the exposure time, the detection geometry and the detector properties are taken from

KamLAND-experiment data [79]. To determine the averaged fission number of the four main nuclei ($^{235}U$, $^{238}U$, $^{239}Pu$, $^{241}Pu$) which induce the antineutrino contributions from the fission products of each of the Japanese reactors in the radius of 1000 km from detector we took the required parameters from the KamLAND-Internet-site [82], for example, the relative fission yields ($^{235}U$ : $^{238}U$ : $^{239}Pu$ : $^{241}Pu$) and the distances to KamLAND-detector for each of the indicated groups of reactors.

Obviously, the approximate values of the oscillation parameters ($sin^2 2\theta_{12} = 0.83$, $\Delta m^2_{12} = 2.5 \times 10^5\ eV^2$) obtained in this way allow us, by a similar calculation procedure, to determine the total geoneutrino spectrum (4.5) which includes the events due to the $\alpha$-decay of $^{238}U$ and $^{232}Th$ (with the estimated radial profile of their distributions in the Earth's interior [69]) and the $^{239}Pu$ fission in the georeactor core. We can also calculate the geoneutrino integral intensity on the Earth's surface

$$\begin{aligned} n_{\tilde{\nu}} &= p_i \varepsilon N_p \Delta t \int\limits_{E=1.804}^{\infty} \frac{d\lambda_{\tilde{\nu}}(U+Th+Pu}{dE} \sigma_{\varepsilon p}(E) dE \qquad (4.23) \\ &= p_i \left[2.70(U) + 0.78(Th) + 12.72(Pu)|_{E_\varepsilon \le 3.272} + 30.24(Pu)|_{E_\varepsilon > 3.272}\right] \\ &= \left[2.10(U+Th) + 7.50(Pu)\right]_{E \le 3.272} + 17.84|_{E>3.272} \end{aligned}$$

Now, the obtained total geoneutrino spectrum (figure 4.5(a), green shaded region) makes it possible to determine the "true"antineutrino spectrum (figure 4.5(b), blue points with bars) detected from the Japanese reactors in geometry of the first KamLAND -experiment [79]. In figure 4.5(b) we show an approximate oscillation fit, i.e., the theoretical antineutrino KamLAND-spectrum with approximate oscillation parameters $sin^2 2\theta_{12} = 0.83$ and $\Delta m^2_{12} = 2.5 \times 10^5\ eV^2$. Here we note that the observed difference discrepancy between the expected no oscillation spectrum shown in figure 4.5 and a similar KamLAND-spectrum [79] is probably explained by the non-identity of the used databases and does not exceed 3% (see figure 4.3).

Finally, let us show the results of verification of the oscillation parameters in the framework of the test problem of comparing the theoretical (which takes into account the georeactor operation) and the experimental spectrum of the reactor antineutrino on the base of new data [51] which have been obtained by the experimental investigation of the geologically produced antineutrinos with KamLAND. For example, the new KamLAND data [51] in the energy range $E_\varepsilon = (1.7 - 3.4)\ MeV$ (with the exposure time $\Delta t = (749.1 \pm 0.5)\ days$, the detection efficiency $\varepsilon \approx 0.687$ and the number of protons in detector sensitive volume $N_P = (3.46 \pm 0.17) \times 10^{31}$) show that the antineutrino spectrum obtained by taking into account the georeactor antineutrinos, and the predicted KamLAND-spectrum are similar (figure

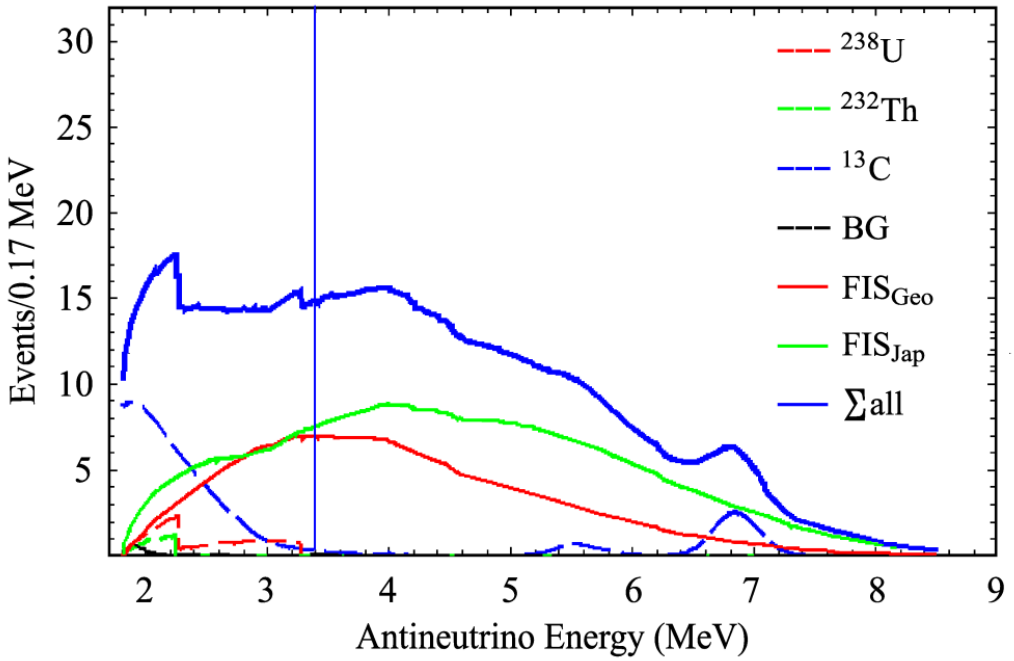


Figure 4.8: The $\tilde{\nu}_e$ energy spectra in KamLAND. Main panel, experimental points (solid black dots with error bars) together the total expectation obtained in KamLAND experiment (dotted black line) [51] and results obtained in this thesis (thick solid blue line). Also shown are expected neutrino spectrum (solid green line) from Japans reactor, the expected neutrino spectrum from georeactor (red line), the expected signals from $^{238}U$ (dashed red line) and $^{232}Th$ (dashed green line) geoneutrinos, $^{13}C(\alpha, n)^{16}O$ reactions (dashed blue line) and accidentals (dashed black line). Inset, expected spectra obtained in KamLAND experiment (solid black line) [51] and results obtained in this thesis (solid green line) extended to higher energy.

4.8). In figure 4.9 the theoretical (which takes into account the georeactor operation) reactor antineutrino spectrum calculated on the basis of the new data [51]for whole energy range of detectable events is presented.

In conclusion, we should note that although the nuclear georeactor hypothesis which we used for the interpretation of KamLAND-experiment seems to be very effective, it can be considered only as a possible alternative variant for describing the KamLAND experimental data. Only direct measurements of the geoantineutrino spectrum in the energy range $> 3.4\ MeV$ in the future underground or submarine experiments will finally settle the problem of the existence of a natural georeactor and will make it possible to determine the

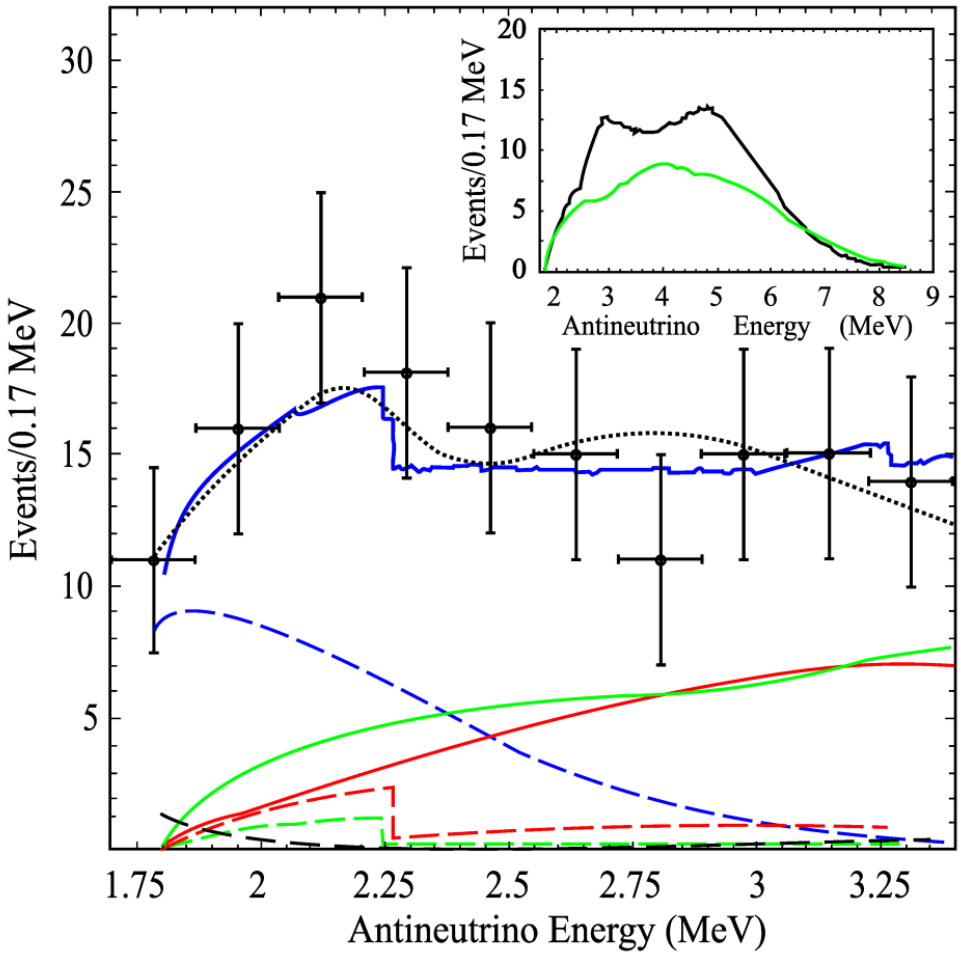


Figure 4.9: Theoretical (which takes into account the georeactor operation) reactor antineutrino spectrum calculated on the base of new data [86] for all energy range of event detection. Designations are like in figure 4.8. Vertical line corresponds to the analysis threshold at 2.6 MeV.

"true"values of the reactor antineutrino oscillation parameters.

On the basis of the analysis of the temporal evolution of radiogenic heat emission power of the Earth in the framework of the geochemical model of the mantle differentiation and the Earth's crust growth [75], [87] complemented by a nuclear energy source on the boundary of the solid and liquid phases of the Earth's core, altentative estimation of the geoantineutrino intensity and the geoantineutrino spectrum on the Earth surface from different radioactive sources ($^{238}U$, $^{232}Th$, $^{40}K$ and $^{239}Pu$) is obtained.

It's also shown that natural nuclear reactors may exist on the boundary

of the solid and liquid phases of the Earth's core as spontaneous reactor-like processes based on Feoktistov $U-Pu$ fuel cycle and/or Teller-Ishikawa-Wood $Th-U$ fuel cycle. Note that, as compared to $^{238}U$-medium, the wave velocity in the $^{232}Th$-medium has the value of about $L/\tau \sim 0.1\,cm/day$ (where $L \sim 5\,cm$ is the diffusion length of the neutron absorption in thorium, $\tau = 39.5/ln257\ days$ is the time of $^{233}U$ generation due to the $\beta$-decay of $^{233}Pa$). It means that the speed of the neutron-fission wave propagation in the $^{232}Th$-medium (Teller-Ishikawa-Wood fuel cycle) is by an order of magnitude less than the similar speed of Feoktistov burning wave.

The solution of the main problem connected with the search of natural neutron sources which locally start the nuclear burning, is unclear and requires serious joint efforts of the theorists. However, concerning the $^3He/^4He$ distribution in the Earths interior and the geoneutrino spectrum on of the Earths surface (KamLAND-experiment), the presence of a georeactor (as nuclear burning progressing wave) makes it possible to obtain a model $^3He/^4He$ distribution and a geoneutrino spectrum which are in good agreement with the experimental data.

Finally, we note that Feoktistov burning wave provides an effective convective mechanism for a sustained hydromagnetic dynamo operation in the Earth's outer core. In fact, it creates natural conditions for gravity convection in the liquid core produced by the effective floating-up of light fission fragments behind the nuclear burning wave front. The condition of continually sustained weak (the temperature being close to adiabatic) convection in the liquid core is the cause of, but also a condition for the differential rotation of different layers in the core, and, consequently, the generating mechanism of the geomagnetic field.

Thus, the hypothesis of slow nuclear burning on the boundary of the liquid and solid phases of the Earth's core is very effective for the explanation of some features of geophysical events. However, strong evidences can be obtained from the independent experiment on geoantineutrino energy spectrum measurements using a multi-detector scheme of geoantineutrino detection with a large base. Finally, solution of the direct and the inverse problems of the remote neutrino-diagnostics for the intra-terrestrial processes which is essential to obtain the pure geoantineutrino spectrum [75] and to determine correctly the radial profile of the $\beta$-sources in the Earth's interior will help to settle the problem of the existence of a natural nuclear reactor on the boundary of the liquid and solid phases of the Earth's core.

# Chapter 5

# Conclusions

This research project has dealt with a conceptual design of a model of an innovative inherently safe nuclear soliton-like fast reactor of Feoktistov type. The main findings are summarized below.

The kinetics of self-stabilising fast uranium-plutonium reactor, which generates self-propagating neutron-fission nuclear burning wave, that satisfies all conditions of inherent safety, was considered for the Feoktistov uranium-plutonium fuel cycle. For simplicity the neutron spectrum was assumed the same as the fission spectrum. A case with little or no moderator was considered – the neutron spectrum is the same as the initial neutron spectrum.

The auto-wave solution for the transmutation chain with necessary condition $n_{crit} < \tilde{n}_{Pu}$ was obtained and analyzing this solution it was shown that the soliton-like propagation of neutron-fission nuclear burning wave is possible in $U_{238}$ medium only under the condition of a certain ratio between equilibrium and critical plutonium concentration ($\tilde{n}_{Pu} > n_{crit}$), which is characterized by Bohr-Sommerfeld quantization condition.

A preliminary model of nuclear fast reactor of Feoktistov type is proposed. The obtained model satisfied the requirement of inherent safety. The numerical experiments of nuclear reactor with uranium-plutonium fuel cycle are made and the solution in the form of soliton-like progressive burning wave is obtained.

The physical conditions of Feoktistov wave mode are generalized and the necessary and sufficient condition of the soliton-like wave origin and propagation are obtained.

The heuristic description of the slow burning process propagation in the reactor core is given.

The simplified one-dimentional model of Pu accumulation and U burnup kinetics was proposed. Taking into account delayed neutrons three-dimentional model for one-group diffusion approximation is offered.

The numerical solution for the obtained physical model of the reactor is provided. In oder to verify theoretical model the computational experiment is performed. The simulation were done for the different initial and boundary condition, with and without initial fuel enrichment. The calculated wave velocity was in good agreement with the necessary and sufficient conditions obtained in chapter 2 of this thesis.

The numerical solution using the method of mesh points in the implicit form is obtained and the simulation results and its verification w.r.t. obtained in the chapter 2 necessary and suffycient conditions of nuclear burning wave origin were given.

On the basis of proposed reactor model the hypothesis of slow nuclear burning on the boundary of the liquid and solid phases of the Earth's core was offered.

On the basis of the analysis of the temporal evolution of radiogenic heat emission power of the Earth in the framework of the geochemical model of the mantle differentiation and the Earth's crust growth [75], [87] complemented by a nuclear energy source on the boundary of the solid and liquid phases of the Earth's core, altentative estimation of the geoantineutrino intensity and the geoantineutrino spectrum on the Earth surface from different radioactive sources ($^{238}U$, $^{232}Th$, $^{40}K$ and $^{239}Pu$) is obtained.

It's also shown that natural nuclear reactors may exist on the boundary of the solid and liquid phases of the Earth's core as spontaneous reactor-like processes based on Feoktistov $U-Pu$ fuel cycle and/or Teller-Ishikawa-Wood $Th-U$ fuel cycle. Note that, as compared to $^{238}U$-medium, the wave velocity in the $^{232}Th$-medium has the value of about $L/\tau \sim 0.1\,cm/day$ (where $L \sim 5\,cm$ is the diffusion length of the neutron absorption in thorium, $\tau = 39.5/ln257\ days$ is the time of $^{233}U$ generation due to the $\beta$-decay of $^{233}Pa$). It means that the speed of the neutron-fission wave propagation in the $^{232}Th$-medium (Teller-Ishikawa-Wood fuel cycle) is by an order of magnitude less than the similar speed of Feoktistov burning wave.

Finally, concerning the $^3He/^4He$ distribution in the Earths interior and the geoneutrino spectrum on of the Earths surface (KamLAND-experiment) the possibility of the existence of soliton-like nuclear reactor with $U-Pu$ or/and $Th-U$ fuel cycle on the boundary of the liquid and solid phases of the Earth's core is shown.

# Appendix A

# Simulation. Program listing.

```
program NY11KT

      USE Numerical_Libraries_e
      USE lin_eig_self_int
      USE rand_int

!*********** PARAMETERS ***********

! real parameters of lenght 8
! where hz - is an iteration on z (cilinder lenght) in sm
!       hr - is a step on r (cilinder radius) in sm
!       ht - is a step on time in sec

real(8),parameter::hz=1.0d0,ht=1.0d2,hr=1.0d0,Rbc=0.5


! integer parameters of lenght 4
! where Nz - is lenght (nuber of "steps") z (cilinder lenght)
!       Nr - is a lenght (nuber of "steps") on r (cilinder radius)
!       Nt - is a lenght (nuber of "steps") on t

integer(4),parameter::Nt=240000,Nr=125,Nz=1000


! real parameters of lenght 8
! where n0 - is an concentration of neutrons on the left bound
!       N80 - is initial concentration of U-238, ro=16.7 - density
! of U-238 at 1500,
```

```
!               Nav - Avogadro constant Nav=6.0247d23
!       Dn - diffusion constant of neutrons
real(8),parameter::n0=1.0d9,N80=(19.0*6.0247d23)/238.0,Dn=2.8d9


! integer parameters of lenght 4
! where  npdes - number of equations
!              uch1, uch2 - size of zones with different structure
!              p - 0 or 1 - initial data reading from file 1,
! or calculating 0
integer(4),parameter::npdes=11,uch1=10,uch2=100,p=0


!*********** VARIABLES AND ARRAYS ***********

!  integer variables of lenght 4
! where i - is an iteration on z
!       j - is an iteration on r (cilinder radius) in sm
!       t - is an iteration on t

integer(5):: k,l,i,j,t


!initial data array  U(:,:,:)
!
real(8)::U(11,0:Nz,Nr)

!  real variables of lenght 8
! where JF - is an initial condition of Bessel equation
!       dTprij - variable for time
!       tt -
real(8)::JF,dTpri,tt


! An(Nr-1,Nr-1)- array of coefficients in sweep method
real(8)::An(Nr-1,Nr-1) !


! CAa(Nz-1,Nr-1,Nr-1) - table of inverse matrixes used
! for calc. of matrix alpha and beta neutrons
!  alfa(Nr-1,Nr-1),beta(Nz,Nr-1) - matrixes in the sweep
```

```
! method equation
real(8)::alfa(Nr-1,Nr-1),beta(Nz,Nr-1),CAa(Nz-1,Nr-1,Nr-1)


real(8)::alfaU(Nr-1),AbF(Nr-1,Nr-1),Fn(0:Nz,Nr-1),fi(Nz,Nr)



open(3,file='dan.dat')
call allopen(npdes,Nz)


dTpri=ht;Tpr=ht


  ! INITIAL CONDITION
!**********************************************************************

t=0

if (p==0) then

   U(:,:,:)=0.0 !All
   U(5,:,:)=N80 !Fragments

   U(2,uch1:uch2,1:Nr)=N80*0.99 !Uranium 238
   U(4,uch1:uch2,1:Nr)=N80*0.01 !Plutonium

   U(2,uch2:(uch2*2),1:Nr)=N80*0.99 !Uranium 238
   U(4,uch2:(uch2*2),1:Nr)=N80*0.01 !Plutonium

   U(2,(uch2*2):(uch2*3),1:Nr)=N80*0.99 !Uranium 238
   U(4,(uch2*2):(uch2*3),1:Nr)=N80*0.01 !Plutonium

   U(2,(uch2*3):Nz,1:Nr)=N80*0.99 !Uranium 238
   U(4,(uch2*3):Nz,1:Nr)=N80*0.01 !Plutonium

   U(5,uch1:Nz,1:Nr)=0.0 !(-uch1) !Fragments


   do j=1,Nr !-1 !!!Boundary condition w.r.t R
```

```
   U(1,0,j)=n0 !0.0
   enddo
else

   call allopen(npdes,t)

   do ur=1,npdes
   l=1000*ur
     do i=1,Nr
    read(l,"(1201(1x,1Pd21.15))")(U(ur,j,i),j=0,Nz)
     enddo
   enddo

   do ur=1,npdes
     l=1000*ur
   close(l)
   enddo

endif


call prir(U,Nr,Nz,t*ht,npdes) !

!*****************************************************************

An(1,1)=ht*Dn/(hz**2)
An(Nr-1,Nr-1)=An(1,1)
 do k=2,Nr-2
An(k,k)=An(1,1)
 enddo

tt=TIMEF()

call CAaK(hr,hz,ht,Nr,Nz,Dn,CAa)

write(*,*)'flag'
tt=TIMEF()
write(3,*)tt
```

```
do t=1,Nt ! Steps on time

call resh(U,Nr,Nz,ht,npdes,fi) !!,qT) !!!!!Source


Fn(0,1:(Nr-1))=U(1,0,1:(Nr-1))

do i=1,Nz-1
Fn(i,1)=(U(1,i,1)+ht*fi(i,1))

 do j=2,Nr-2
dFUr=(U(1,i,j+1)-U(1,i,j-1))/(2.0*j*(hr**2))
+(U(1,i,j-1)-2*U(1,i,j)+U(1,i,j+1))/(hr**2)

Fn(i,j)=(U(1,i,j)+ht*fi(i,j))
 enddo
j=Nr-1
dFUr=(U(1,i,j+1)-U(1,i,j-1))/(2.0*j*(hr**2))
+(U(1,i,j-1)-2*U(1,i,j)+U(1,i,j+1))/(hr**2)

JF=Rbc*U(1,i,Nr-1)*ht*Dn*(1.0+1.0/(2.0*j))/(hr**2)
!!Boundary cond on R

Fn(i,j)=(U(1,i,j)+JF+ht*fi(i,j))
!!FT(i,j)=(U(6,i,j)+JFT+ht*qT(i,j))
enddo

Fn(Nz,1:(Nr-1))=U(1,Nz,1:(Nr-1))

U(1,:,Nr)=Rbc*U(1,:,Nr-1) !,1)

U(1,Nz,:)=Rbc*U(1,Nz-1,:)

!*********************************************************************
!*********************************************************************

! Sweep method

! neutrons

beta(:,:)=0.0
```

```
beta(1,:)=Fn(0,:)
do i=1,Nz-1

alfaU(:)=beta(i,:)

alfaU(:)=An(1,1)*alfaU(:)

do k=1,Nr-1
 alfaU(k)=alfaU(k)+Fn(i,k)
enddo


AbF(:,:)=CAa(i,:,:)
alfaU=MATMUL(AbF,alfaU)
beta(i+1,:)=alfaU(:)

enddo

!-------------------------------------------------------------


do i=Nz-1,1,-1

alfa(:,:)=CAa(i,:,:)
alfa(:,:)=An(1,1)*alfa(:,:)    !!!!!!!!!!!!!!!

do j=1,Nr-1
 alfaU(j)=U(1,i+1,j)
enddo

alfaU=MATMUL(alfa,alfaU)
do j=1,Nr-1
U(1,i,j)=alfaU(j)+beta(i+1,j)
enddo

   do k=1,(Nr-1)
    do j=1,(Nz-1)
 if (U(1,j,k)<0.0) U(1,j,k)=0.0
    enddo
   enddo
```

```
enddo

  dTpri=dTpri+Tpr
  endif
     write(*,*)t*ht,' c',100*t/Nt,'%'


enddo

   call prir(U,Nr,Nz,Nt*ht,npdes)

call allclose(npdes)

tt=TIMEF()
write(3,*)tt
close(3)

end program NY11KT

!*********************************************

!-----------------------------------------------------

subroutine prir(U,Nr,Nz,t,npdes) ! !Data  saving

integer(4):: i,j,Nr,Nz,ur,npdes,f !,ko,Nzf
real(8)::U(npdes,0:Nz,Nr),t !,Tprprir,dTpri,ht

do ur=1,npdes

f=1001*ur !+ko

    write(f,"(1202(1x,1Pd8.2))")(U(ur,j,1),j=0,Nz)

 enddo

 do ur=1,npdes-5

  f=10*ur !+ko
    do i=1,Nr
```

```
      write(f,"(1202(1x,1Pd8.2))")(U(ur,j,i),j=0,Nz)

    enddo

 write(f,*)T    !*
enddo

call allopen(npdes,f-f)

do ur=1,npdes
 f=1000*ur
   do i=1,Nr
     write(f,"(1201(1x,1Pd21.15))")(U(ur,j,i),j=0,Nz)
   enddo
enddo

do ur=1,npdes
 f=1000*ur
 close(f)
enddo


end subroutine prir
!-------------------------------------------------------

subroutine allopen(npdes,Nz)

integer(4)::ur,Nz,npdes,f !,ko,Nzf
character(len=4),parameter::obsh='.dat' !,o='o',z='z'
character(len=8)::name,nach(11)=(/'n','U8','U9','Pu',
'osk','os1','os2','os3','os4','os5','os6'/)
if (Nz.ne.0) then

do ur=1,npdes
 name=trim(nach(ur))//obsh !//trim(kon)
 f=1001*ur !+ko
 open(f,file=name)
enddo

do ur=1,npdes
 name=trim(nach(ur))//obsh !//trim(kon)
```

```
  name=trim(name)
  f=10*ur !+ko
  open(f,file=name)
 enddo
 else

 do ur=1,npdes
  name=trim(nach(ur))//'z'//obsh
  name=trim(name)
  f=1000*ur
  open(f,file=name)
 enddo

endif

end subroutine allopen
!-------------------------------------------------------

subroutine allclose(npdes) !,Nz

integer(4)::npdes,ur,f !,Nzf,Nz,ko

 do ur=1,npdes
  f=10*ur !+ko
  close(f)
  f=1001*ur !+ko
  close(f)
 enddo

end subroutine allclose
!-------------------------------------------------------

subroutine resh(U,Nr,Nz,ht,npdes,q)

integer(4):: i,j,Nr,Nz,ur,npdes
real(8):: U(npdes,0:Nz,Nr),q(Nz,Nr),ht
real(8)::Sum1
real(8),parameter::sifPU=2.0d-24,sia8=5.38d-26,
sia9=2.12d-26,siaPu=2.12d-26
real(8),parameter::To(6:11)
/55.0,22.0,5.5,2.1,0.55,0.22/
```

```
real(8),parameter::Po(6:11)
/0.0002,0.0018,0.0013,
0.0020,0.0005,0.0003/,Sump=0.0061
real(8),parameter::taub=2.85d5,
Vn=1.0d9,nu=2.9,czap=1.0

  q(:,:)=0.0

  do i=1,(Nr-1)

   do j=1,(Nz-1)

 Sum1=0.0;Sumzap=0.0;Sum1o=0.0
do ur=6,11
 Sumzap=Sumzap+U(ur,j,i)/To(ur)
 Sum1o=Sum1o+U(ur,j,i)
enddo

Sum1=sia8*U(2,j,i)+sia9*U(3,j,i)+siaPu*U(4,j,i)
+sia8*(Sum1o+U(5,j,i))
q(j,i)=(nu*(1-Sump)-1)*U(1,j,i)*Vn*sifPu*U(4,j,i)
+czap*0.693*Sumzap-Vn*U(1,j,i)*Sum1
U(2,j,i)=-ht*Vn*U(1,j,i)*sia8*U(2,j,i)
+U(2,j,i) !+Vn*U(1,j,i)*siaPu*U(4,j,i)

U(3,j,i)=ht*Vn*U(1,j,i)*sia8*U(2,j,i)
-ht*U(3,j,i)/taub+U(3,j,i)

U(4,j,i)=ht*U(3,j,i)/taub-ht*Vn*U(1,j,i)
*(siaPu+sifPu)*U(4,j,i)+U(4,j,i)

! Fragments
do ur=6,11
Uk(ur,j,i)=ht*Po(ur)*Vn*sifPu*U(4,j,i)*U(1,j,i)
-ht*0.693*U(ur,j,i)/To(ur)+U(ur,j,i)
 U(ur,j,i)=ht*Po(ur)*Vn*sifPu*U(4,j,i)*U(1,j,i)
  -ht*0.693*U(ur,j,i)/To(ur)+U(ur,j,i)
enddo
U(5,j,i)=ht*(1-Sump)*Vn*U(1,j,i)*sifPu*U(4,j,i)
+ht*0.693*Sumzap+U(5,j,i)
```

```
  enddo

  enddo

  do ur=2,npdes
   do i=1,(Nr-1)
    do j=1,(Nz-1)
 if (U(ur,j,i)<0.0) U(ur,j,i)=0.0
    enddo
   enddo
  enddo
end subroutine resh
!-------------------------------------------------
subroutine CAaK(hr,hz,ht,Nr,Nz,Dn,CAa)
real(8)::hr,hz,ht
integer(4):: k,l,i !,j !,t !Nr,Nz,Nt,
integer(4)::Nr,Nz

real(8)::An(Nr-1,Nr-1),ZAPt(Nr-1,Nr-1),C(Nr-1,Nr-1)
real(8)::alfa(Nr-1,Nr-1),CAa(Nz-1,Nr-1,Nr-1)



real(8)::Dn

An(1,1)=ht*Dn/(hz**2)
C(1,1)=1.0+2.0*ht*Dn/(hz**2)+2.0*ht*Dn/(hr**2)
C(1,2)=-2.0*ht*Dn/(hr**2)
An(Nr-1,Nr-1)=An(1,1)
C(Nr-1,Nr-1)=1+2.0*ht*Dn/(hz**2)+2.0*ht*Dn/(hr**2)
C(Nr-1,Nr-2)=ht*Dn*(1.0/((Nr-1-1)*2.0)-1.0)/(hr**2)
 do k=2,Nr-2
  do l=k-1,k+1
   if (l==k) then
An(k,l)=An(1,1)
C(k,l)=C(Nr-1,Nr-1)
   else
    C(k,l)=ht*Dn*((k-l)*(1.0/((k-1)*2.0))-1.0)/(hr**2)
   endif
  enddo
 enddo
```

```
!-------------------------------------------------------

alfa(:,:)=0.0
CAa(:,:,:)=0.0
do i=1,Nz-1ZAPt=MATMUL(An,alfa)

do k=1,Nr-1
do l=1,Nr-1
ZAPt(k,l)=C(k,l)-ZAPt(k,l)
enddo
enddo

call obr(ZAPt,Nr-1)

CAa(i,:,:)=ZAPt(:,:)
alfa=MATMUL(ZAPt,An)

write(*,*)i

enddo
end subroutine CAaK


!*******************************************************



subroutine obr(a,n)
 integer(4)::n
 integer(4)::j,ipvt(n)
 real(8)::a(n,n),fac(n,n),e(n),ainv(n,n)

 call Lufac2(n,a,fac,ipvt)
 do j=1,n
  e=0.0; e(j)=1.0
  call useLU2(n,fac,ipvt,e,ainv(1,j))
 end do
a(:,:)=ainv(:,:)
end subroutine obr !
```

```
subroutine Lufac2(n,a,fac,ipvt)
integer(4)::n,ipvt(n),i,j,k
real(8)::a(n,n),fac(n,n),p(n),hold
fac=a;ipvt=(/(i,i=1,n)/)
do k=1,n-1

ipvt(k:k)=k+maxloc(abs(fac(k:n,k)))-1
if(ipvt(k)/=k) then
p(k:n)=fac(k,k:n)
fac(k,k:n)=fac(ipvt(k),k:n);fac(ipvt(k),k:n)=p(k:n)


do j=1,k-1
 hold=fac(ipvt(k),j);fac(ipvt(k),j)=fac(k,j);fac(k,j)=hold
end do
end if
p(k+1:n)=fac(k+1:n,k)/fac(k,k)
 do i=k+1,n
  fac(i,k+1:n)=fac(i,k+1:n)-fac(k,k+1:n)*p(i)
 end do
 fac(k+1:n,k)=-p(k+1:n)
end do
end subroutine Lufac2

subroutine useLU2(n,fac,ipvt,b,x)
 integer(4)::n,ipvt(n),k
 real(8)::fac(n,n),x(n),b(n),s,hold
 do i=1,n
  if(ipvt(i)/=i) then
   hold=b(ipvt(i));b(ipvt(i))=b(i);b(i)=hold
  end if

 end do
 do k=2,n !
  b(k)=b(k)+dot_product(fac(k,1:k-1),b(1:k-1))
 end do

 x(n)=b(n)/fac(n,n)
 do k=n-1,1,-1
  s=sum(fac(k,k+1:n)*x(k+1:n))
  x(k)=(b(k)-s)/fac(k,k)
```

```
 end do

end subroutine useLU2
```

# Bibliography


[1] Feoktistov L.P. *The safety is the key moment of revival of nuclear power*, Progress in Phys. Sciences, 1993.

[2] Feoktistov L.P. *A Weapon that Outlived itself*, RK VMPYaV, Snezhinsk, Russia, 1999.

[3] Feoktistov L.P. *From past to the future: from hopes about bomb to safe reactor*, RK VMPYaV, Snezhinsk, Russia, 1998, p.326.

[4] Nuclear Regulatory Commission USA, Preliminary Notification of Event of Unusual Occurrence, PNO-III-02-006 *Significant Metal Loss Observed n Reactor Vessel Head*, March 8, 2002.

[5] Feoktistov L.P. *The analysis of one concept of physical safety of the reactor*, Preprint of the Kurchatov University of nuclear energy N4605/4, Moscow, 1988.

[6] Feoktistov L.P. *The perspective systems of nuclear reactors with inherent safety*, Soviet school on theoretical nuclear physics, MIFI , 1988.

[7] Feoktistov L.P. *The variant of safe reactor*, Nature, 1, in russian, 1989.

[8] Feoktistov L.P. *Is the nuclear power engineering necessary?*, Nature, 4, in russian, 1989

[9] Zarezky N.P. *Feoktistov inverse task and megajoule chemical laser with self-triggering*, RK VMPYaV, International conference on high energy density physics "7th Zababakhin Scientific Talks", Snezhinsk, Russia, 2003, 8-12 September, pp. 1-16.

[10] Mitsuru KAMBE *RAPID Operator-Free Fast Reactor Concept without Any Control Rods. Reactor Concept and Plant Dynamics Analyses*, Journal of NUCLEAR SCIENCE and TECHNOLOGY, Vol. 42, No. 6, p. 525-536, June 2005.

[11] *http : //news.bbc.co.uk/2/hi/science/nature/*1504564.*stm BBSNews, 22 August, 2001*

[12] *http : //technology.newscientist.com/channel/tech/nuclear/dn*1186 *New Scientist magazine, 22 August 2001*

[13] Akhiezer A.I., Belozorov D.P., Rofe-Beketov F.S., Davydov L.N., Spolnik Z.A. *To the theory of propagating of the nuclear chain reaction in the diffusion approximation*, Nuclear Physics, Issue 5, pp. 1567-1575, 1999.

[14] Akhiezer A.I., Belozorov D.P., Rofe-Beketov F.S., Davydov L.N., Spolnik Z.A. *Slow nuclear burning*, The problems of nuclear physics, Issue 6, pp. 276-278, 2001.

[15] Bohm D., *A Suggested Interpretation of the Quantum Theory in Terms of Hidden Variables*, Phys.Rev., 1952, V. 85, P.166-179

[16] Holland P.R. *Quantum Theory the Motion. An account of the de Brogie-Bohm causal interpretation of quantum mechanics.* Cambridge University Press 1993.

[17] Rusov V.D., Vlasenko D. *On the Quantization Procedure in Classical Mechanics and Problem of Hidden Variables in Bohmian Mechanics*, arHive: quant-ph/0806.4050.

[18] Rusov V.D. *On the Quantization Procedure in Classical Mechanics and the Reality of the Bohm's $\psi$-field*, arHive: quant-ph/0804.1427.

[19] Ershov, A.P., Anisichkin,V. F., *Natural Neutron-Fission Wave*,Combustion, Explosion, and Shock Waves, Vol. 39, No. 2, pp. 226231, 2003

[20] Principal Research Results *Operator-Free Super Safe Fast Reactor Concept RAPID-L*, Japan Atomic Energy Research Institute, Annual Research Report 2002

[21] Teller et al., 1995 Teller, E., Ishikawa, M., Wood, L., *Completely automated nuclear reactors for long-term operation.* In: "Fronters in Physics Symposium", 26-28 Okctober, Lubbock, Texas.

[22] Teller et al., 1996 Teller, E., Ishikawa, M., Wood, L., *Completely automated nuclear reactors for long-term operation II.* In: Proceedings ICENES'96, 24-28 June, Obninsk, Russia, pp. 151-158 .

[23] Sekimoto, H., and Udagawa, Y., *Effects of Fuel and Coolant Temperatures and Neutron Fluence on CANDLE Burnup Calculation*Journal of NUCLEAR SCIENCE and TECHNOLOGY, Vol. 43, No. 2, p. 189197 (2006)

[24] Sekimoto, H., *Recent Research Activities on CANDLE Burnup*International Conference on Advances in Nuclear Science and Engineering in Conjunction with LKSTN 2007 (125-131)

[25] Sekimoto, H., *Light a CANDLE. An Innovative Burnup Strategy of Nuclear Reactors* The 21st Century Center of Excellence Program Innovative Nuclear Energy Systems for Sustainable Development of the World (COE-INES), Tokyo Institute of Technology, 2005.

[26] Fomin,S.P.,Melnik,Yu.P., Pilipenko,V.V., Shul'ga,N.F. *Self-sustained regime of nuclear burning wave in U-Pu fast neutron reactor with Pb-Ni coolant*, Problems of Atomic Science and Thechnology 3 (2007) 156.

[27] Fomin,S.P.,Melnik,Yu.P., Pilipenko,V.V., Shul'ga,N.F. *Investugation of self-organization of the non-linear nuclear burning regime in fast neutron reactor.*, Annals of Nuclear Energy 32 (2005) 1435.

[28] Arnold, B.I., *Small denominators and problem of stability in classical and celestial mechanics*, Uspekhi Mat. Nauk, 1963

[29] Kolmogorov, A.N., *On conservation of conditionally periodic motions under small perturbations of the Hamiltonian*, Dokl. Akad. Nauk. SSR, 1954

[30] Moser,J., *On invariant curves of area preserving mappings of an annulus*, Nachr. Akad. Wiss. Gottingen, Math. Phys. Kl, 1962

[31] Einstein A. *Zum Quantensatz von Sommerfeld und Epstein.*, Verh. Deutsch. Phys. Ges. 19 (1917) 82.

[32] Gutzwiller M.C., *Chaos in Classucal and Quantum Mechanics.*, N.Y.: Springer-Verlag, 1990.

[33] Tabor, M., *Chaos and Integrability in Nonlinear Dynamics.*, Wiles, New York,in English, 2001

[34] Persival, I.C.*Semiclassical theory of bound states*, Adv. Chem. Phys. 36 (1977) 1.

[35] Stokmann H.-J. *Quantum Chaos.* Cambridge University Press. 2000, 375 p.

[36] Zirnbauer M.R. *Riemannian symmetric superspases and their origin in random-matrix theory* J. Math. Phys. 37 (1996) 4986.

[37] Mehta M.L. Random *Matrices*. San Diego: Academic Press, 1991.

[38] Bohigas O., Giannoni M.J., Schmit C. *Characterization of chaotic spectra and universality of level fluctuation laws*, Phys. Rev. Lett. 52 (1984) p.1.

[39] G. G. Bartolomei, G. A. Bat', V. D. Baibakov, M. S. Alkhutov *Nuclear power theory fundamentals and nuclear reactors calculation methods*, (in Russian), M. Energoatomizdat,1989, 512 p.

[40] Stacey W. M. *Nuclear reactors Physics*, 2nd Ed. John Wiley Sons, 2007, 736 p.

[41] Lewis E. *Fundumental of Nuclear Reactors Physics*, Academic Press, 2008, 280 p.

[42] Van Dam, 2000 H. Van Dam, *Self-stabilizing criticality waves,* Annals of Nuclear Energy 27 (2000), pp. 1505-1521.

[43] Seifritz W. *What is Sustainable Development? An Attempt to Interpret it as a Soliton like Phenomenon*, Chaos, Solitons and Fractals 7 (1996) 2007 2018.

[44] Xue-Nong Chen and Werner Maschek, *Transverse buckling effects on solitary burn up waves,* Annals of Nuclear Energy 32 (2005) 1377-1390.

[45] Dall'Osso A. *A transverse bucling based methods in core neutronics models equivalence*, Annals of Nuclear Energy 29 (2002) 659-671.

[46] L. Landau, E. Lifshitz *The Classical theory of fields*, Pergamon Press / Addison-Wesley Publishing Company, INC. (1961)

[47] Samarsky *The Classical theory of fields*, Pergamon Press / Addison-Wesley Publishing Company, INC. (1961)

[48] Samarsky *The Classical theory of fields*, Pergamon Press / Addison-Wesley Publishing Company, INC. (1961)

[49] Samarsky *The Classical theory of fields*, Pergamon Press / Addison-Wesley Publishing Company, INC. (1961)

[50] Smelov, V. V.*Lectures of Neutron Transport Theory*, (1978) Atomizdat, Moscow, pp. 247.

[51] Araki, T., et al.,*Measurement of neutrino oscillation with KamLAND: Evidence of spectral distortion*, Phys. Rev. Lett, 94, 0818011-0818015, 2005.

[52] Lay, T., J. Hernlund, E.J. Garnero et al., *A post-perovskite lens and Dheat flux beneath the Central Pacific*, Scince, 314, 1272-1276, 2006.

[53] Driscoll,*Nuclear disruption of a planet with convective outer core*, Bull. Amer. Phys. Soc., Series II, 33, 1031-1037, (1988).

[54] Herndon, J.M.*Feasibility of a nuclear fission reactor at the center of the Earth as the energy source for the geomagnetic field*Geomagnetism and Geoelectricity, 45, 423-437, 1993.

[55] Anisichkin V.F., A.A. Bezborodov, and I.P. Suslov*Chain fission reactions of nuclides in the Earths core during billions years*,Atomic Energy (Russia) 98(5), 370-379,2005.

[56] Hollenbach, D.F., and J.M. Herndon*Deep-Earth reactor: nuclear fission, helium, and the geomagnetic field*,Proc. of Nat. Acad. Sci., 98, 11085-11090,2001.

[57] Anisichkin, V.F., A.P. Ershov, A.A. Bezborodov et al.*The possible modes of chain nuclear reactions in the Earths core*, paper presented at Int. Conf. VII Zababakhin's Sientific Lectures, Snezhinsk, Russia, 8-12 September, 2003.

[58] Wood, B.J., M.J. Walter, J. Wade*Accretion of the Earth and segregation of its core,* (2006), Nature, 441, 825-833.

[59] Ershov, A.P., and V.F. Anisichkin*About neutron-fissioning wave*, Burning and Explosion Phys. (Russia), 39, 121-127.

[60] Anderson, D.L.,*Theory of the Earth.*, 366 pp., Blackwell Scientific Publications, Boston,1989.

[61] Anderson, D.L., *The statistics and distribution of helium in the mantle*,Int. Geology Rev., 42, 289-311, 2000.

[62] Kuznetsov, V.V.,*Anisotropy of the Earths inner core properties*, Usp. Fiz. Nauk (Russia), 167, 1001-1012,1997.

[63] Julian, B.R., D. Davies, and R.M. Sheppard, *PKJKP*, Nature, 235, 317-318, 1972.

[64] Su, W.J., A.M. Dziwonski, *Inner core anisotropy in three dimensions,* J. Geophys. Res., 100 (B6), 9831-9852, 1995.

[65] Adushkin et al.,*On the density jump at the inner boundary of the Earths core from observations of PKiKP waives at distances of about 6o*, Dokl. Russ. Acad. Sci./Earth Sci., 334, 595-598,1997.

[66] Lobkovsky, L.I., A.M. Nikishin, and V.E. Khain, *Current Problems of geotectonics and geodynamics*, 612 pp., Scientific World, Moscow, 2004.

[67] Kuroda, P.K., *On the nuclear physical stability of the uranium minerals*, J. Chem. Phys., 4, 781-782, 1956.

[68] Tromp, J., *Normal-mode splitting observations from the great 1994 Bolivia and Kuril Islands earthquakes: constraints on the structure of the mantle and inner core*,1995, GSA Today, 5, 137-141.

[69] Rusov, V.D., et al.*Geoantineutrino Spectrum and Slow Nuclear Burning on the Boundary of the Liquid and Solid Phases of the Earth's Core*, JOURNAL OF GEOPHYSICAL RESEARCH, VOL. 112, B09203, doi:10.1029/2005JB004212, 2007

[70] Hofmeister, A.M., and R.E. Criss, Earths heat flux revised and linked to chemistry, Tectonophysics, 395, 159-177.

[71] van den Berg,A.P., Yuen,D.A.*Non-linear effects from variable thermal conductivity and mantle internal heating: implications for massive melting and secular cooling of the mantle*, Physics of the Earth and Planetary Interiors 129 (2002) 359375

[72] Fiorentini, G., M. Lissia, F. Mantovani,. and R. Vannucci*How much uranium is in the Earth? Predictions for geo-neutrinos at KamLAND*, hep-ph/0501111 v1., 2005.

[73] Vorobev et al.,*Triple fission of plutonium-239*, Nucl. Phys. (USSR), 20, 461-468, 1974.

[74] Stuart, F.M., S. Lass-Evans, J.G. Fitton, and R.M. Ellam $^3He/^4He$ *in picritic basalts from Baffin Island: the role of a mixed reservoir in mantle plumes*, Nature, 424, 57-59.,2003.

[75] Rusov, V.D., T.N. Zelentsova, V.A.Tarasov, and D. Litvinov*Inverse problem of remote neutrino diagnostic of intrareactor processes*J. of Appl. Phys., 96, 1734-1739,2004.

[76] Kellogg and Wasserburg,*The role of plumes in mantle helium fluxes*, Earth planet. Sci. Lett., 99, 276-289, 1990.

[77] Barger, V., D. Marfatia and K. Whisnant*Progress in the physics of massive neutrinos,*hep-ph/0308123.

[78] Achmed et. al., *Measurement of the total active 8B solar neutrino flux at the Sudbury neutrino observatory with enhanced neutral current sensitivity*, Phys. Rev. Lett., 92, 1813011-1813016,2004.

[79] Eguchi, K., S. Enomoto, K. Furuno et al., *First results from KamLAND: Evidence for reactor anti-neutrino disappearance*, Phys. Rev. Lett., 90, 041801-041805, 2003.

[80] Vogel,P., *Analysis of the antineutrino capture on protons*, Phys. Rev., D29, 1918-1930, 1984

[81] Fogli, G.L., E. Lisi, A. Marrone et. al. *Solar neutrino oscillation parameters after first KamLAND results*, hep-ph/0212127,2002.

[82] *KamLAND collaboration. Data release accompanying the 2nd KamLAND reactor result*,2005, is available at http:/www.Awa.tohoku.ac.jp/KamLAND/datarelease/2ndresult.html.

[83] Tuli, J.K.,*Evaluated Nuclear Structure Data File. A manual for preparation of Data Sets*,BNL-NCS-51655-01/02-Rev2001.

[84] England, T.R. and B.F. Rider, *Evaluation and Compilation of Fission Product Yields*,LA-UR-94-3106, ENDF-349, 1993.

[85] Hagivara, K., et al., 2002*Review of particle properties*Phys. Rev. D, 66, 010001, doi:10.1103 v.1.

[86] Araki, T., et al.*Experimental investigation of geologically produced antineutrinos with KamLAND*Nature, 436, 499-503, 2005..

[87] ONions, R.K., N.M. Evensen, and P.J. Hamilton*Geochemical modeling of mantle differentiation and crustal grouth*, J. Geophys. Res., 84 (B11) 6091-6098,1979.